CRANFIELD UNIVERSITY

Hyo-Sang Shin

Study on Cooperative Missile Guidance for Area Air Defence

Department of Informatics & Systems Engineering,
Autonomous Systems Group

PhD

CRANFIELD UNIVERSITY

Defence Academy - College of Management and Technology

Department of Informatics & Systems Engineering,
Autonomous Systems Group

PhD
2010

Hyo-Sang Shin

Study on Cooperative Missile Guidance for Area Air Defence

Supervisors:
Professor Antonios Tsourdos

Nov 2010

© Cranfield University, 2010. All rights reserved. No part of this publication may be reproduced without the prior written permission of the copyright owner.

Abstract

This research investigates the necessary components to design cooperative guidance strategies for area air defense applications, as a part of a project supported by UK MoD and French DGA MCM-ITP (Materials and Components for Missile - Innovation and Technology Partnership) programme. The main considerations in developing the cooperative guidance scheme are the uncertainty of the target manoeuvre and the zone defence concept. For the interception of unpredictable targets before they reach any asset in the defended area, Earliest Intercept Geometry (EIG) and Intercept Geometry (IG) are introduced; EIG is analytically obtained and IG is numerically computed in consideration of physical constraints of the missile and target. Then, two mid course guidance laws are proposed using the geometries, termed the Earliest Intercept Geometry Guidance Law (EIGGL) and Intercept Geometry Guidance Law (IGGL). Since the EIG or IG represents a capture zone of the missile, the defended assets can be protected if the guidance law guarantees no overlapping between the geometry (EIG or IG) and the defended area. In many-on-many engagement scenarios, it is clear that the performance of the guidance scheme depends on the target allocation policy, thus an optimal target allocation algorithm is designed using the EIG and IG to maximize the reachability and safety margin. Multiple co-existing hypotheses about future target trajectory in the mid course and homing phase result in an initial angular difference between actual flight path and the flight path demanded by the homing guidance law at handover, termed the heading error. Even if a hypothesis of future target trajectory is common to mid course and homing guidance laws, heading error can be caused by errors in uplink data because of radar/launcher misalignment, tracker lag, radar measurement error etc. Since this error might result in an abrupt change of the missile acceleration, it is undesirable. In order to resolve this problem, an optimal homing guidance law is developed by introducing a second order polynomial function into the cost function of the guidance problem. The performance of the optimal guidance law heavily depends on the accuracy of the time-to-go estimates. Because the optimal guidance laws are used in the calculation of the IG and the terminal homing guidance, a time-to-go estimation algorithm is also proposed. The performance of each algorithm is demonstrated using simple numerical examples. Furthermore, the overall perfor-

mance of the cooperative guidance algorithm is verified using scenarios in naval and ground context and a Simulink Common Model (CM). For the algorithm test and development, these scenarios and CM have been shared between partners and have evolved during the project. Future work within this research area is discussed further in the last chapter of this thesis, along with other applications for the cooperative guidance scheme

To
my wife Sun Mi, the joys of my life

Acknowledgements

I would like to first thank my supervisor, Professor Antonios Tsourdos, for giving me an opportunity to undertake this research and helping me in many ways. Antonios has invested considerable time and effort to support me, understand my situation, and guide me in a right direction for the research. I still clearly remember when he came to Korea and gave us a talk in 2006. That short moment became the most important milestone of my life. I am also most grateful to Professor Brian A White who always inspires me. It was blessing for me to know someone with clear vision and ability to direct future work through a simple but inspiring question.

I would like to also thank my partners in the joint project supported by UK MoD and French DGA MCM-ITP programme. Dr Keith Markham, MBDA UK, always listened what we are trying to say through the project meeting or in some conferences, and endeavoured to guide the project in a right direction at all time. Dr Stéphane Le Ménec, MBDA France, and Hélène Piet-Lahanier, ONERA, collaborated with me and gave me different point of views to solve the problem as ever. Dr Graham Wallis, MDBA UK, I was really amazed by his keen and deep insight about the future and passion for improving the current weapon systems. They were my industrial mentors and guided me throughout the project with encouragement and inspiration.

I would like to also thank Professor Min-Jea Tahk and Dr Hanju Cho. Professor Min-Jea Tahk allowed me to come to Cranfield University while I was doing my research in KAIST. Although everything has gone in a slightly different way from what we expected, he always understood it and advised me to have a right decision. Dr Hanju Cho, ADD, came to Cranfield University for his sabbatical year in 2010 and carried some work with me. Not to mention his help for the research, he showed me how I can carry out not only my research, but also my life. My thanks also go to Mr Hyun-Dong Oh. He spent most of his time with me in the office, about 15 hours per day. It is a bit sad, but he is now more than my family to me.

My family deserve a sincere vote of thanks too. Due to the long distance between Korea and UK, I couldn't spend much time with my family, parents, two

sisters, parent-in-law and sister-in-laws. However, they trust and support me as always and as will. I really appreciate to my wife, Sun Mi. My wife had been waiting for me to come back to Korea for two years and then accepted me as her husband. Without her trust and understanding, I am for sure I couldn't finish this research.

Contents

List of Tables

List of Figures

Nomenclature

All units are in SI unless otherwise stated

Abbreviations

ALCPOV	Approximated Length of the Curved Path Over Velocity
CM	Common Model
DGGL	Differential Geometry Guidance Law
DGT	Differential Game Theory
IAC	Impact Angle Control
IACG	Impact Angle Control Guidance
IATG	Impact Angle and Time Guidance
IG	Intercept Geometry
IGGL	Intercept Geometry Guidance Law
LOS	Line-of-Sight
LQ	Linear Quadratic
LQR	Linear Quadratic Regulator
OGL	Optimal Guidance Law
PN	Proportional Navigation
SPT	Singular Perturbation Technology
UAV	Unmanned Aerial Vehicle
UCAV	Unmanned Combat Aerial Vehicle
UGV	Unmanned Ground Vehicle

Chapter 1

Introduction

1.1 Motivation and Objectives

Technology developments in the field of modular data links may allow the creation of a multi-link communication network to be established between anti-air missiles and the launch platform. The future prospect of such ad hoc networks with many existing guidance schemes makes it possible to consider cooperative strategies for missile guidance. Over the past decades, a range of missile genres have been developed mostly on the basis of one-on-one engagements which are then optimized for many-on-many scenarios. A priori allocation rules and natural missile dispersion can allow a salvo of missiles to engage a swarm of targets; however, this does not always avoid some targets leaking through the salvo, whilst other targets may experience overkill. Therefore, cooperative guidance places greater demands on the guidance chain compared with one-on-one guidance. UK MoD and French DGA launched a project in MCM-ITP (Materials and Components for Missile - Innovation and Technology Partnership) programme[1] to investigate the cooperative guidance problem. This research has focused on the problem of air defence systems, especially naval based systems, which must defend against attacks from multiple targets as a part of this project.

If missiles within a salvo can communicate with each other, the possibility exists for a more optimal assignment of missiles to targets. Sharing homing sensor measurements and tracked object information, the missiles will be able to collate a consistent air picture which is available to maintain the allocation of missiles to targets. Further, if the communication includes the exchange of zero effort miss (ZEM) data, the allocation can be adapted according to which missile has the best chance of engaging which target in terms of attainability.

The primary task of the area air defence is to protect all defended assets against incoming weapon systems (targets) which have a high kill probability and low detectability; the missile must intercept the incoming threats before they reach

[1] http://www.mcmitp.com/

their targets in the defended area. It is obvious that one of guidance strategies for the protection of an area is to intercept the incoming threat as soon as possible. Siouris & Leros (1998), Tahk et al. (2002), investigated this concept to develop the guidance strategy, termed Minimum Time Guidance (MTG) or earliest intercept guidance. This minimum time concept can be converted as a purely geometric concept; the earliest intercept guidance strives to intercept the target at the longest distance from the defended asset. This research mainly examined how the earliest intercept concept can be used to develop cooperative guidance for the protection of the area.

1.2 An Overview of the Thesis

Cooperative guidance combines a number of guidance technology strands to deliver this enhanced capability and these have been studied as part of the research programme:

- Mid course to place the missile in position to acquire and engage the target;
  - An algorithm using the Earliest Intercept Geometry (EIG), which is named Earliest Intercept Geometry Guidance Law (EIGGL) ;
  - An algorithm using the Intercept Geometry (IG), which is named Intercept Geometry Guidance Law (IGGL) ;
- Target allocation algorithm based on the intercept geometries (EIG or IG) and target behaviour;
- Terminal homing guidance to achieve an intercept;
- Time-to-go estimation algorithm;
- Estimation and prediction of the target behaviour.

Figure 1.1 shows the links between the proposed algorithms. Each algorithm is investigated in a different chapter and the performance of the whole cooperative guidance system is carefully examined. Note that, in this research, we use the set estimation for the target prediction and estimation developed by Dr Hélène

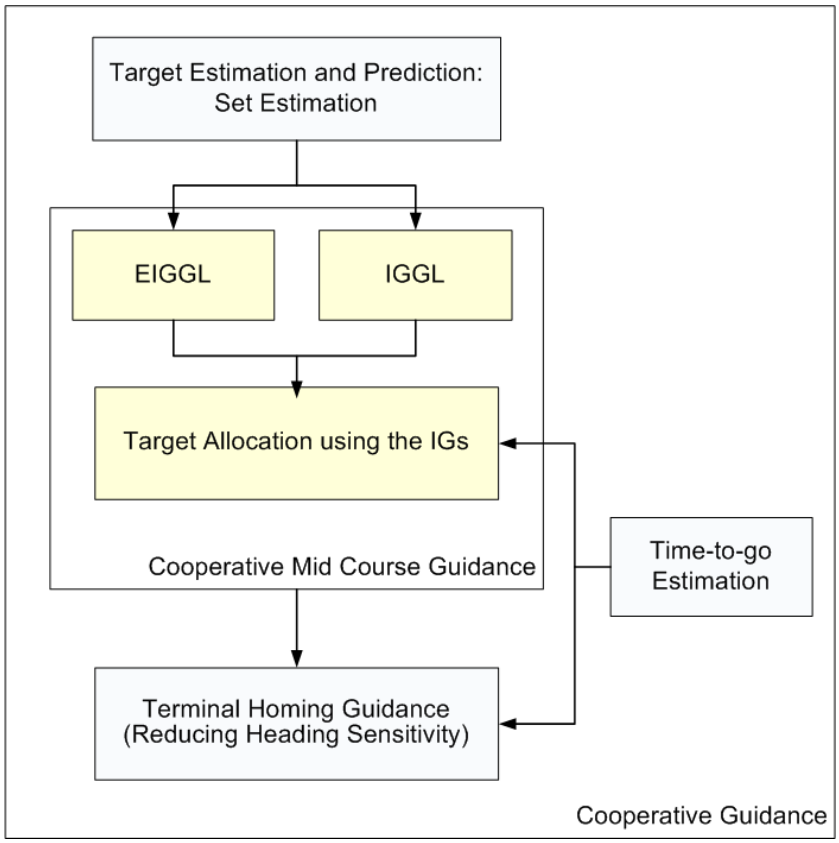

Figure 1.1: Framework of the proposed algorithms

Piet-Lahanier[2], who is one of partners[3] in the our joint project developing a cooperative guidance scheme. This technique considers target constraints, such as maximum lateral acceleration, and combines these with measurements to maintain an evolving ellipsoid which bounds the target state. It is possible to collate bundles of target trajectories to an array of intended goals.

Chapter 2 describes the general mid course problem for the area air defence and develops a mid course guidance law to overcome the problem with the uncertainty of the target manoeuvre. The guidance solution is analytically derived using the Earliest Intercept Guidance, obtained from the locus of all possible Earliest Intercept Points (EIPs) against the target. The EIG represents the capture zone. If the guidance algorithm can guarantee that EIG is not overlapped with the defended area (keep out zone), it can protect the assets in the defended

[2]Dr Hélène Piet-Lahanier is Research Fellow at Direction des Etudes de Synthése - Mécanique et Systémes Aérospatiaux, ONERA, BP 72, F-92322 Châtillon Cedex, France

[3]MBDA UK, MBDA-Fr, ONERA and Cranfield University

area. As will be shown, the EIG law depends on the missile heading and is analytically derived so as to establish the mid course guidance strategy. Unlike typical guidance schemes, the derived guidance strategy leads the missile toward one of the EIPs which most pushes the EIG from the defended assets.

In Chapter 3 , another mid course guidance algorithm, termed Intercept Geometry Guidance Law (IGGL), is proposed to take operational and physical constraints of the missile and target into consideration. Because the optimal guidance minimizing the energy loss can leave more manoevrability to the terminal homing guidance, the optimal guidance law is introduced and used to compute the IG. Under the assumption that the missile constraints such as velocity loss are given, the general optimal solution is derived. When the missile guidance is determined, the hypothesis on the target acceleration ultimately changes the shape of the IG. Therefore, the characteristic of the IG change is also examined using a couple of target acceleration profiles. After computing the IG, the guidance strategy of the IGGL is the same as that of the EIGGL.

In previous chapter, we proposed a mid course guidance algorithm, named Earliest Intercept Guidance Law (EIGGL). Since missiles must destroy the incoming threat before it intercepts any defended asset, the proposed guidance algorithm endeavours to guarantee that all assets will be located outside the capture zone. The EIGGL was analytically derived under the assumption that the missile can instantaneously change its heading angle. Although it can deal with the worst case, it is difficult to consider the operational and physical constraints of the missile and target. To take the operational and physical constraints of the missile and the target into consideration, we propose a mid course guidance law, called Intercept Geometry Guidance Law (IGGL), based on the optimal control theory and the concepts of the Intercept Geometry (IG).

Chapter 4 addresses a target allocation problem and proposes a numerical allocation algorithm using the intercept geometry concept and the optimal control theory. Since there are many players in the cooperative mid course guidance problem, the allocation policy is one of most important components determining the guidance performance. Certain distances between the defended assets and intercept geometries guarantee the protection of the defended assets against incoming threats. This implies that the bigger the distance between the intercept geometry and asset, the more satisfactory the target allocation is. Therefore, the

optimal target allocation algorithm endeavours to maximize these distances. Although the optimal allocation plan can be derived using both of the EIG and IG, we describe the algorithm using the EIG because all parameters to find an optimal allocation can be analytically derived by using simple algebra. In order to reduce the computational load, we divide the optimization procedure into several simple steps. The performance of the optimal allocation algorithm is demonstrated using simple numerical examples.

In Chapter 5, a new homing guidance is developed to reduce sensitivity to the heading error at the beginning of the terminal guidance phase. There can be different respective hypotheses of future target trajectory in mid course and homing guidance laws, or errors in uplink data due to radar/launcher misalignment, tracker lag, radar measurement error etc. This causes an angular difference between the actual flight path and the desired flight path when the guidance law is changed from the mid course to homing phase. Any initial angular deviation of the actual flight path angle from the demanded angle, known as a heading error, can result in undesirable phenomena such as abrupt acceleration commands at the handover point. This problem can be resolved by reducing the sensitivity of the heading error. In order to shape the control input alleviating the sensitivity, a new performance index is proposed by introducing distribution functions on the input weighting. The distribution functions are expressed in terms of second order polynomials of time-to-go, so that it is possible to distribute the input weighting over the flight. Then, a homing guidance law is derived by applying the LQ optimal control theory to the guidance problem with the new performance index. Whilst the navigation gain is constant in the general Proportional Navigation (PN) guidance, the proposed guidance laws have time varying gains to ease the heading error sensitivity. The performance of the terminal guidance law is verified by the mathematical analysis and numerical examples.

The optimal guidance laws are used in the IGGL and the terminal homing guidance. Since the command of those optimal guidance is represented as a function of time-to-go, the time-to-go estimation problem is one of major parameters determining the performance of various optimal guidance laws. Therefore, Chapter 6 introduces the time-to-go estimation problem. The strong curvature of the trajectory is a main factor that increases the time-to-go estimation error and the curvature is determined by the given guidance command history over the

flight. The optimal guidance with unpredictable target manoeuvres can cause a strongly curved trajectory of the missile. Thus, a time-to-go estimation algorithm is proposed using guidance command histories. Since the proposed method involves trigonometric integrands in estimating the time-to-go, we approximate the sinusoidal functions by polynomial functions of the time of flight through the Talyor series expansion. The performance of the proposed time-to-go estimation algorithm is investigated by various numerical examples, and the results show that it works effectively.

Although the technology strands have been developed separately it is necessary to consider their interaction closely. In order to check the interaction, Chapter 7 investigates the overall performance of the cooperative guidance system using scenarios and a Simulink Common Model (CM) designed and shared between the partners for algorithm test and development. The simulation results of the cooperative guidance scheme are compared to those of the conventional PN guidance (navigation gain 4) with the most common allocation policy. The mid course, target allocation, terminal homing guidance algorithms are assumed to use the target prediction and estimation data obtained from the set estimation algorithm. Since the update is relative slow and the uplink can be lost during the mid course phase, the performance of the mid course guidance integrated with the set estimation algorithm is also examined.

Chapter 8 provides a brief review of the thesis to highlight the key points and identify the remaining challenges. Then, future work to complete this research along with possible applications of the cooperative guidance scheme are discussed.

Under this research, 10 papers have been generated: 6 conference papers, 1 journal paper, and 3 papers under review

- Earliest Intercept Geometry Guidance to improve mid-course guidance in area air-defence, presented at Mediterranean Conference on Control and Automation 2009 (Shin et al., 2009);
- Cooperative Missile Guidance Strategies for Maritime Area Air Defense, presented at IFAC NecSys 2009 (Le Ménec et al., 2009);
- Cooperative Guidance, presented at MCM-ITP conference 2009;

- Cooperative Guidance for Naval Area Defence, presented at IFAC ACA 2010 (Shin et al., 2010a);
- Cooperative Mid Course Guidance for Area Air Defence, presented at AIAA GNC 2010 (Shin et al., 2010b);
- Cooperative Guidance, presented at MCM-ITP conference 2010;
- Earliest Intercept Geometry Guidance to improve mid-course guidance in area air-defence, published in Int'l J. of Aeronautical & Space Sci. in 2010 (Shin et al., 2010);
- Time-to-go Estimation using Guidance Command History, submitted to IFAC WC 2010;
- Membership set-based mid course guidance: application to manoeuvreing target interception, submitted to IFAC WC 2010;
- Cooperative Allocation and Guidance for Air Defence Application, submitted to IFAC WC 2010.

Several papers are also in preparation.

1.3 Area Air Defence Scenario and Assumption

As stated the cooperative guidance problem for area air defence is considered in this research. Figure 1.2 illustrates the description of area air defence. Key components supporting the cooperative guidance are generally developed based on this description in a 2D plane. A range of the values for key characteristics of the missile and target is not specified during developing the guidance components. However, for the numerical example of each algorithm, a specific range is considered to verify the algorithm in the context of the area air defence, as shown in Table 2.1. These values are selected using numerous open literature sources, especially using the MBDA website and Jane's (2002). In this research, the assumptions for developing a cooperative guidance scheme are:

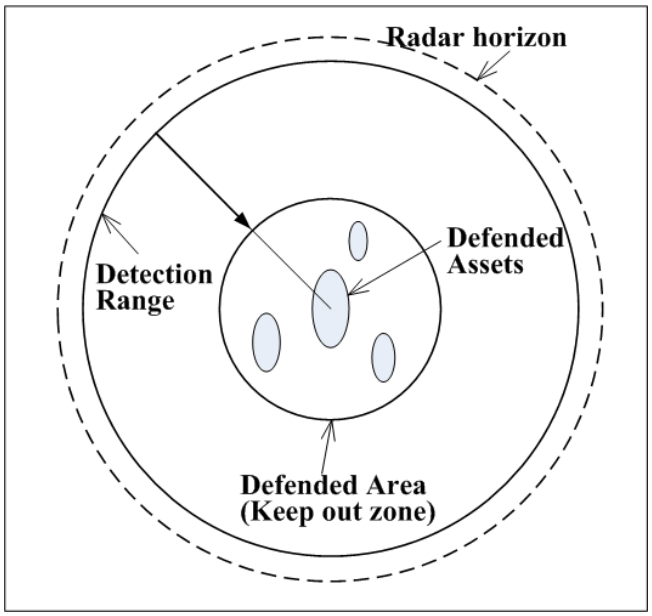

Figure 1.2: Area air defence description

- For the medium range missiles, mid course guidance and terminal homing guidance phases are considered
- During mid course, target information is uplinked from the command station (ship or ground base) and uplink rate is about 2Hz to 1Hz
- Missile equips a radar seeker of which measurement update rate is about 100 Hz
- When the missile locks on the target and can track it, guidance authority changes from a uplink driven mid course guidance law to a seeker driven guidance law (handover)
- Target velocity and position vectors can be computed or measured from the data provided by either the uplink or seeker
- Since control and command logic for the launch phase is not a scope of this research, the missile is assumed to be fired when target is within the shooting range and it can be tracked by the radar from the command station
- Speeds of the missile and target are generally assumed to be constant. However, velocity changes (Longax) are considered in the IGGL and time-to-go estimation algorithm.

Table 1.1: Range of values for key characteristics of the missile and target

Feature	Target	Missile
Velocity (m/sec)	200 to 1000+	800 to 1200+
Range (Km)	10 to 200	2 to 100
Manoeuvrability (G)	3 to 15	25 to 70
Guidance	Inertial Navigation with active or passive homing	inertial navigation with mid course guidance and active radar homing
Warhead	High explosive	High explosive

In order to investigate the overall cooperative guidance system, several scenarios for air defence in ground and naval context have been defined and shared between partners. For the purpose of comparison, the conventional PN guidance is implemented into the scenarios together with the common target allocation policy. In many-on-many engagement cases, the engagement policy is usually given as:

- Detect target;
- Form a track on the target;
- Create a firing solution;
- Launch first salvo;
- Carry out kill assessment;
- Launch second salvo

Therefore, the common policy considered for the comparison purpose is sequential: the first missile tries to intercept the target which is first assigned, the second missile the second target, and so on.

Due to classification issue[4], in this thesis, only "scenario 3" is used to demonstrate the performance of the overall system. Scenario 3 deals with ground defense

[4]Notice that the scenarios proposed in our joint work are classified as Cat A except scenarios 3

where several Fire Units (FU) are located within the defended area and protect the assets in the area. It is assumed that an aircraft launches one missile and then escapes the radar zone. The velocities of incoming threats, the aircraft and incoming missile, are also assumed be supersonic.

1.4 Previous Studies

With development of the guided weapon system over the past decades, there has been an abundance of studies and implementations covering every aspect of the guidance system such as detection, state estimation and prediction, target tracking, guidance and control laws, and dynamics and hit kill probability. Even only on the guidance law which is tackled with in this thesis, there is a wide range of material available. Therefore, our group[5] has reviewed the literature on the missile guidance system and presented an overview at IFAC ACA 2010 (White & Tsourdos, 2011).

The missile guidance laws can be classified by two primary genres. PN guidance is commonly used in current missiles and often referred to as classical guidance. The advantage, and limitation of the PN guidance and its various family have been well addressed in a number of studies (Becker, 1990; Chakravarthy & Ghose, 1996; Ghose, 1992; Guelman, 1972; Mahapatra & Shukla, 1989; Becker, 1990; Rusnak & Meir, 1990; Kim et al., 1998). Moreover, by numerous studies and practical implementations, it is shown that the guidance law has good performance against non-manoeuvring and moderately manoeuvring targets at the terminal homing phase (Zarchan, 1994; Shukla & Mahapatra, 1990; Yuan & Chern, 1992). The strength of the PN laws is their simplicity; it is possible to intercept a target by regulating the rate of the Line-of-Sight (LOS) angle. However, this simplicity could limit its capability.

Another primary genre in modern guidance is the Optimal Guidance Law (OGL). This guidance law optimizes a predetermined performance index to enhance the guidance performance. Therefore, the performance of the OGL heavily depends on the performance index; often determined as the control energy (Ryoo

[5]Autonomous systems group in Department of Informatics and Systems Engineering (DISE) at Cranfield Univerisity

et al., 2006; Cho et al., 1999; Zarchan, 1994), flight time (Imado et al., 1998), final speed (Yang, 1996; Imado et al., 1998), or combination of these cost functions Shneydor (1998). The PN guidance law can be derived from the problem of minimizing the control energy. Kreindler (1973) proved that the conventional PN guidance is an optimal solution for the non-manoeuvring target case. It is also proved by Ryoo et al. (2005) that PN with arbitrary constant gains are also the optimal solutions if appropriate time-to-go weighted functions are imposed into the cost function of the conventional linear quadratic energy optimal problem. The optimal guidance problem can also handle several constraints. For example, Ryoo et al. (2006) and Ben-Asher & Yaesh (1998) proposed the optimal guidance laws with the terminal impact angle constraint, Jeon et al. (2006) also solved the optimal guidance problem with the flight time constraint and Lee et al. (2007) proposed the optimal guidance laws called the Impact Angle and Time Guidance (IATG). Since these optimal guidance laws satisfy the zero miss distance and control the engagement geometry, they might be able to improve the hit kill probability or the survivability.

Several approaches have been proposed to solve the optimal mid course guidance problem. Song and Tahk have addressed artificial neural networks for the mid course guidance algorithms to generate suboptimal guidance commands in a feedback fashion (Song & Tahk, 1998, 1999, 2001). Whilst this approach can overcome the difficulty in deriving an on-board optimal guidance law, it is difficult to cover all the region of the input vector for neural network training and the stability cannot be guaranteed. To find a real time sub-optimal guidance algorithm, Singular Perturbation Technology(SPT) (Cheng & Gupta, 1986; Dougherty & Speyer, 1997; Menon & Briggs, 1990) and Linear Quadratic Regulator (LQR) (Imado et al., 1990; Imado & Kuroda, 2009) have been proposed. However, a guidance law based on SPT does not result in a true feedback control and the LQR type guidance algorithm needs a large set of database.

One of the characteristics of the optimal guidance laws is that they generally require accurate time-to-go estimation. In fact, precise time-to-go estimations play important roles in ensuring good performance of the optimal guidance laws. The time-to-go estimation algorithms can be classified into two categories. In the first category, the time-to-go computation formulae are derived from optimal guidance problems with free terminal time. Although a set of time-to-go equations

is a part of the optimal solution, this defies simple solutions. As shown in the recent papers (Glizer, 1996; Yang & Yang, 1997), the optimal time-to-go estimation equations are highly nonlinear and complicated. The time-to-go algorithm in the second category tries to provide the best time-to-go estimation possible for a given guidance law. A recursive time-to-go calculation is proposed by Tahk et al. (2002). This method first calculates the minimum time-to-go and then recursively compensates the time-to-go error resulting from the path curvature. Since this time-to-go estimation algorithm is originally devised for the missile having a velocity profile, it works effectively to various types of guidance laws for both varying and constant velocity missiles. However, the main error source considered here for the compensation of the time-to-go error is the initial heading angle error, not the terminal impact angle constraint. Ryoo et al. (2005) suggested time-to-go calculation method efficient for the impact angle control guidance laws. Although this method works fine, it considered only the case of stationary target. Moreover, the time-to-go estimation error of this method is increasing as the desired impact angle constraint is getting bigger.

There are several other guidance technologies, such as Differential Game Theory (DGT) and nonlinear control theory. From the literature review on guidance using the DGT mostly proposed by Shinar (Shinar et al., 1988; Shinar & Shima, 1996; Shinar, 2001; Shinar & Turetsky, 2002), it is clear that:

> *"... key innovative idea is not to engage the current trajectory, but to employ the worst case evasive trajectory to predict a suitable engagement strategy (Shinar et al., 1989)."*

This approach can address the reachability problem with the uncertainty problem of the target manoeuvre (Isaacs, 1665). Since the manoeuvre of target is likely programmed not only to improve survivability against the incoming missile, but also to guarantee the interception of an asset in the defended area, it would require some modification to be used in area air defence problem.

In order to design a cooperative guidance scheme, we freely borrow the key principles of the cooperative missile guidance problem from the literature. As stated, the intercept geometries were used to develop two mid course guidance algorithms. The first paper of a new guidance concept using the Earliest Intercept Line (EIL), called Earliest Intercept Line Guidance (EILG), was proposed by our

group in 2005 Robb et al. (2005). Since then, several papers were presented at some conferences (Robb et al., 2005, 2006). As has been mentioned in these papers, the key challenge to develop a capable guidance system using this concept was:

> *"Unlike common guidance genres, the EIL was a tool without closed form and not formulatic,"*

thus, it was employed classical game theory to derive the guidance command. This concept was named as the Earliest Intercept Line Guidance (EIGL). However, for the implementation, there were a couple of issues to be resolved such as high computational load and difficulty dealing with physical constraints. Theses issues are addressed in this thesis.

Chapter 2

Mid Course Guidance I: EIGGL

Over the past decades, not only a wide range of missile guidance algorithms have been developed, but also they have been successfully implemented into real systems. Despite the recent developments on missile guidance algorithms, research on area air defence is still an open and active research topic. Primary objective of the guidance laws is to strike threats in order to protect an area in which the defended assets are placed. For example, two primary tasks of the missiles in naval defence are protections of sea traffic or convoys, and coast line against incoming threats. In the area air defence problem, there exist various types of air threat from the sea skimmer to the high diving missile in addition to attacking aircraft and weapon carrying Unmanned Aerial Vehicles (UAVs). For ground stations to continue their primary role, it is essential that air defence for a single unit, a close escort or a major surface group provides a comprehensive defence against all types of these threats (Robb et al., 2005, 2006).

In order to directly consider area air defence in the mid course missile guidance problem, we investigate an Earliest Intercept Geometry Guidance Law (EIGGL) with the concept of the Differential Geometry Guidance Law (DGGL). The key idea of the mid course guidance based on the EIGGL and DGGL concepts is shown in Figure 2.1. The Earliest Intercept Geometry (EIG) is the contour of the earliest intercept points along with all possible heading angles of the target, i.e. the largest boundary where the target can travel. Therefore, it is the capture zone. In area air defence, missiles must destroy the incoming target threat before it reaches any protected assets. Therefore, a mid course algorithm should hold the target inside this capture region, guaranteeing that all assets remain outside the capture zone. However, in some circumstances, defend assets could be located in or near the capture zone. If the mid course guidance could control the intercept geometry, it might be able to push the EIG away from the assets inside the capture zone. Figure 2.2 shows this concept.

In this chapter, the EIG is analytically derived under the assumption that the missile changes its heading angle instantaneously. In practice, the missile takes a minimum of $\theta V/a_{max}$ secs to achieve a flight path angle change of θ when flying at

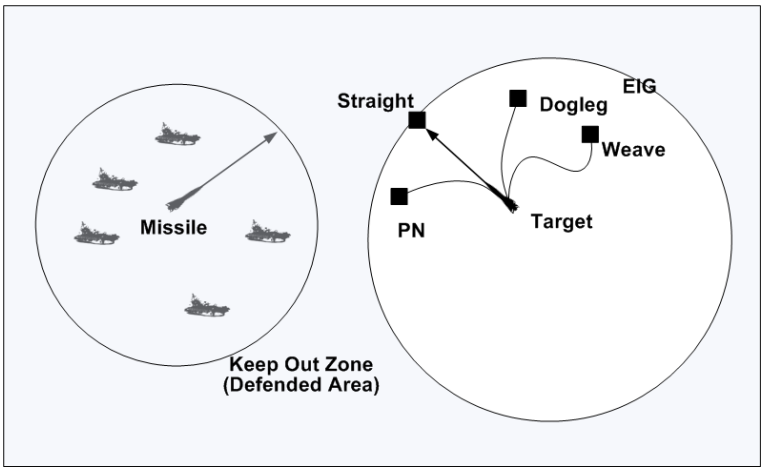

Figure 2.1: Concept of the mid course guidance using EIGGL

Vm/s with maximum acceleration bound of a_{max}. The assumption of zero time is reasonable only if time-to-go is much bigger than this turn time. This issue issue will be discussed in 7.2. We also address how to control the intercept geometry and a guidance strategy using the EIG control.

2.1 Earliest Intercept Geometry

In engagement scenarios, a target tries to reach a defended asset before the defending missile intercepts the target. It is obvious the distance between the initial target point and an intercept point is longest when the path of the target is straight, as shown in Figure 2.1. Since the EIG considers the capture zone in worst case in terms of the distance, we only consider the non-manoeuvring target in this section.

2.1.1 Earliest Intercept Point

In order to derive EIG we need first to consider the intercept geometry, that is the collision geometry. The collision geometry of homing guidance for a non-manoeuvring target and missile is shown in figure 2.3. It shows the direct intercept case, where both the target and the missile respectively are flying in straight lines at constant velocities v_T and v_M. Their trajectories are assumed to meet at a point **I**, called intercept point. The target and missile together with the intercept point

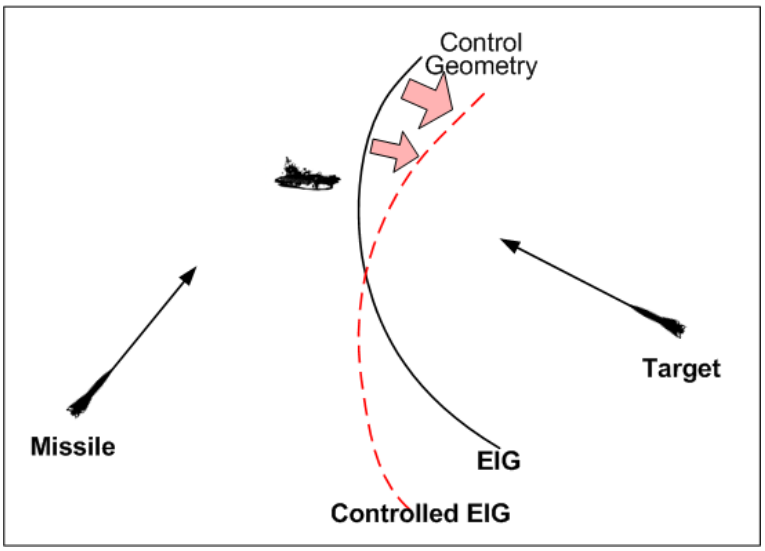

Figure 2.2: EIG control

form a triangle, which will be called the intercept triangle or perfect collision triangle. In order to establish the matching condition for intercept, consider a time T such that the target has traveled in a straight line and at constant velocity from its initial position to the intercept point as shown in in Figure 2.3. The length of this trajectory s_T will be:

$$s_T = v_T T. \tag{2.1}$$

In order for the missile to intercept the target, it must travel a distance s_M in the same time T. i.e.,

$$s_M = v_M T. \tag{2.2}$$

The ratio of the trajectory lengths is then given by:

$$\gamma \equiv \frac{s_M}{s_T} = \frac{v_M}{v_T}. \tag{2.3}$$

Equation (2.3) shows that the missile must manoeuvre until the trajectory lengths of the intercept triangle are in the same ratio as the target and missile velocities to impact on a non-manoeuvring target. Since the target velocity and heading are either unknown or estimated, there must be an active control system to acquire and maintain this intercept geometry. As shown in Figure 2.3, the intercept triangle does not change shape, but shrinks as the missile and target move along their respective straight line trajectories. If the missile is on the perfect collision course

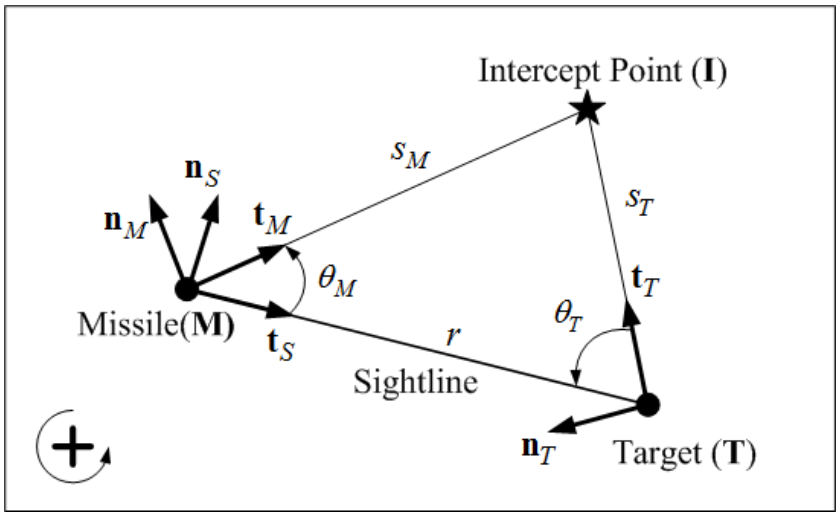

Figure 2.3: Direct intercept geometry

(intercept geometry), the missile-to-sightline angle θ_M and the target-to-sightline angle θ_T remain constant over the whole engagement. From the intercept triangle in Figure 2.3 and matching condition in Equation (2.3), we have

$$s_M \boldsymbol{t}_M = r\boldsymbol{t}_S + s_T \boldsymbol{t}_T, \tag{2.4}$$

and

$$\begin{aligned} \gamma s_T \boldsymbol{t}_M &= r\boldsymbol{t}_S + s_T \boldsymbol{t}_T \\ \boldsymbol{t}_M &= \frac{1}{\gamma}\left[\frac{r}{s_T}\boldsymbol{t}_S + \boldsymbol{t}_T\right] \end{aligned} \tag{2.5}$$

Equation (2.5) is in a non-dimensional form and will thus represent the solution for all ranges r between the missile and the target. Given the geometry of the target basis vector $\boldsymbol{t}_T$ and the sightline basis vector $\boldsymbol{t}_S$, the direction of the missile basis vector $\boldsymbol{t}_M$ is fixed. Thus, if we derive the angle between sightline and missile basis vector θ_M, it is possible to obtain the intercept solution tangent $\boldsymbol{t}_M$. The angle θ_M can be obtained by applying the sine rule to intercept triangle which gives

$$\sin\theta_M = \frac{\sin\theta_T}{\gamma} \tag{2.6}$$

There are two solutions for the angle θ_M, which satisfy Equation (2.6): one is an acute angle and the other an obtuse angle. Thus, we have to determine which

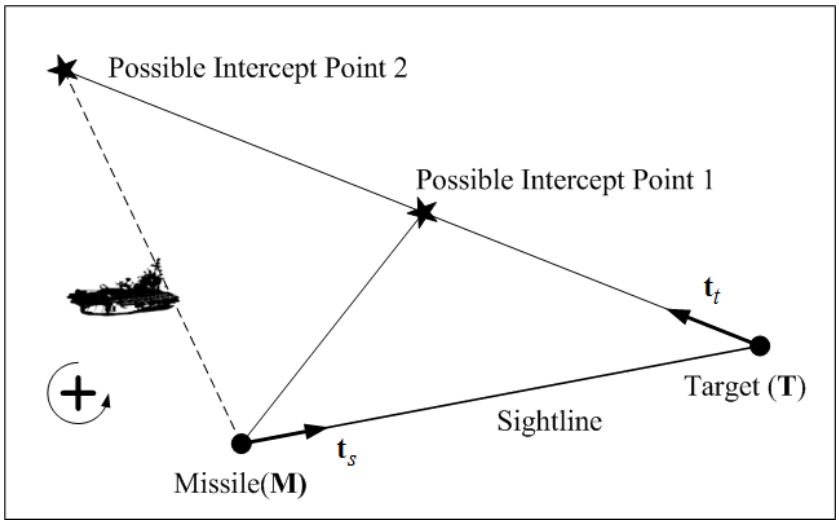

Figure 2.4: Two possible intercept geometries for $\gamma < 1$

angle is real solution. Implementing cosine rule to the intercept triangle, we have:

$$\begin{aligned} \frac{1}{\gamma^2} + \frac{1}{\gamma^2}\left(\frac{r}{s_T}\right)^2 - 2\frac{1}{\gamma^2}\frac{r}{s_T}\cos\theta_T &= 1 \\ \left(\frac{r}{s_T}\right)^2 - 2\cos\theta_T\frac{r}{s_T} - (\gamma^2 - 1) &= 0 \end{aligned} \tag{2.7}$$

This quadratic in (r/s_T) can be factorised, to give:

$$\frac{r}{s_T} = \cos\theta_T \pm \sqrt{\cos^2\theta_T + \gamma^2 - 1} \tag{2.8}$$

If $\gamma \geq 1$, only positive sign is valid in Equation (2.8). Figure 2.4 shows two possible solutions for $\gamma < 1$. Since we consider the EIG, only the earlier intercept geometry is taken into account. Thus, the solution in this study is an acute angle and the matching condition is given by

$$\begin{aligned} \frac{r}{s_T} &= \cos\theta_T + \gamma\cos\theta_M \\ \cos\theta_M &= \frac{\sqrt{\gamma^2 - \sin^2\theta_T}}{\gamma}. \end{aligned} \tag{2.9}$$

The intercept geometry of a manoeuvring missile with a constant lateral acceleration is illustrated in figure 2.5. Following the same procedure as the zero intercept case, the intercept triangle is determined by the target tangent vector $\boldsymbol{t}_T$

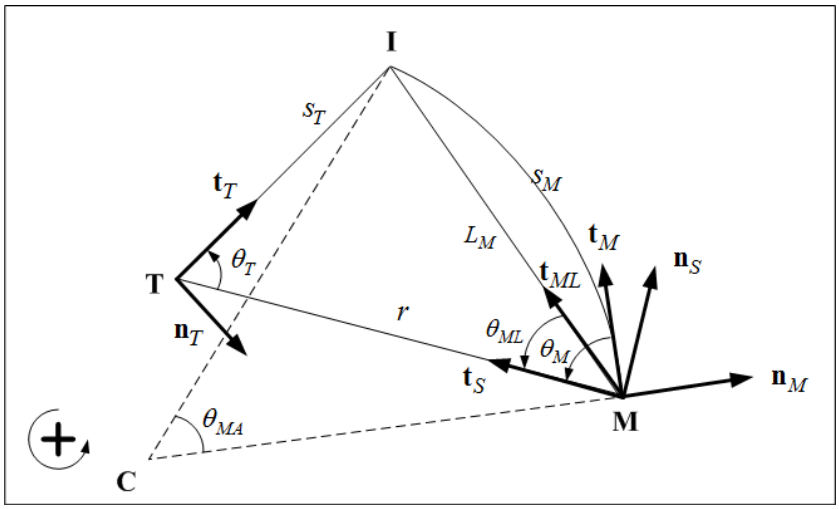

Figure 2.5: Intercept geometry for a manoeuvring missile

and the missile arc chord defined by the vector $\boldsymbol{t}_{ML}$ as shown in figure 2.5. From the figure the intercept condition can be represented by a vector sum of the form

$$L_M \boldsymbol{t}_{ML} = r\boldsymbol{t}_S + s_T \boldsymbol{t}_T, \tag{2.10}$$

where the arc chord basis vector $\boldsymbol{t}_{ML}$ can be obtained from the target basis vector by a rotation through $\theta_{MA}/2$. The arc length is obtained as

$$s_M = \frac{\theta_{MA}}{\kappa_M}, \tag{2.11}$$

where κ_M denotes the curvature of the missile trajectory. Then, the chord length L_M is obtained as

$$L_M = \frac{\sin(\theta_{MA}/2)}{\kappa_M/2} = \frac{\sin(\theta_{MA}/2)}{\theta_{MA}/2} s_M = \gamma\beta s_T, \tag{2.12}$$

where

$$\beta = \frac{\sin(\theta_{MA}/2)}{\theta_{MA}/2}. \tag{2.13}$$

From Equation (2.12) and simple algebra, Equation (2.10) is rewritten as

$$\boldsymbol{t}_{ML} = \frac{1}{\gamma\beta}\left[\frac{r}{s_T}\boldsymbol{t}_S + \boldsymbol{t}_T\right]. \tag{2.14}$$

This matching condition can be solved by applying the sine rule to the intercept triangle:

$$\sin\theta_{ML} = \frac{\sin\theta_T}{\gamma\beta}. \tag{2.15}$$

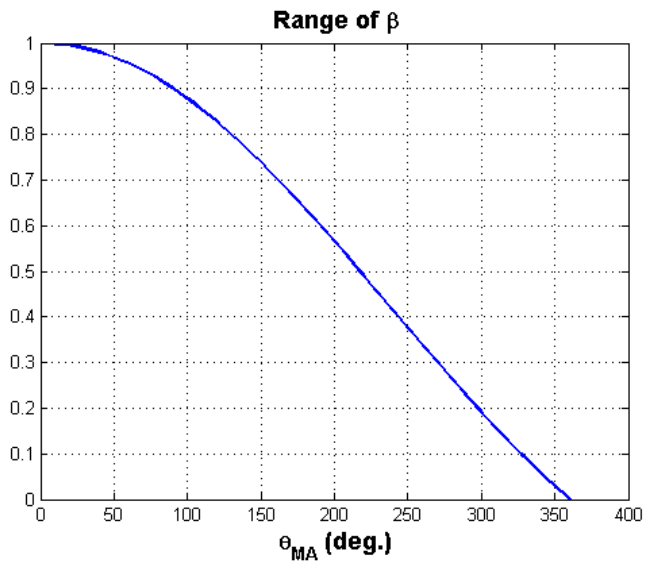

Figure 2.6: Range of β

Due to unknown parameter β, which is causing nonlinearity, Equation (2.15) with Equation (2.13) can be solved by implementing numerical methods. However, since trajectory shaping gives one more degree-of-freedom to the intercept guidance problem, we can control endgame geometry by adjusting the curvature.

For the manoeuvring missile with a constant lateral acceleration, it is possible to control the intercept point by setting appropriate value for β as shown in Equation (2.15). Note that β controls the curvature of the missile trajectory. Figure 2.6 represents β values for $2\pi \geq \theta_{MA} \geq 0$. Hence, the boundary of β is given by

$$0 \leq \beta \leq 1. \tag{2.16}$$

A matching condition derived by the cosine rule to the intercept triangle is given by

$$1 = \frac{1}{\gamma^2\beta^2} + \frac{1}{\gamma^2\beta^2}\left(\frac{r}{s_T}\right)^2 - 2\frac{1}{\gamma^2\beta^2}\frac{r}{s_T}\cos\theta_T. \tag{2.17}$$

Here, β can be rewritten as

$$\beta = \frac{1}{\gamma}\sqrt{\frac{s_T^2 + r^2 - 2rs_T\cos\theta_T}{s_T^2}}. \tag{2.18}$$

From Equation (2.17), (2.16) and Figure 2.6, it is clear:

$${s_T}^2\sin^2\theta_T \leq s_T^2 + r^2 - 2rs_T\cos\theta_T \leq \gamma^2 s_T^2. \tag{2.19}$$

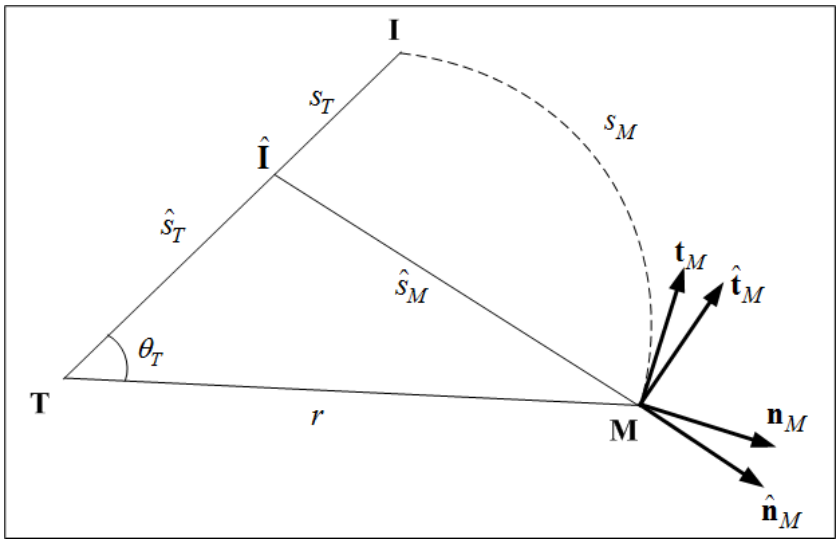

Figure 2.7: Guidance geometries comparison

Left inequality in Equation (2.19) is always satisfied:

$$\begin{aligned} 0 &\leq s_T^2(1-\sin^2\theta_T) + r^2 - 2rs_T\cos\theta_T = s_T^2\cos^2\theta_T - 2rs_T\cos\theta_T \\ &\leq (s_T\cos\theta_T - r)^2 \end{aligned} \tag{2.20}$$

To find the boundary of the intercept points, let us consider the direct intercept. In this figure, superior, ˆ, represents the value for the direct intercept solution.

From the right inequality in Equation (2.19), we have:

$$\hat{s}_M^2 = (\gamma\hat{s}_T)^2 = \hat{s}_T^2 + r^2 - 2\hat{s}_T r\cos\theta_T \tag{2.21}$$

$$s_M = \gamma s_T = \gamma(\hat{s}_T + a) \tag{2.22}$$

$$L_M^2 = (\hat{s}_T + a)^2 + r^2 - 2(\hat{s}_T + a)r\cos\theta_T \tag{2.23}$$

and

$$\begin{aligned} s_M^2 - L_M^2 =& \gamma^2(\hat{s}_T + a)^2 - (\hat{s}_T + a)^2 - r^2 + 2(\hat{s}_T + a)r\cos\theta_T \\ =& (\gamma^2 - 1)(\hat{s}_T + a)^2 - r^2 + 2\hat{s}_T r\cos\theta_T + 2ar\cos\theta_T \\ =& (\gamma^2 - 1)(\hat{s}_T + a)^2 - \hat{s}_M^2 + \hat{s}_T^2 \\ &+ 2a\hat{s}_T\left[\cos^2\theta_T + \sqrt{\cos^2(\theta_T)\left(\gamma^2 - \sin^2\theta_T\right)}\right] \\ =& \left(\gamma^2 - 1\right)\left(2a\hat{s}_T + a^2\right) + 2a\eta\hat{s}_T \end{aligned} \tag{2.24}$$

where:

$$r/\hat{s}_T = \cos(\theta_T) + \sqrt{\gamma^2 - \sin^2\theta_T} \tag{2.25}$$

$$\eta = \cos^2(\theta_T) + \sqrt{\left(\gamma^2 - \sin^2\theta_T\right)\cos^2\theta_T} > 0 \tag{2.26}$$

Therefore

$$\begin{cases} s_M < L_M & for \ -s_T \leq a < 0 \\ s_M \geq L_M & for \quad a \geq 0 \end{cases} \tag{2.27}$$

Thus, the boundary of possible intercept points is derived as:

$$\hat{s}_T \leq s_T \tag{2.28}$$

This means the intercept point of the missile with a straight line (non-manoeuvring) is earliest interception point.

2.1.2 Intercept Geometry

Since a heading angle of the target can change and its acceleration is hard to be predicted, the intercept geometry is not determined. However, it is possible to derive the locus of possible intercept triangles, i.e. the intercept geometry, by considering all viable heading of the target. As has been stated, the locus of the EIP for all heading angles of the target is the worst intercept geometry, that is the EIG.

The conditions for the EIG can be examined by exploring the geometry in Figure 2.8 The geometry is drawn using the sightline axes centred in the missile, thus x is along the sightline and y is normal to the sightline. As the target angle to the sight line θ_T varies, the intercept point **I** will change. The locus of the intercept points can be determined by using Pythagoras on two triangles. The first is (**M I N**), made up of the missile position **M**, the intercept point **I** and the intercept of the normal from the intercept point onto the sightline **N**. The second is triangle (**T I N**), replacing the missile position with the target position **T**. Hence:

$$s_M^2 = x^2 + y^2, \tag{2.29}$$

$$s_T^2 = (r - x)^2 + y^2. \tag{2.30}$$

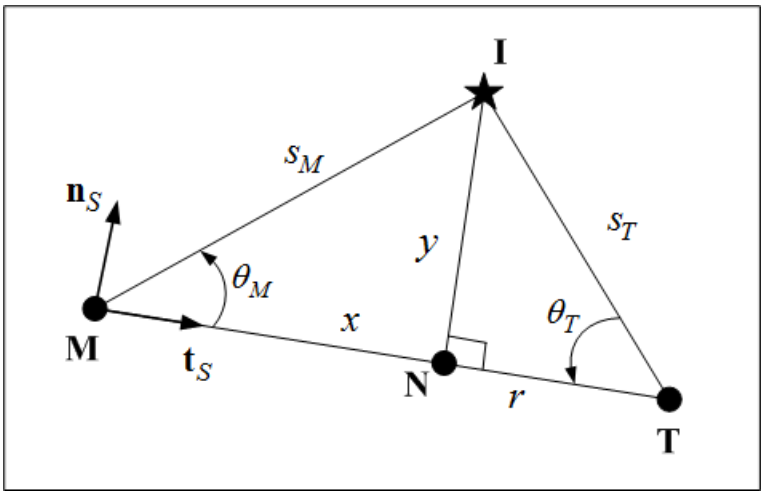

Figure 2.8: Intercept Triangle

From the definition of the velocity ratio γ, we have

$$s_M^2 = \gamma^2 s_T^2. \tag{2.31}$$

Substituting Equation (2.29) and (2.30) into this equation yields

$$x^2 + y^2 = \gamma^2 \left\{(r - x)^2 + y^2\right\} \tag{2.32}$$

Hence, we have

$$(x - r_l)^2 + y^2 = c_l^2 \tag{2.33}$$

where

$$r_l = \frac{\gamma^2 r}{\left|\gamma^2 - 1\right|}, \quad c_l = \frac{\gamma r}{\left|\gamma^2 - 1\right|}. \tag{2.34}$$

This equation represents the locus of the all EIPs, i.e. the EIG, and can be used to asses the guidance strategy. All possible EIGs are shown in Figures 2.9 – 2.11.

The speed ratio is an important parameter to determine the EIG. As shown in equation (2.34), since subtracting the radius from the distance between the centre and the target is as follows

$$(c_l - r) - r_l = -\frac{\gamma + 1}{\gamma^2 - 1} r < 0 \qquad \text{for } \gamma > 1 \tag{2.35}$$

the circle encloses the target as shown in Figure 2.9. However, for $\gamma < 1$, there is

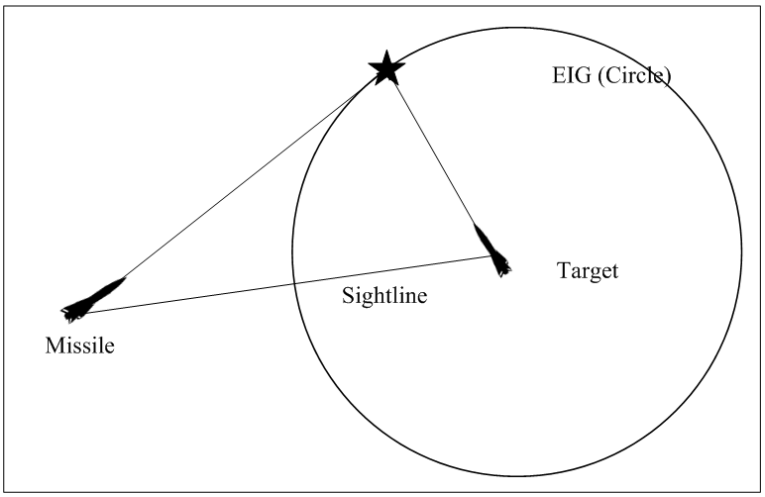

Figure 2.9: Locus of the impact triangles (EIG) for $\gamma > 1$

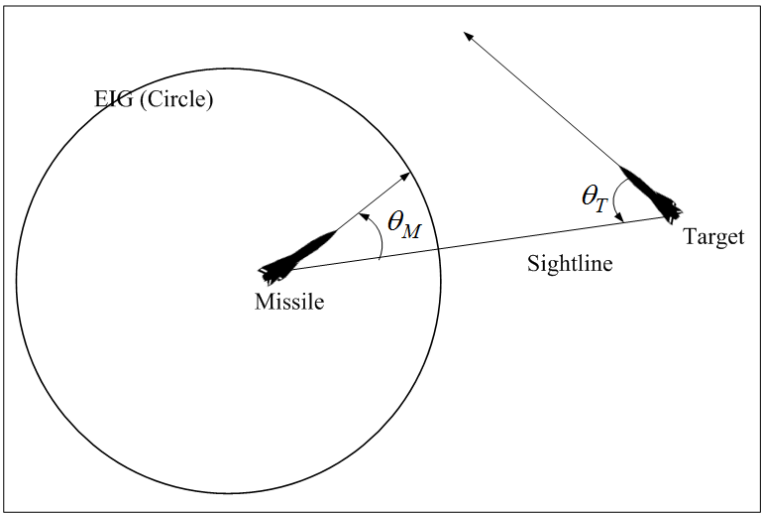

Figure 2.10: Locus of the impact triangles (EIG) for $\gamma < 1$

the range of θ_T for which:

$$\gamma^2 - \sin^2(\theta_T) < 0 \qquad \text{for } \gamma < 1 \tag{2.36}$$

which implies that r/s_T in the matching condition Equation (2.9) can an imaginary value in some engagement condition, i.e. missile is not able to intercept the target as shown in Figure 2.10. The EIG for $\gamma < 1$ can be used to determine when another missile should be launched. If the missile and target speeds are same, γ is equal to unity and the intercept geometry is no longer a circle. The matching condition

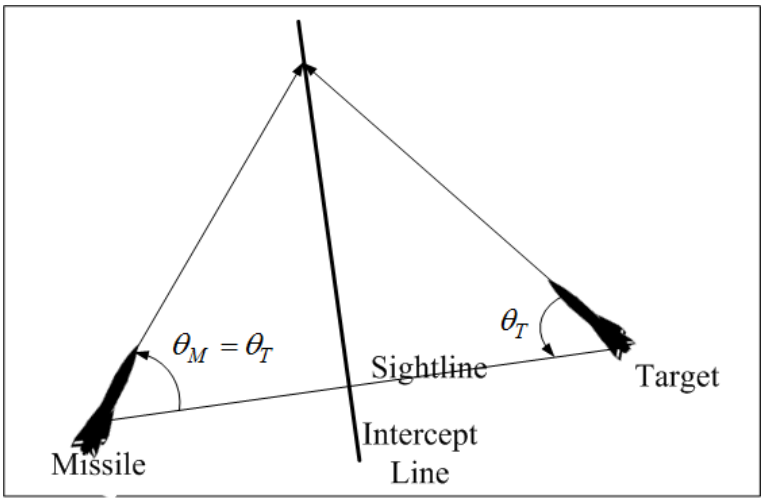

Figure 2.11: Locus of the impact triangles (EIG) for $\gamma = 1$

for this case becomes:

$$\frac{r}{s_T} = \cos(\theta_T) \pm \cos(\theta_T) \tag{2.37}$$

There are now two real solutions given by:

$$\frac{r}{s_T} = 2\cos(\theta_T) \quad \text{or} \quad 0 \tag{2.38}$$

The first solution implies a geometry which gives rise to an isosceles triangle solution as before, for s_T equal to s_m. For the second solution, $s_T = \infty$ and $s_m = \infty$. In this case, the missile can not intercept the target and protect the defended objects. Therefore, only the first solution is valid. Substituting $\gamma = 1$ into Equation (2.32) yields

$$x = \frac{r}{2} \tag{2.39}$$

Note that this means, for $\gamma = 1$, the intercept geometry is a line as shown in Figure 2.11.

For simplicity, we considered the case of that $\gamma > 1$ in this study. However, this is not the restriction of the application of this approach. The same concepts and methodologies of the proposed cooperative guidance algorithms can be extended for $\gamma \leq 1$

2.2 Guidance Strategy

2.2.1 Geometry Control

Let us first analytically derive the EIG change to establish a mid course guidance strategy. The intercept point **I** is stationary for the missile and target velocity vectors lying along the impact triangle sides. In order to see this, consider the velocity of the impact point v_{EIP} in the inertial reference frame. The position vector of the intercept point **I** can be represented with respect to the target position **T**

$$\boldsymbol{r}_{EIP} = \boldsymbol{r}_T + s_T \boldsymbol{t}_T, \tag{2.40}$$

where $\boldsymbol{r}_{EIP}$ and $\boldsymbol{r}_T$ are the position vectors of the intercept point and the target. From the first time derivative of the position vector $\boldsymbol{r}_{EIP}$, we have

$$\begin{aligned} \boldsymbol{v}_{EIP} &= \boldsymbol{v}_T + \dot{s}_T \boldsymbol{t}_T + s_T \dot{\boldsymbol{t}}_T \\ &= v_T \boldsymbol{t}_T + \dot{s}_T \boldsymbol{t}_T - s_T \dot{\psi}_T \boldsymbol{n}_T, \end{aligned} \tag{2.41}$$

where ψ_T is the heading angle of the target in the inertial reference frame. From the matching condition, the relative distance r is obtained as

$$r = \left(\cos\theta_T + \sqrt{\gamma^2 - \sin^2\theta_T} \right) s_T. \tag{2.42}$$

Differentiating this equation with respect to time gives

$$\dot{r} = \left(\cos\theta_T + \sqrt{\gamma^2 - \sin^2\theta_T} \right) \dot{s}_T - \left(\sin\theta_T + \frac{\sin\theta_T \cos\theta_T}{\sqrt{\gamma^2 - sin^2\theta_T}} \right) \dot{\theta}_T s_T. \tag{2.43}$$

$\dot{s}_T$ is derived as:

$$\dot{s}_t = \frac{1}{\cos\theta_T + \sqrt{\gamma^2 - \sin^2\theta_T}} \dot{r} + \frac{\sin\theta_T}{\sqrt{\gamma^2 - \sin^2\theta_T}} s_T \dot{\theta}_T \tag{2.44}$$

Figure 2.12 shows a guidance geometry of an engagement scenario in which the missile heading angle is either the same as or intentionally different from the desired angle for the interception. From the geometry, the first time derivative of the range is obtained as:

$$\dot{r} = -\left(v_M \cos\theta_M + v_T \cos\theta_T \right) = -\left(\gamma \cos\theta_M + \cos\theta_T \right) v_T, \tag{2.45}$$

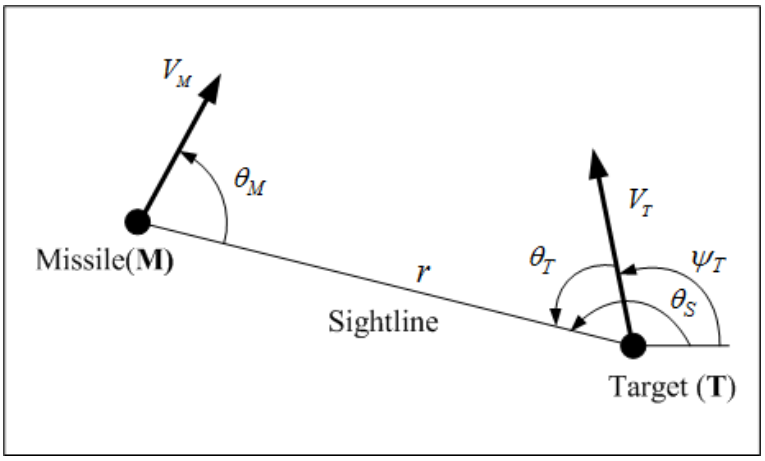

Figure 2.12: Sightline geometry

and the rate of sightline angle is given by

$$\dot{\theta}_S = -\frac{v_M \sin\theta_M - v_T \sin\theta_T}{r} = -\frac{\gamma \sin\theta_M - \sin\theta_T}{r} v_T. \tag{2.46}$$

where θ_M represent the real heading angle of the missile relative to the current target sightline and it could be different from the desired angle. Substituting Equation (2.45) into Equation (2.44) yields

$$\dot{s}_T = -\frac{\gamma \cos\theta_M + \cos\theta_T}{\cos\theta_T + \sqrt{\gamma^2 - \sin^2\theta_T}} v_T + \frac{\sin\theta_T}{\sqrt{\gamma^2 - \sin^2\theta_T}} s_T \dot{\theta}_T \tag{2.47}$$

Since θ_M^* denotes the desired heading angle for the earliest intercept and it is given by

$$\theta_M^* = \sqrt{\gamma^2 - \sin^2\theta_T}, \tag{2.48}$$

substituting this equation into equation (2.41) gives the velocity of the intercept point of the form:

$$\begin{aligned}
\boldsymbol{v}_{EIP} &= \left(1 - \frac{\gamma\cos\theta_M + \cos\theta_T}{\cos\theta_T + \sqrt{\gamma^2 - \sin^2\theta_T}}\right) v_T \boldsymbol{t}_T \\
&\quad + \frac{\sin\theta_T}{\sqrt{\gamma^2 - \sin^2\theta_T}} s_T \dot{\theta}_T \boldsymbol{t}_T - s_T \dot{\psi}_T \boldsymbol{n}_T, \\
&= \frac{\cos\theta_M^* - \cos\theta_M}{\cos\theta_T + \sqrt{\gamma^2 - \sin^2\theta_T}} \gamma v_T \boldsymbol{t}_T \\
&\quad + \frac{\sin\theta_T}{\sqrt{\gamma^2 - \sin^2\theta_T}} s_T \dot{\theta}_T \boldsymbol{t}_T - s_T \dot{\psi}_T \boldsymbol{n}_T
\end{aligned} \tag{2.49}$$

The EIG is the contour of EIPs, so that Equation (2.49) implies that the intercept geometry can be controlled.

For the analysis of the EIG change, let us first assume that the missile can change its heading angle instantaneously and heads for the EIP:

$$\theta_M = \theta_M^*. \tag{2.50}$$

The time derivative of the angle θ_T is obtained as

$$\dot{\theta}_T = \dot{\theta}_S - \dot{\psi}_T. \tag{2.51}$$

Substituting these two equations and into Equation (2.49) yields

$$\boldsymbol{v}_{EIP} = \frac{\sin\theta_T}{\sqrt{\gamma^2 - \sin^2\theta_T}} s_T (\dot{\theta}_S - \dot{\psi}_T) \boldsymbol{t}_T - s_T \dot{\psi}_T \boldsymbol{n}_T. \tag{2.52}$$

From the intercept matching condition, we have

$$\gamma \sin\theta_M - \sin\theta_T = 0, \tag{2.53}$$

and substituting this equation into Equation (2.47) yields $\theta_S = 0$. Hence, the intercept point velocity becomes

$$\begin{aligned}
\boldsymbol{v}_{EIP} &= -\frac{\sin\theta_T}{\sqrt{\gamma^2 - \sin^2\theta_T}} s_T \dot{\psi}_T \boldsymbol{t}_T - s_T \dot{\psi}_T \boldsymbol{n}_T \\
&= -(\sin\theta_T \boldsymbol{t}_T + \cos\theta_T \boldsymbol{n}_T) \frac{s_T}{\sqrt{\gamma^2 - \sin^2\theta_T}} \dot{\psi}_T.
\end{aligned} \tag{2.54}$$

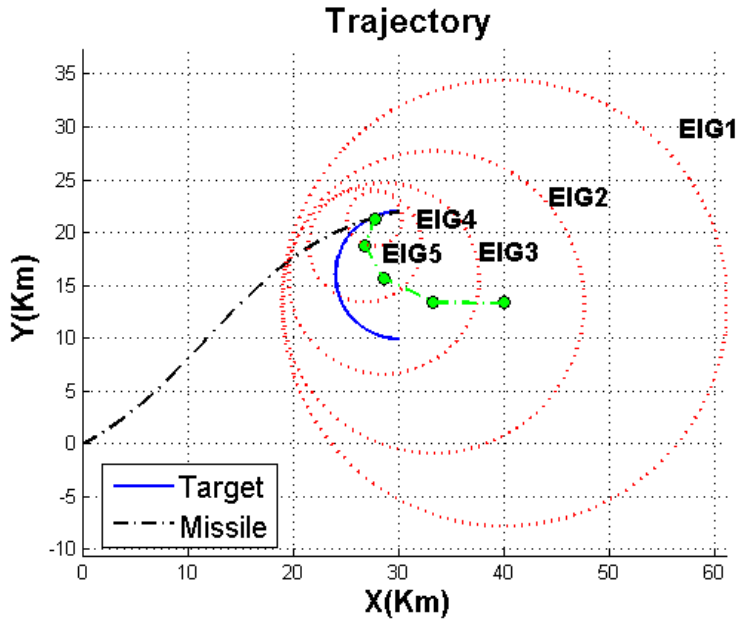

Figure 2.13: EIG change for the direct intercept when a target is manoeuvring (γ = 2)

Table 2.1: Initial conditions of the EIGGL simulation

	Target	Missile
Position(Km,Km)	(30, 10)	(0, 0)
Velocity(m/s)	300	600
Heading angle(deg)	180	0

Note that the velocity of the intercept point is tangent to the EIG, because the intercept position r_{EIP} is given by

$$r_{EIP} = \frac{s_T}{\sqrt{\gamma^2 - \sin^2\theta_T}}, \tag{2.55}$$

and the tangent vector at the intercept point, $\boldsymbol{t}$, can be represented as

$$\boldsymbol{t} = -\left(\sin\theta_T \boldsymbol{t}_T + \cos\theta_T \boldsymbol{n}_T\right), \tag{2.56}$$

In this case, as the missile homes to the EIP, the EIG not only shrinks, but also moves tangent to the current EIG. Figure 2.13 depicts the EIG change of the direct intercept, when the missile is manoeuvring with a constant lateral acceleration $15m/s^2$. Initial conditions of the missile and target are given in Table 2.1. As has been stated, the missile intercepts the target in the capture zone. If the target is

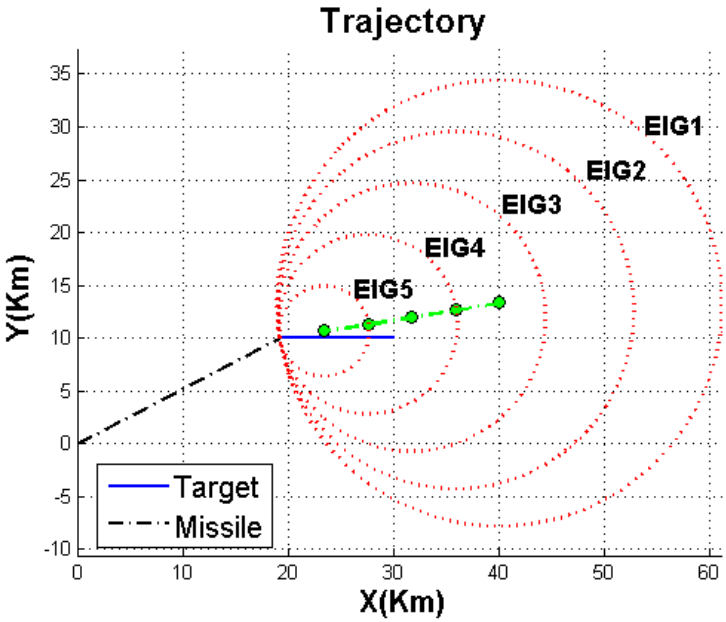

Figure 2.14: EIG change for the direct intercept when a target is flying in a straight line ($\gamma = 2$)

flying in a straight line, i.e. the rate of its heading angle is zero, then the intercept point is stationary in space

$$v_{EIP} = 0. \tag{2.57}$$

This implies that the size of the EIG decreases, whilst its shape and the intercept point are fixed. The EIG change in this case is illustrated in Figure 2.14. As shown in the figure, if the target is directly heading to a defended asset, the best guidance strategy is to guide the missile to the EIP with the straight line.

Now, consider the EIG change when the missile intentionally flies with a heading angle θ_M different from the desired angle θ_M^* on the purpose of controlling the intercept geometry. The velocity of the EIP is derived in Equation (2.49). The worst scenario for the missile is that the target directly heads for a defended asset as shown in figure 2.18. In this scenario, the heading angle of the target is locked on its target and its rate is zero:

$$\dot{\psi}_T = 0. \tag{2.58}$$

Furthermore, the rate of the target-to-sightline angle is given by

$$\dot{\theta}_T = \dot{\theta}_S. \tag{2.59}$$

Substituting these two equations and equation (2.46) into equation (2.49) yields

$$\boldsymbol{v}_{EIP} = \frac{s_T}{r}\gamma v_T \left(\cos\theta_M^* - \cos\theta_M - \frac{\sin\theta_M - \sin\theta_M^*}{\sqrt{\gamma^2 - \sin^2\theta_T}} \sin\theta_T \right) \boldsymbol{t}_T. \tag{2.60}$$

Now, let us define θ_M as

$$\theta_M \equiv \theta_M^* + \alpha \tag{2.61}$$

Then, the velocity of the intercept point can be rewritten as

$$\begin{aligned} \boldsymbol{v}_{EIP} &= \left\{ \left(1 - \cos\alpha - \frac{\sin\alpha \sin\theta_T}{\gamma \cos\theta_M^*} \right) \cos\theta_M^* \right. \\ &\quad \left. + \left(\sin\alpha + \frac{1 - \cos\alpha}{\gamma \cos\theta_M^*} \sin\theta_T \right) \sin\theta_M^* \right\} \frac{s_T}{r}\gamma v_T \boldsymbol{t}_T \end{aligned} \tag{2.62}$$

From the following relationship

$$\sin\theta_T = \gamma \sin\theta_M^* \tag{2.63}$$

we have

$$\boldsymbol{v}_{EIP} = \frac{1 - \cos\alpha}{\cos\theta_M^*} \frac{s_T}{r} \gamma v_T \boldsymbol{t}_T \tag{2.64}$$

Since s_T/r, γ, and v_T are always positive values and it is clear that

$$\frac{1 - \cos\alpha}{\cos\theta_M^*} \geq 0, \tag{2.65}$$

the velocity vector of the intercept point is positive a scaled vector of the target velocity vector. This finding is intuitive since EIP is defined for as straight-flying target assumption, so if the missile deliberately delays intercept then target moves a little further along the current heading before the interception. Figure 2.15 and 2.16 show the EIG change if the missile flies not to the intercept point on a purpose.

2.2.2 Guidance Policy

As shown in Figure 2.1, if all defended assets are outside the capture zone defined by the EIG, the missile directly heading to the intercept point can intercept the

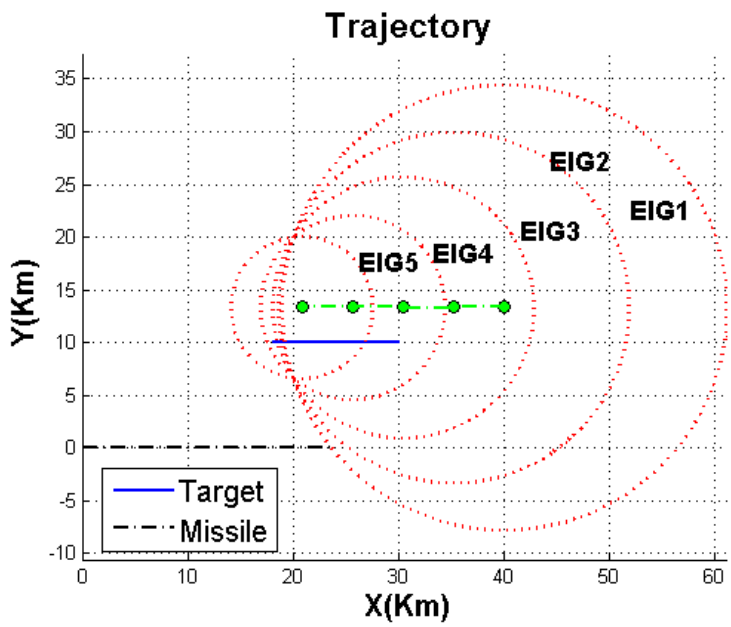

Figure 2.15: EIG change for the direct intercept when a target directly heads to an asset (γ = 2 and θ_{MF} = 0 deg.): θ_{MF} is the heading angle of the missile in inertial reference frame

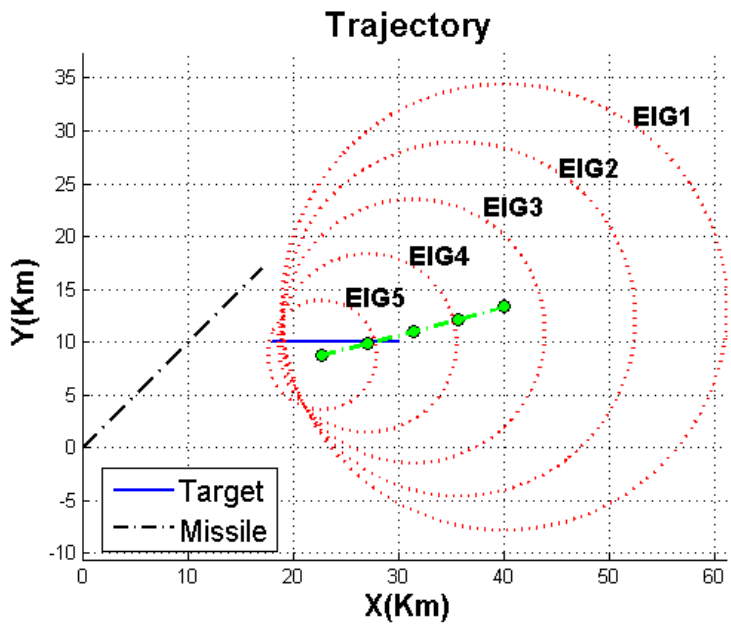

Figure 2.16: EIG change for the direct intercept when a target directly heads to an asset (γ = 2 and θ_{MF} = 45 deg.)

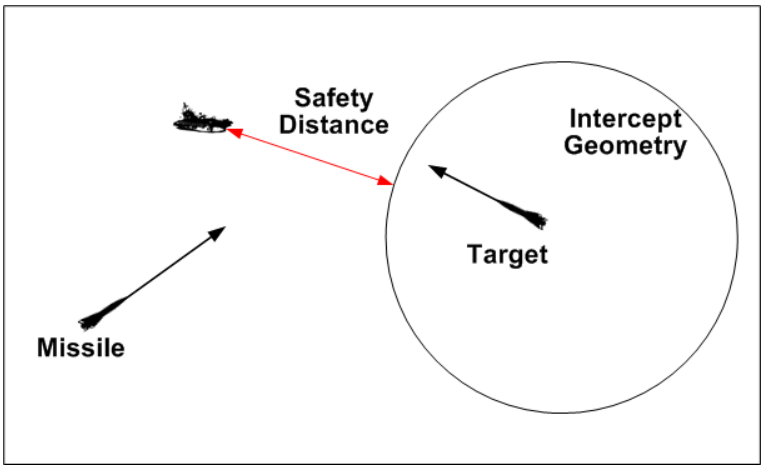

Figure 2.17: Safety distance

target before it reaches any asset. Therefore, the proposed mid course guidance strategy is keeping all the defended assets away from the capture zone. The mid course algorithm guides the missile to the EIP when all protected assets are located outside the capture zone and the safety distances are greater than the safety margin. The safety distances are defined the closest distances between the intercept geometry and asset as shown in Figure 2.17. The safety margin is introduced here because of possible deformation of the EIG resulting from the heading error between the real heading angle and the desired one on the perfect collision geometry (intercept geometry). Note that the heading error can be caused by many factors such as radar measurement error, misalignment, tracking lag, autopilot bandwidth etc. A target might penetrate an asset due to the possible change of the EIG, even though all protected assets are outside the capture zone. When all the protected defended assets are initially outside the capture zone (EIG), the mid course guidance strategy guarantees the intercept of the target and area defence as shown in Figure 2.13 and 2.14.

In some engagement scenarios, the missile might not be able to protect some asset even though it homes to the intercept point . Figure 2.18 represents one of these cases. If it is possible to push the EIG away from a defended asset in danger, the missile can still protect the assets and intercept the target. As illustrated in Figure 2.15 and 2.16, for the target heading to an asset inside the capture zone, missile cannot intercept the target before it strikes a defended asset using any methods. In this case, the best guidance strategy is to guide the missile to the

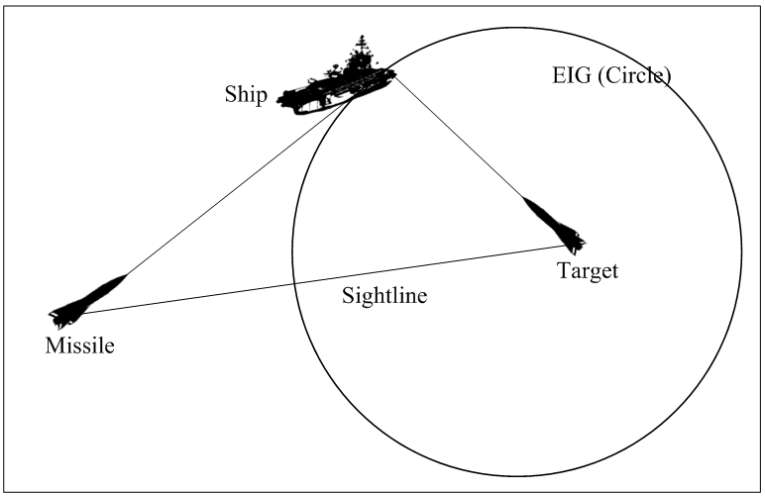

Figure 2.18: Engagement scenario: an asset is in danger

EIP. However, in many scenarios, especially in naval engagement scenarios, the target manoeuvres to an asset at the end of the flight, whilst it intentionally flies not toward the asset. The EIG can be pushed away from the asset by controlling the heading angle of the missile in these scenarios. Figure 2.19 and 2.20 show the result of a numerical example to illustrate the mid course guidance strategy base on the EIG control. In these figure, a defended asset, the black coloured diamond, was initially located in the capture zone. As shown in Figure 2.20, however, it can be outside the capture zone after the missile heading angle is controlled for some time. Therefore, when any asset is within the safety distance from the target and the target is not directly heading to the asset, the mid course guidance strategy controls the EIG away from the asset using Equation (2.49).

The key issue of the EIGGL is the change of the EIG by guiding the missile to one of EIPs, not to the EIP against current heading angle of the target. This can be mathematically derived. Let us consider the scenario that there exists an asset in danger and the target is directly not heading to the asset as shown in Figure 2.21. The EIP of interest is the interception of the EIG and the straight line from the target to the asset in danger. The position vector of the intercept point **I** of interest can be represented with respect to the target position **T**

$$\boldsymbol{r}_I = \boldsymbol{r}_T + s_T^* \boldsymbol{t}_T^*, \tag{2.66}$$

where $\boldsymbol{r}_I$ and $\boldsymbol{r}_T$ are the position vectors of the intercept point and the target. Note that motion information with superscript * denotes the desired one for the EIP of

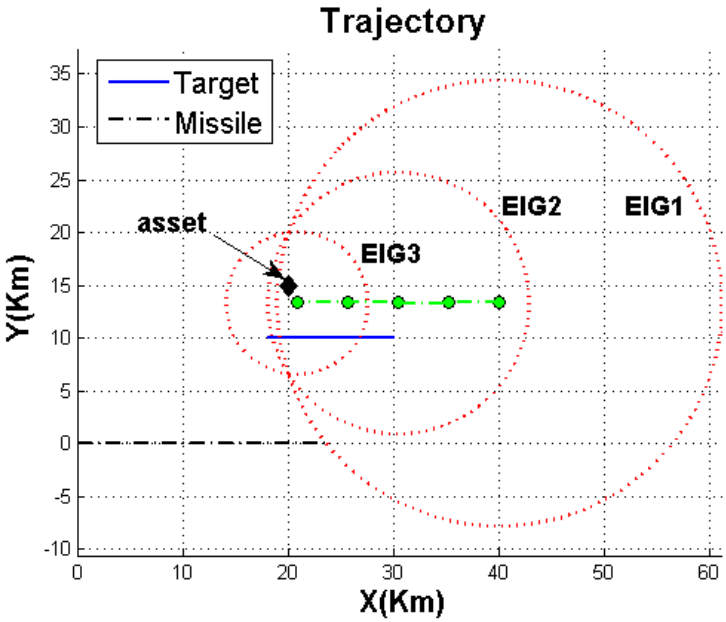

Figure 2.19: EIG control concept for $\gamma = 2$ and $\theta_{MF} = 0$ deg.

interest. From the first time derivative of the position vector $\boldsymbol{r}_I$, we have

$$\boldsymbol{v}_I = \boldsymbol{v}_T + \dot{s}_T^* \boldsymbol{t}_T^* + s_T^* \dot{\boldsymbol{t}}_T^* \tag{2.67}$$

The velocity of the considering EIP is obtained as:

$$\begin{aligned}
\boldsymbol{v}_I &= \left(\cos(\theta_T^* - \theta_T) - \frac{\gamma \cos\theta_M + \cos\theta_T^*}{\cos\theta_T^* + \sqrt{\gamma^2 - \sin^2\theta_T^*}} \right) v_T \boldsymbol{t}_T^* \\
&\quad - v_T \sin(\theta_T^* - \theta_T) \boldsymbol{n}_T^* + \frac{\sin\theta_T^*}{\sqrt{\gamma^2 - \sin^2\theta_T^*}} s_T^* \dot{\theta}_T^* \boldsymbol{t}_T^* - s_T^* \dot{\psi}_T^* \boldsymbol{n}_T^*, \\
&= \frac{\left(\cos(\theta_T^* - \theta_T) - 1\right)\cos\theta_T^* + \left(\cos(\theta_T^* - \theta_T)\cos\theta_M^* - \cos\theta_M\right)\gamma}{\cos\theta_T^* + \sqrt{\gamma^2 - \sin^2\theta_T^*}} v_T \boldsymbol{t}_T^* \\
&\quad - v_T \sin(\theta_T^* - \theta_T) \boldsymbol{n}_T^*
\end{aligned} \tag{2.68}$$

since θ_T^* and ψ_T^* are identical to zero. The control parameter in the equation is θ_M. If the missile head to the EIP of interest, i.e. $\theta_M = \theta_M^*$, we have

$$\cos(\theta_T^* - \theta_T)\cos\theta_M^* - \cos\theta_M = \left(\cos(\theta_T^* - \theta_T) - 1\right)\cos\theta_M^* \leq 0 \tag{2.69}$$

and Figure 2.22 shows the velocity of the EIP.

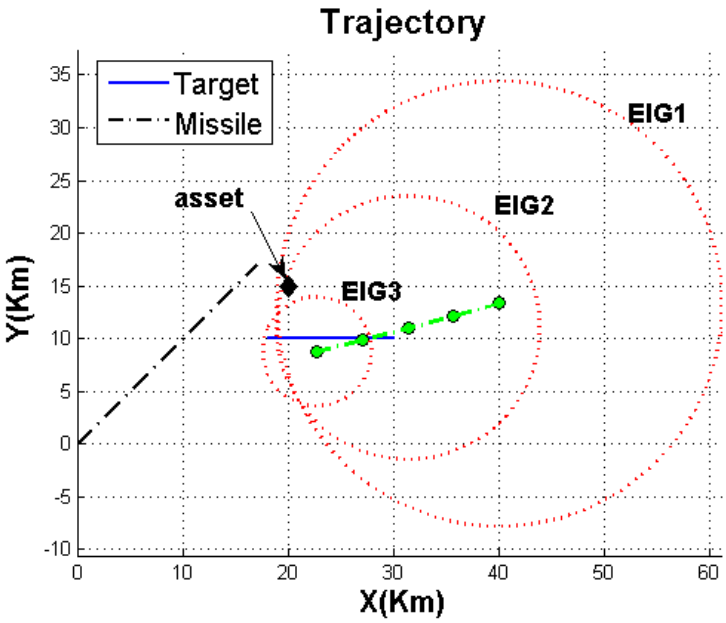

Figure 2.20: EIG control concept for $\gamma = 2$ and $\theta_{MF} = 45$ deg.

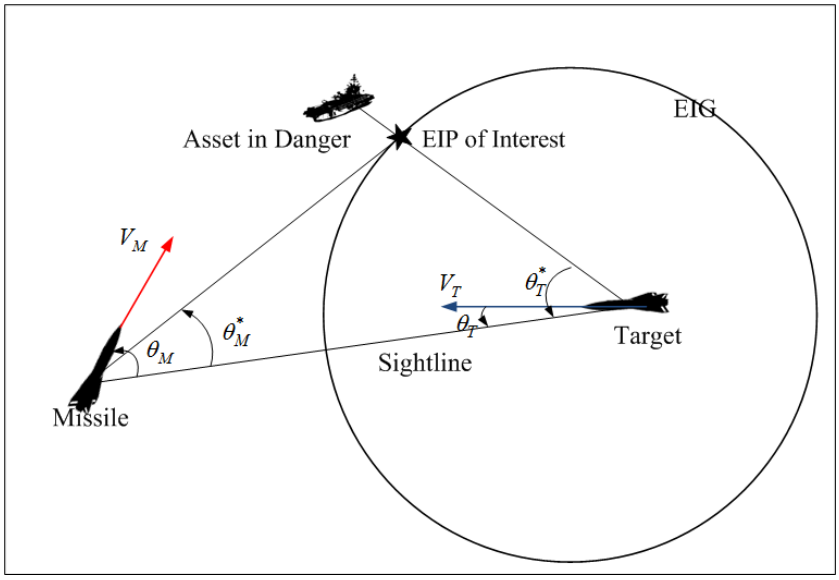

Figure 2.21: Engagement geometry to illustrate the geometry control

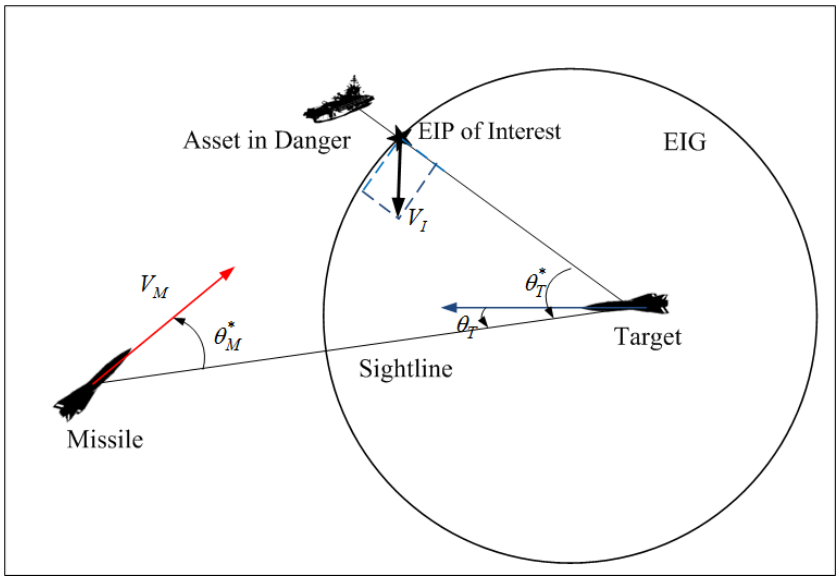

Figure 2.22: Velocity of the EIP of interest

Chapter 3

Mid Course Guidance II: IGGL

In previous chapter, we proposed a mid course guidance algorithm, named Earliest Intercept Guidance Law (EIGGL). Since missiles must destroy the incoming threat before it intercepts any defended asset, the proposed guidance algorithm endeavours to guarantee that all assets will be located outside the capture zone. The EIGGL was analytically derived under the assumption that the missile can instantaneously change its heading angle. Although it can deal with the worst case, it is difficult to consider the operational and physical constraints of the missile and target. To take the operational and physical constraints of the missile and the target into consideration, we propose a mid course guidance law, called Intercept Geometry Guidance Law (IGGL), based on the optimal control theory and the concepts of the Intercept Geometry (IG). Note that the IG can be numerically computed because it is hard to find an analytical solution.

Similar to the EIG, IG is the boundary that target can travel against the guidance law applied to the missile. Therefore, the IG represents a capture zone of the guidance law. As shown in Figure 3.1, if the guidance algorithm ensures no overlapping between this capture zone and keep out zone (defended area), all assets inside the defended area can be protected. From this IG concept, it is

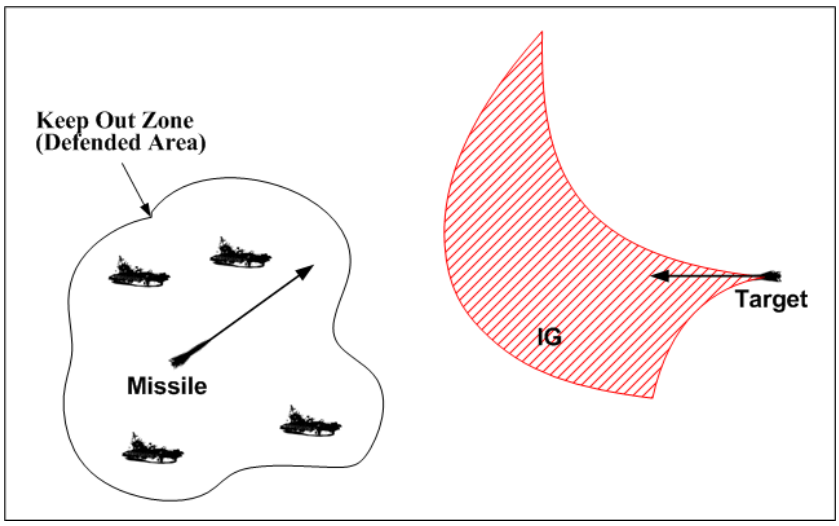

Figure 3.1: Concept of the mid course guidance law based on the IG concept

possible to calculate the distances between the defended assets and the IG. These distances are used to determine which assets are in danger; if the distance between the IG and an asset is smaller than the safety margin, the asset is in danger. In the case that there is no asset within the safety distance from the IG, the missile is guided to the intercept point. However, when any of these distances are less than the safety distance, the missile is guided to the point on the IG which can most push the IG away from the asset in danger.

The key idea of the proposed guidance algorithm is to confine the target within intercept geometries, regardless of the target manoeuvres. Therefore, the shape of the IG is an important factor determining the proposed guidance strategy. The IG shape ultimately depends on the choice among candidates of the target acceleration profiles. In the EIGGL, straight line (zero acceleration) trajectories with all possible target heading angles are used for the analytical derivation of the EIG. In this chapter, we will consider several types of the target acceleration profiles and investigate their effects on the IG shape to determine.

3.1 Optimal Guidance Law

In this section, we will introduce optimal guidance algorithms not only to consider physical and operational constraints in the computation of the IG, but also to provide more energy and manoeuvrability to the terminal homing phase. Since PN guidance is most common, a Proportional Navigation (PN) type optimal guidance law for the manoeuvring target will be first addressed. Then, we will derive an Impact Angle Control Guidance (IACG) law for the manoeuvring target. IACG can increase the hit kill probability by controlling engagement geometry.

3.1.1 PN Type Optimal Guidance

Consider a two-dimensional missile homing guidance as shown in Figure 3.2. Subscripts $_M$ and $_T$ on the parameters in this figure represent their motion information of the missile and target. For example, the position vectors of the missile and target are denoted as $(x_M,\ y_M)$ and $(x_T,\ y_T)$. The flight path angle and line-of-sight angle with respect to the inertial reference frame are denoted as ψ and σ,

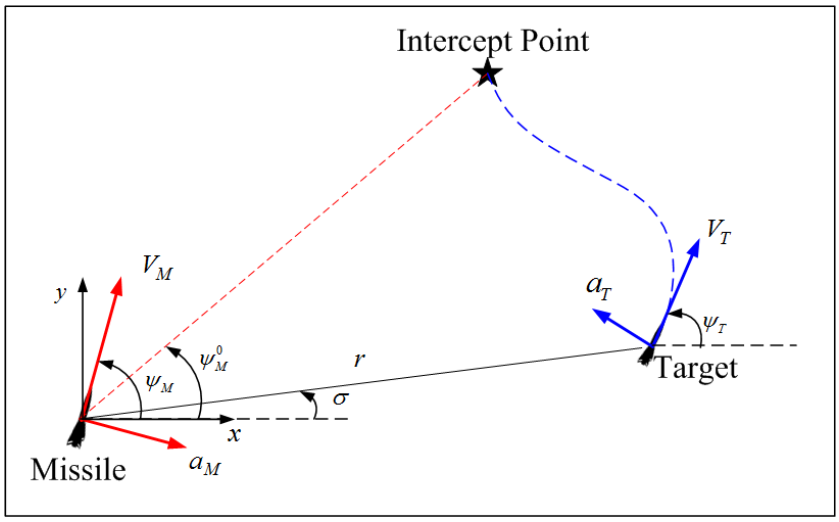

Figure 3.2: Guidance geometry

respectively. ψ_M^0 is the flight path angle for the perfect collision path that is determined at the beginning of engagement. The acceleration command to change ψ is denoted as a. Note that the relation between the sightline angle θ_S and LOS angle σ is given by

$$\sigma = \theta_S - 180(deg). \tag{3.1}$$

The relative position between the missile and target on y axis is obtained as:

$$y(t) = y_T(t) - y_M(t). \tag{3.2}$$

The equation of motion of homing guidance is, then, given by

$$\dot{y}(t) = V_T(t)\sin\psi_T(t) - V_M(t)\sin\psi_M(t) \tag{3.3}$$

$$\dot{\psi}_M(t) = \frac{a_M(t)}{V_M(t)} \tag{3.4}$$

Since $V_M \sin\psi_M(t)$ can be represented as

$$V_M \sin\psi_M = V_M \sin\psi_M^0 \cos\Delta\psi_M + V_M \cos\psi_M^0 \sin\Delta\psi_M \tag{3.5}$$

where $\Delta\psi_M \equiv \psi_M - \psi_M^0$, Equation (3.3) is rewritten as:

$$\dot{y} = V_T \sin\psi_T - V_M \sin\psi_M^0 \cos\Delta\psi_M - V_M \cos\psi_M^0 \sin\Delta\psi_M. \tag{3.6}$$

We define V_y as linearized $\dot{y}$ about $\Delta\psi_M = 0$ by assuming small $\Delta\psi_M$

$$\begin{aligned}\dot{y} &\simeq V_T \sin\psi_T - V_M \sin\psi_M^0 - V_M \cos\psi_M^0 \Delta\psi_M \\ &= V_y^0 - V_M \cos\psi_M^0 \Delta\psi_M \equiv V_y,\end{aligned} \tag{3.7}$$

where

$$V_y^0 \equiv V_T \sin\psi_T - V_M \sin\psi_M^0. \tag{3.8}$$

The first time derivative of $V_y(t)$ is given by

$$\dot{V}_y(t) \equiv c(t)V_y(t) + u(t) - c(t)V_y^0(t) + \dot{V}_y^0(t), \tag{3.9}$$

where

$$c \equiv \frac{\dot{V}_M}{V_M}, \quad u \equiv -a_M \cos\psi_M^0, \quad \dot{V}_y^0 \equiv \frac{\mathrm{d}V_y^0}{\mathrm{d}t} \tag{3.10}$$

The state equations for the homing guidance problem is represented of the form

$$\dot{\boldsymbol{x}} = A\boldsymbol{x} + Bu + \Delta \tag{3.11}$$

where

$$\boldsymbol{x} \equiv [x_1,\ x_2]^T = \left[y,\ V_y\right]^T \tag{3.12}$$

$$A = \begin{bmatrix} 0 & 1 \\ 0 & c \end{bmatrix}, \quad B = \begin{bmatrix} 0 \\ 1 \end{bmatrix}, \quad \Delta = \begin{bmatrix} 0 \\ \dot{V}_y^0 - cV_y^0 \end{bmatrix}. \tag{3.13}$$

Consider the following optimal control problem: find optimal control command $u(t)$ which minimizes the performance index given by:

$$J = \frac{1}{2}\int_{t_0}^{t_f} u^T(s)R(s)u(s)\,\mathrm{d}s, \tag{3.14}$$

subject to Equation (3.11) with terminal constraints given by

$$D\boldsymbol{x}(t_f) = E, \tag{3.15}$$

where

$$R(s) = (t_f - s)^n, \tag{3.16}$$

for a integer n greater than or equal to zero, and

$$D = [1\ \ 0], \quad E = 0. \tag{3.17}$$

Note that the weighting function $R(s)$ in Equation (3.16) is getting smaller as the time-to-go is getting smaller. Since this can prevent the actuator saturation resulting from the target manoeuvre at the late phase of the engagement, this can improves the robustness of the guidance algorithm.

The general form of the optimal solution is given in Ref. Cho et al. (1999).

$$u(t) = -\frac{N(t)}{t_g^2} \cdot ZEM, \tag{3.18}$$

where ZEM denotes the zero-effort miss of the form

$$ZEM = y(t) + t_g(t)V_y(t) + \int_t^{t_f} t_g(s)(\dot{V}_y^0(s) - c(s)V_y^0(s))\ \mathrm{d}s, \tag{3.19}$$

and t_g is defined as

$$t_g \equiv \frac{\int_t^{t^f} V_M(s)\ \mathrm{d}s}{V_M(t_f)}. \tag{3.20}$$

The the guidance navigation gain $N(t)$ is obtained as

$$N(t) = \frac{R^{-1}t_g^3}{\int_t^{t_f} R^{-1}(s)t_g^2(s)\ \mathrm{d}s}, \tag{3.21}$$

When the speed of the missile is constant and the target flies in a straight line with a constant speed, the optimal guidance command is given by

$$u(t) = -\frac{n+3}{t_{go}^{n+2}}\Big(y(t) + t_{go}V_y(t)\Big). \tag{3.22}$$

where $t_{go} = t_f - t$. Since

$$y(t) + t_{go}V_y(t) \simeq r\dot{\sigma}t_{go}, \quad r \simeq t_{go}V_C, \tag{3.23}$$

where V_C denotes the closing velocity, Equation (3.22) can be rewritten

$$u(t) \simeq -\frac{n+3}{t_{go}^n}V_C\dot{\sigma}. \tag{3.24}$$

If $n = 0$, the derived guidance law is the same as the conventional PN guidance law:

$$u(t) \simeq -3V_C\dot{\sigma} = u_{PN}. \tag{3.25}$$

3.1.2 Impact Angle Control Guidance

Now, let us consider an optimal impact angle control problem: find optimal control command $u(t)$ minimizing the performance index defined by Equation (3.14), subject to Equation (3.11) with terminal constraints given by

$$D\boldsymbol{x}(t_f) = E, \tag{3.26}$$

where

$$D = I_{2x2}, \quad E \equiv [e_1 \; e_2]^T = [0 \quad V_y^0(t_f)]^T. \tag{3.27}$$

Here, the second terminal constraint, e_2, is introduced to constrain the impact angle at the intercept point.

This optimal problem is a linear optimal control problem with additional forcing term. Note that, in this optimal guidance problem, Q, C, and S_f in Equations (A.3) and (A.4) are zero. The general solution for this problem is derived in Appendix A:

$$u = -R^{-1}B^T\boldsymbol{\lambda}, \tag{3.28}$$

where $\boldsymbol{\lambda}$ is the influence function vector. From $\dot{S}$ in Equations (A.68) and $\dot{S}(t_f)$ (A.69), we have

$$S(t) = 0. \tag{3.29}$$

Using system matrices and $\dot{F}$ in Equations (A.68) and $\dot{S}(t_f)$ in Equation (A.69), F can be derived as follows

$$F = \begin{bmatrix} 1 & 0 \\ t_g & 1_g \end{bmatrix}, \tag{3.30}$$

where

$$1_g \equiv \frac{V_M(t)}{V_M(t_f)}. \tag{3.31}$$

If we assume the costate vector $\boldsymbol{\lambda}$ as

$$\boldsymbol{\lambda} = F\boldsymbol{\nu}, \tag{3.32}$$

where $\boldsymbol{\nu}$ is a constant vector, then we have

$$\dot{\boldsymbol{\lambda}} = \dot{F}\boldsymbol{\nu}; \quad \boldsymbol{\lambda}(t_f) = D^T\boldsymbol{\nu} = F(t_f)\boldsymbol{\nu}. \tag{3.33}$$

Hence

$$\boldsymbol{\lambda} = F\boldsymbol{\nu} = \begin{bmatrix} 1 & 0 \\ t_g & 1_g \end{bmatrix} \begin{bmatrix} \nu_1 \\ \nu_2 \end{bmatrix} = \begin{bmatrix} \nu_1 \\ t_g\nu_1 + 1_g\nu_2 \end{bmatrix}. \tag{3.34}$$

Substituting Equation (3.34) into Equation (A.9) results in general solution of the optimal IACG problem:

$$u(t) = -R^{-1}(t)B^T(t)\boldsymbol{\lambda}(t) = -t_{go}^N \left(t_g\nu_1 + 1_g\nu_2\right). \tag{3.35}$$

As shown in Equation (A.63), $\boldsymbol{\nu}$ is given by:

$$\boldsymbol{\nu} = [\nu_1 \ \nu_2]^T = G^{-1}(t_0)[E - F^T(t_0)\boldsymbol{x}_0 + G_\Delta(t_0)]. \tag{3.36}$$

From $F(t)$ derived and $\dot{G}(t)$ in Equation (A.68), $G(t)$ can be obtained as

$$G(t) = -\begin{bmatrix} \int_t^{t_f}(t_f - s)^n t_g^2(s)\ \mathrm{d}s & \int_t^{t_f}(t_f - s)^n t_g(s)1_g(s)\ \mathrm{d}s \\ \int_t^{t_f}(t_f - s)^n t_g(s)1_g(s)\ \mathrm{d}s & \int_t^{t_f}(t_f - s)^n 1_g^2(s)\ \mathrm{d}s \end{bmatrix}. \tag{3.37}$$

Since

$$\dot{F}_\Delta = -AF_\Delta; \quad F_\Delta(t_f) = 0, \tag{3.38}$$

it is clear that $F_\Delta = 0$. We can also obtain $G_\Delta(t)$ from F, Δ and $\dot{G}_\Delta$ in Equation (A.68):

$$G_\Delta = -\int_t^{t_f} F^T(t)\Delta(t)\ \mathrm{d}t = -\begin{bmatrix} \int_t^{t_f} t_g(s)(\dot{V}_y^0(s) - c(s)V_y^0(s))\ \mathrm{d}s \\ \int_t^{t_f} 1_g(s)(\dot{V}_y^0(s) - c(s)V_y^0(s))\ \mathrm{d}s \end{bmatrix}. \tag{3.39}$$

Therefore, we have

$$\boldsymbol{\nu} = G^{-1}(t)\begin{bmatrix} -y - t_gV_y - \int_t^{t_f} t_g(s)(\dot{V}_y^0(s) - c(s)V_y^0(s))\ \mathrm{d}s \\ V_y^0(t_f) - 1_gV_y - \int_t^{t_f} 1_g(\dot{V}_y^0(s) - c(s)V_y^0(s))\ \mathrm{d}s \end{bmatrix}. \tag{3.40}$$

If the speeds of the missile and target are assumed to be constant, we have

$$c(t) = 0, \quad t_g = t_{go}, \quad 1_g = 1, \quad \Delta = \left[0,\ \dot{V}_y^0\right]^T. \tag{3.41}$$

$F(t)$ is obtained as:

$$F(t) = \begin{bmatrix} 1 & 0 \\ t_{go} & 1 \end{bmatrix}. \tag{3.42}$$

Moreover, $G(t)$ and $G_\Delta(t)$ are given by

$$G = -\frac{t_{go}^n}{(n+1)(n+2)(n+3)} \begin{bmatrix} (n+1)(n+2)t_{go}^2 & (n+1)(n+3)t_{go} \\ (n+1)(n+3)t_{go} & (n+2)(n+3) \end{bmatrix}, \tag{3.43}$$

$$G_\Delta = \begin{bmatrix} -t_{go}V_y^0(t) + y_T(t_f) - y_T(t) \\ V_y^0(t_f) - V_y^0(t) \end{bmatrix}. \tag{3.44}$$

We plug these matrices and parameters in Equation (3.41) into Equation (3.40):

$$\boldsymbol{\nu} = -G^{-1}(t) \begin{bmatrix} y(t) + t_{go}V_y(t) - (t_f - t)V_T \sin\psi_T(t) + y_T(t_f) - y_T(t) \\ V_y(t) - V_y^0(t) \end{bmatrix}. \tag{3.45}$$

For $t \neq t_f$ $G(t)$ is nonsingular so that $G^{-1}(t)$ can be derived from Equation (3.43):

$$G^{-1}(t) = -\frac{N+2}{t_{go}^{n+3}} \begin{bmatrix} (n+2)(n+3) & -(n+1)(n+3)t_{go} \\ -(n+1)(n+3)t_{go} & (n+1)(n+2)t_{go}^2 \end{bmatrix}. \tag{3.46}$$

Therefore, the optimal guidance command is given by

$$u(t) = -t_{go}^N \left(t_{go}\nu_1 + \nu_2\right), \tag{3.47}$$

where

$$\nu_1 = \frac{(n+2)(n+3)}{t_{go}^{n+3}} \left[(n+2)\{y_T(t_f) - y_M(t)\} + t_{go}\{V_y - V_y^0(t)\}\right], \tag{3.48}$$

$$\nu_2 = -\frac{(n+1)(n+2)}{t_{go}^{n+2}} \left[(n+3)\{y_T(t_f) - y_M(t)\} + t_{go}\{V_y - V_y^0(t)\}\right]. \tag{3.49}$$

Note that we define $\dot{\psi}_M$ as

$$\dot{\psi}_M = \frac{a_M}{V_M} \equiv t_{go}^n(c_1 + t_{go}c_2). \tag{3.50}$$

Since a_M can be derived from the definition of u

$$a_M = -\frac{u}{\cos\psi_M^0}, \tag{3.51}$$

we have

$$c_1 = \frac{\nu_2}{V_M \cos\psi_M^0}, \quad c_2 = \frac{\nu_1}{V_M \cos\psi_M^0}. \tag{3.52}$$

If the target is flying with a constant velocity vector, $V_z^0 = 0$. Then, G_Δ is given by

$$G_\Delta = [0 \quad 0]^T. \tag{3.53}$$

Moreover, $\boldsymbol{\nu}$ is obtained as:

$$\boldsymbol{\nu} = \frac{n+2}{t_{go}^{n+3}} \begin{bmatrix} (n+2)(n+3)y(t) + (n+3)t_{go}V_y(t) \\ -(n+1)(n+3)t_{go}y(t) - (n+1)t_{go}^2 V_y(t) \end{bmatrix}, \tag{3.54}$$

and then c_1 and c_2 are given by

$$c_1 = -\frac{(n+1)(n+2)}{V_M t_{go}^{n+2} \cos\psi_M^0} \left\{(n+3)y(t) + t_{go}V_y(t)\right\}, \tag{3.55}$$

$$c_2 = \frac{(n+2)(n+3)}{V_M t_{go}^{n+3} \cos\psi_M^0} \left\{(n+2)y(t) + t_{go}V_y(t)\right\}. \tag{3.56}$$

Note that if target is moving with a constant velocity vector,

$$V_y = V_M \cos\psi_M^0 \Delta\psi_M = V_M \cos\psi_M^0 (\psi_M - \psi_M^0), \tag{3.57}$$

and ψ_M^0 is given by

$$\psi_M^0 = \psi_T - \psi_I, \tag{3.58}$$

where ψ_I is the terminal impact angle constraint.

3.2 Intercept Geometries

Using the capture zone defined by the IG, we can resolve one of main issues in the area defence, namely unpredictability of the target acceleration; if the capture zone is bounded outside the defended area regardless of the target manoeuvres then all assets in a defended area can be protected. The shape of the capture zone mainly depends on the missile guidance law and the target acceleration profiles used for the IG computation. Since we determined the missile guidance law, the shape of the capture zone now only depends on the target acceleration profiles. This shape ultimately establishes the mid course guidance strategy.

In order to investigate the effect of the acceleration profiles on the IG, we consider three acceleration types in the calculation of the IG:

- Target changes its heading angle instantaneously (no limitation in the target acceleration)
- Target manoeuvres with a constant acceleration

Table 3.1: Initial conditions for the IGGL simulation

	Target	Missile
Position(m,m)	(1700, 500)	(0, 0)
Velocity(m/s)	100	200
Heading angle(deg)	180	60

- Target turns with the maximum acceleration and then flies in a straight line (Dubins path)

When it is assumed that the target can change its heading angle as assumed in the EIGGL, the boundary that the target can reach is the contour of the intercept points for all viable heading angles of the target. Figures 3.3 shows the results of a numerical example. Throughout this chapter, the initial conditions for the examples are the same as represented in Table 3.1. The IG for the PN type optimal guidance is illustrated in Figure 3.3(a) and Figure 3.3(b) depicts the IG for the IAC type guidance. Since the assumption that target can instantaneously change its heading angle is invalid, this assumption provides the largest IG, that is the worst case. However, in this case, we cannot consider physical constraints on the target.

For the implementation of the guidance laws, it is required to obtain the current position and velocity vectors of the missile and target, and the future acceleration profile of the target. Although most of these motion information can be measured or estimated, the future target acceleration is difficult to be predicted. Therefore, it is usually assumed to be constant for a practical reason. Under this assumption, the IG can be obtained from the contour of the intercept points for all constant target accelerations. In order to examine the IG with this concept, a numerical example is considered. The initial conditions for the example are represented in Table 3.1. The constant target accelerations used in computation of the IG are $[-30, -28, -25, -20, -15, -5, 0, 5, 15, 20, 25, 28, 30]$. The results of the numerical examples are illustrated in Figure 3.4. This concept can consider the operational and physical constraints.

In a previous research (Robb et al., 2005, 2006), the Dubins (Dubins, 1957) path is used to derive the Earliest Intercept Line (EIL) because the Dubins path is the shortest path to get reach a certain point. To derive the EIL, the missile

and target are assumed to fly in a straight line after turning with the maximum acceleration to align its heading angle to the intercept point. In this study, this concept is also used to compute the IG. However, it is assumed that the proposed optimal guidance laws are applied to the missile. Since the Dubins path is one of the optimal solutions, the EIL proposed by Robb et al. (2005, 2006) is one of the IG solutions. Figure 3.5 depicts the IG with the Dubins concept of the numerical example. Since the Dubins path is the shortest path when the maximum turning radius is given, the computed IG is the EIG and considers the physical constraints of the target.

The comparisons of the IGs are shown in Figures 3.6 and 3.7. As expected, the IG with straight lines is the largest and other IGs are similar. It is shown that the IGs for the IAC type guidance law are bigger than those for the PN type guidance law. Since the proposed mid course guidance algorithm tries to remove the overlapping between the IG and defended area, large IG is not desirable. However, the IAC type optimal guidance law can increase the hit kill probability by controlling the terminal impact angle. Selecting of the target acceleration profile and the type of optimal guidance laws depends on the properties of the engagement scenarios. In order to provide more options, we leave the decision of the best algorithm to the mid course guidance designers.

3.3 Guidance Strategy

The guidance strategy for the IGGL is the same as that of the EIGGL. As shown in Figure 2.2, the guidance endeavours to keep all assets outside the capture zone and control this zone away from the defended assets. The capture zone is defined by the IG, which is computed using one of methods proposed in 3.2. Since guiding the missile to a different intercept points results in different IG, the guidance strategy delivers the missile to the certain intercept point so as to push the IG away from the defended assets. For the illustration of the proposed guidance concept, an numerical example is applied. Figure 3.8 shows the results of the numerical simulation. Here, the IG is calculated using the assumption that target manoeuvres with a constant lateral acceleration. When the missile intentionally flies to the intercept point for the non-manoeuvring target, the IG after 3 *sec* is IG1 in Figure 3.8. If the missile is guided to the intercept point against

the manoeuvring target with 30 m/s^2 lateral acceleration, the IG after 3 *sec* is IG 2 in the figure. In this numerical example, IG 2 is more satisfactory since the distance between the IG and defended asset is longer.

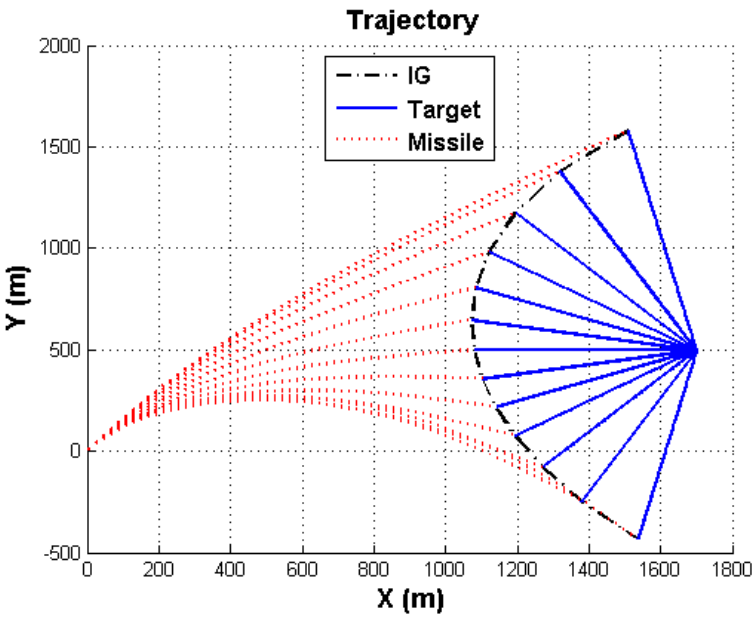

(a) PN type optimal guidance

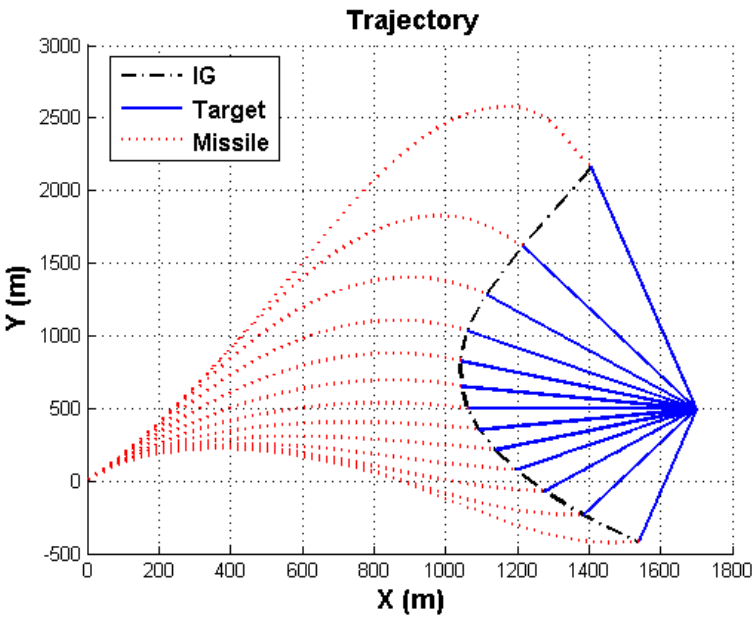

(b) IAC type optimal guidance law (terminal angle constraint = 160deg.)

Figure 3.3: IGs when it is assumed that the target can change its heading angle instantaneously

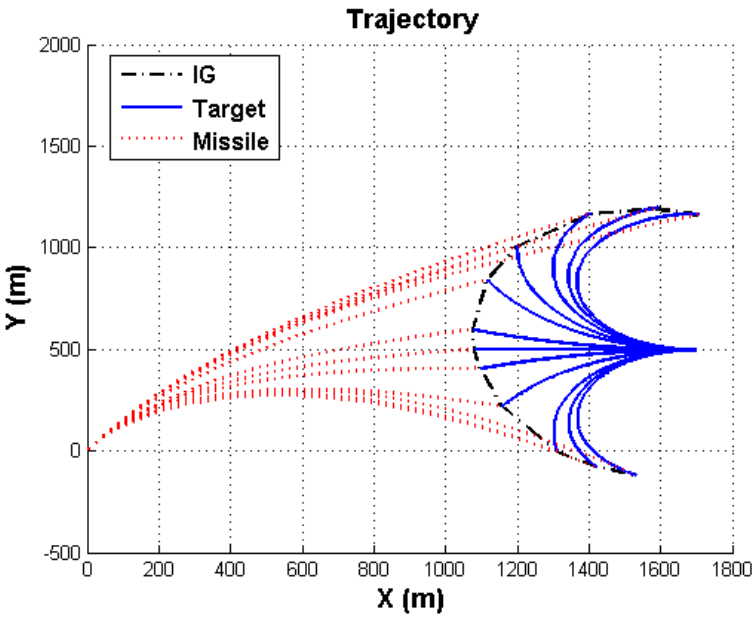

(a) PN type optimal guidance

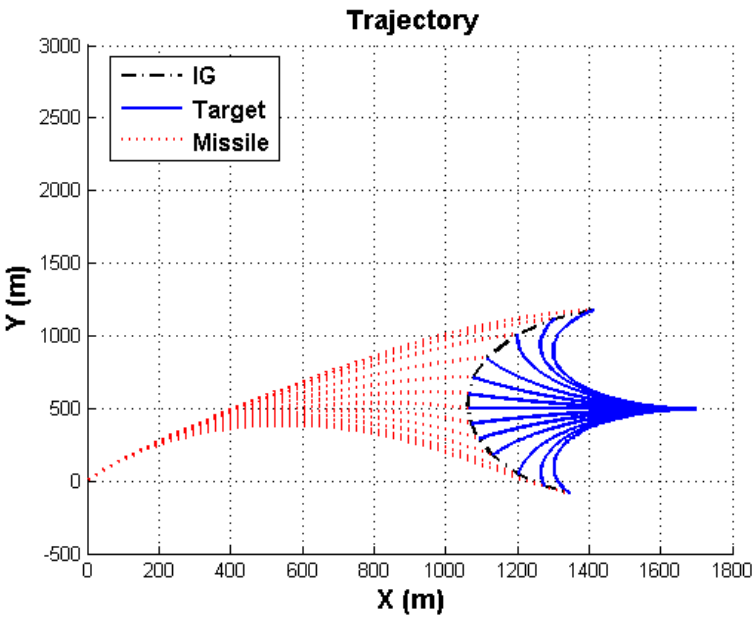

(b) IAC type optimal guidance law (terminal angle constraint = 160deg.)

Figure 3.4: IGs when when it is assumed that the target manoeuvres with a constant lateral acceleration

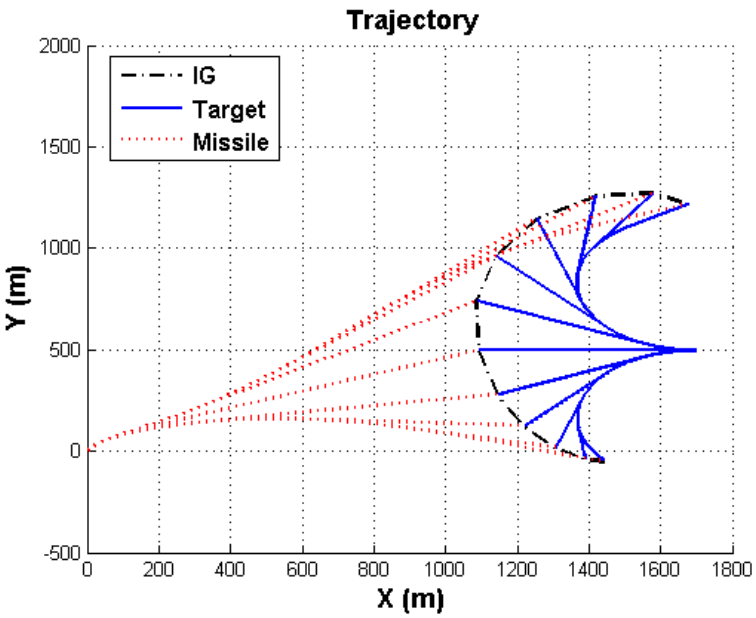

(a) PN type optimal guidance

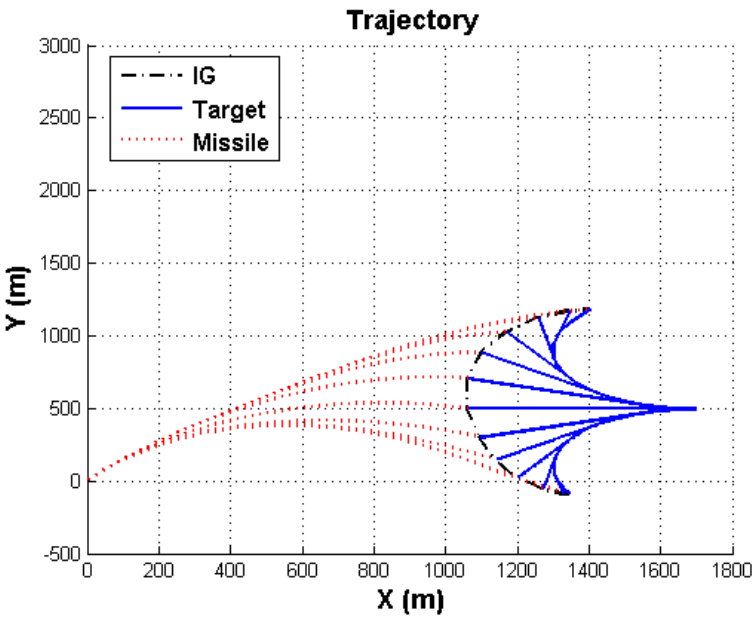

(b) IAC type optimal guidance law (terminal angle constraint = 160deg.)

Figure 3.5: IGs when it is assumed that the target turns with the maximum acceleration and then flies in a straight line

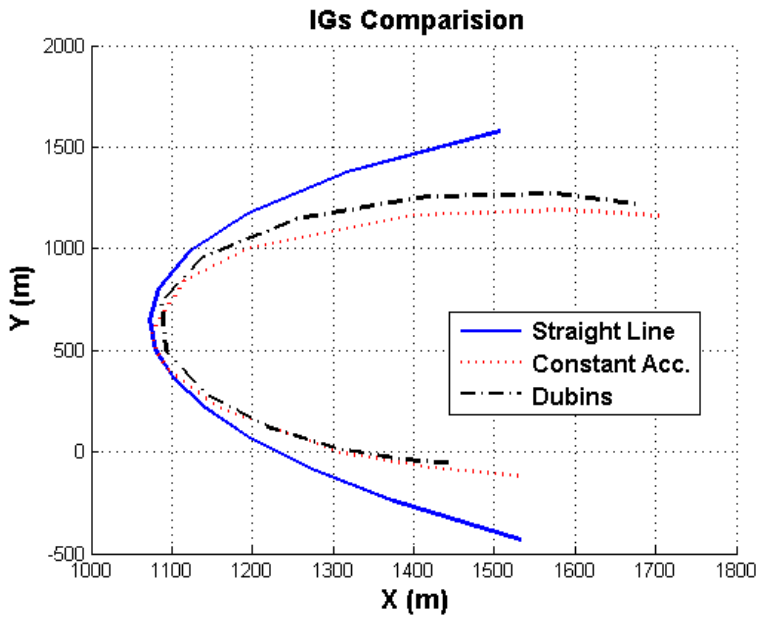

Figure 3.6: Comparison of IGs for the PN type optimal guidance law

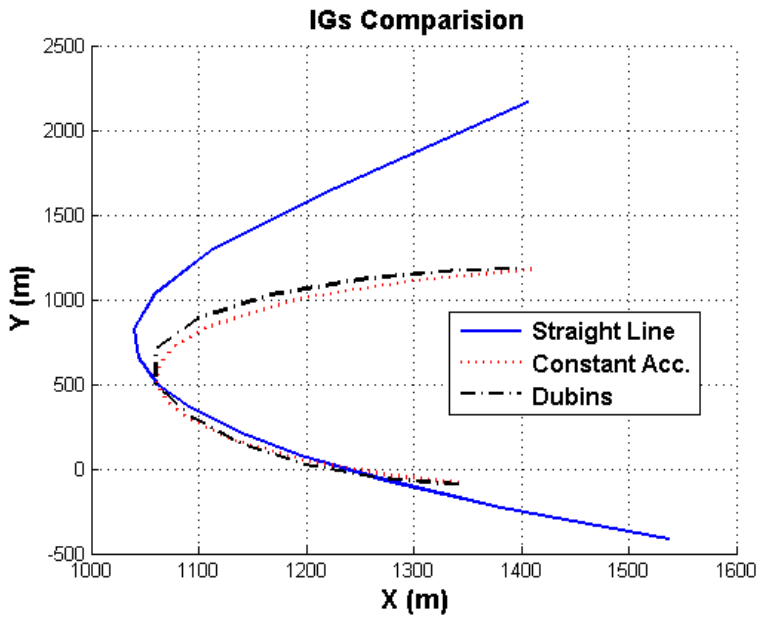

Figure 3.7: Comparison of IGs for the IAC type optimal guidance law

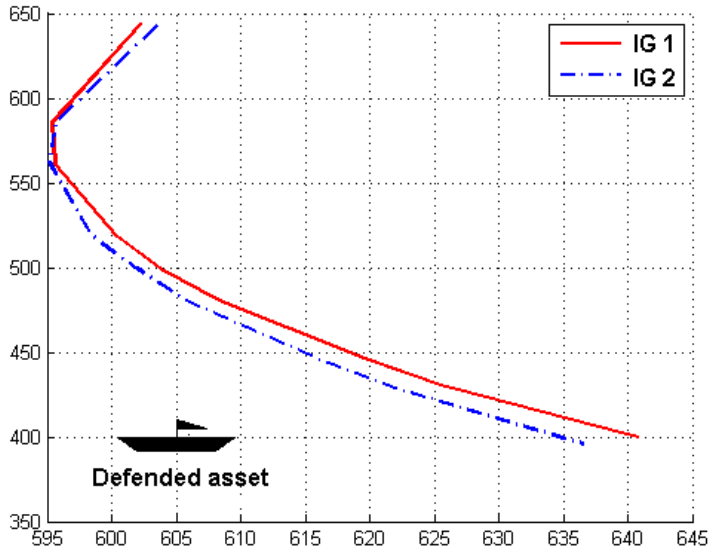

Figure 3.8: Illustration of the IGGL concept

Chapter 4

Target Allocation

In previous two chapters, the intercept geometry is investigated to develop the mid course guidance algorithms. Although these guidance algorithms are mainly described for the one-on-one scenarios, they can be also used for the many-on-many engagement scenarios with the target allocation policy. In this chapter, we will examine the concepts of intercept geometry to develop a target allocation plan for the many-on-many engagement scenarios.

Figure 4.1 shows a many-on-many engagement scenario. As illustrated in

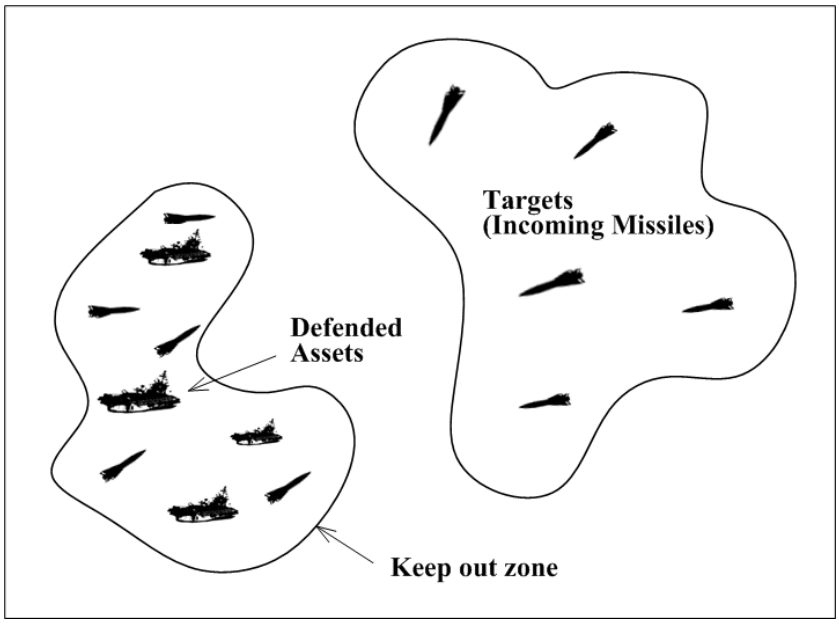

Figure 4.1: Many-on-many engagement scenario

this figure, in the many-on-many engagements, multiple missiles strive to protect assets in a defended area (keep out zone) against many targets. The cooperative mid course guidance problem is to find a guidance algorithm which provides engagement conditions, in which the terminal homing guidance law intercepts all targets before they strike any of assets in the defended area. The concepts of the intercept geometry guidance algorithms can be directly extended to the cooperative mid course guidance algorithm. Figure 4.2 illustrates a simple example

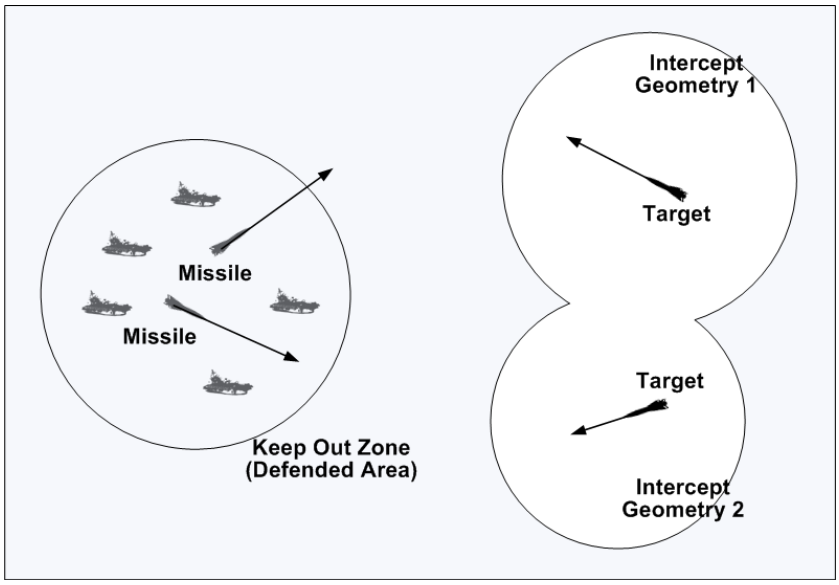

Figure 4.2: Concept of the cooperative mid course guidance strategy using the intercept geometry

describing the implementation of the intercept geometry concept to the cooperative guidance algorithm. The defended assets can be protected, if the cooperative guidance strategy guarantees that all assets are outside the capture zone. Note that the capture zone for the many-on-many engagement is defined as the area inside the union of the intercept geometries, and it is represented as the white coloured geometry in Figure 4.2.

The framework of the cooperative guidance algorithm can be illustrated in Figure 4.3. In this research, it is assumed that each missile uses either the EIGGL or IGGL. Under this assumption, the cooperative mid course guidance problem is to design the best target allocation plan.

4.1 Target Allocation Using the Intercept Geometries

As stated, all defended assets should be outside the capture zone for the area defence. However, as shown in Figure 4.4, the capture zone changes as target allocation plan changes. In the top figure, the first missile is allocated to the first target and the second missile to the second target. Whereas, in the bottom figure,

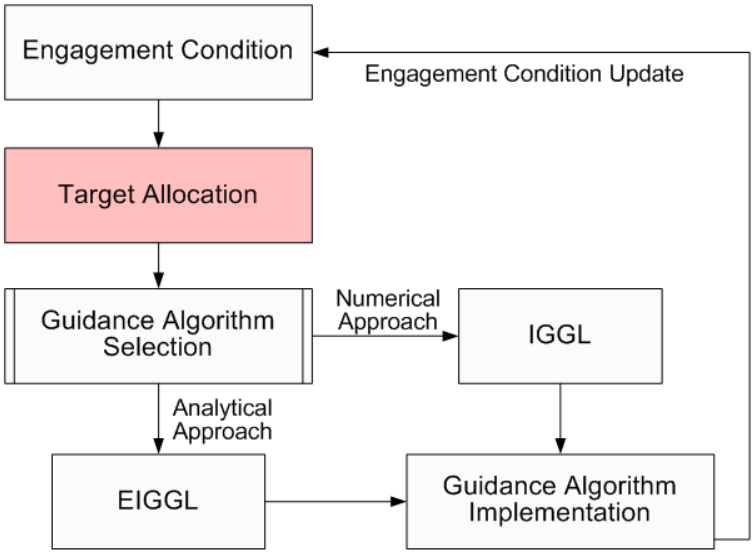

Figure 4.3: Framework of the cooperative guidance algorithm

the first missile is allocated to the second target and the second missile to the first missile. The change of the capture zone implies that it is possible to enhance the performance of the cooperative guidance algorithm using the allocation plan. In this study, an optimal target allocation algorithm is developed using the concept of the safety distance as shown in Figure 2.17. The distances between the intercept geometries and defended assets also vary depending on the geometry change. It is clear that the greater distance the target allocation algorithm can guarantee, the better performance the guidance algorithm can have. Therefore, the optimal allocation problem is to find the allocation plan which can maximize the safety distance.

It is difficult to find an analytical solution for this optimal problem. Thus, we need to implement a numerical algorithm. In order to reduce computational load for the real time implementation, we divide the optimal problem into several simple algebraic steps:

- Find the set of all possible allocation plans
- Derive the intercept geometries (EIGs or IGs) of each element (allocation) of the set
- Calculate the set of minimum distances between the defended assets and intercept geometries

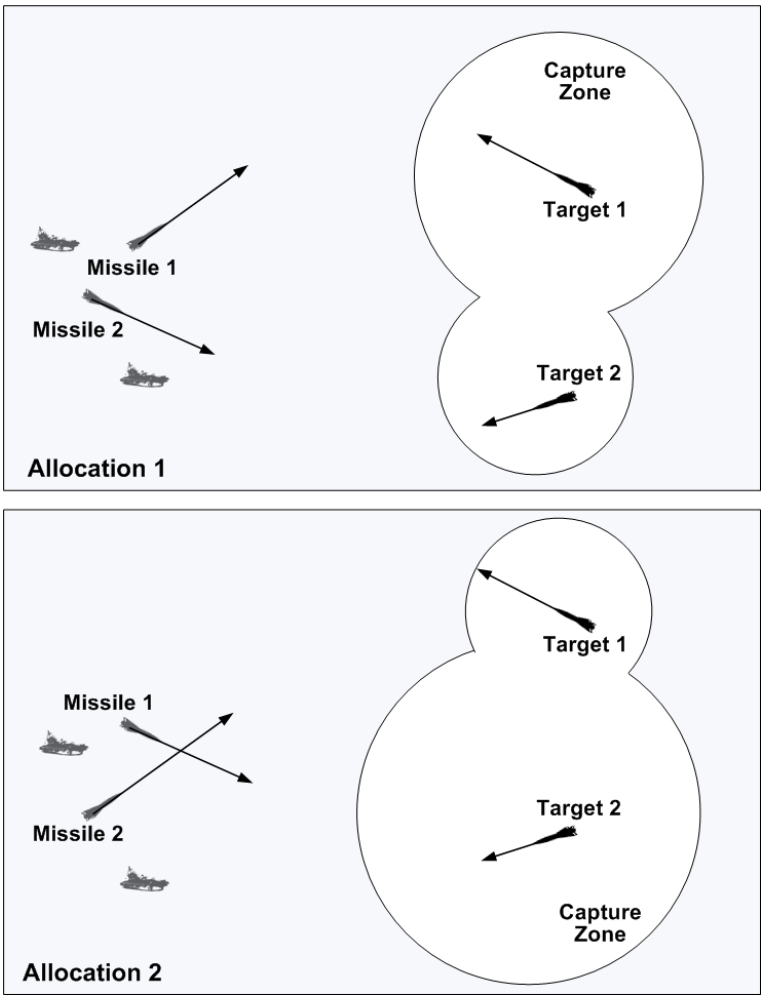

Figure 4.4: Change of the capture zone in accordance with allocation plans

- Find the optimal allocation set maximizing the minimum safety distance by using simple algebra

The allocation problem in this study is to obtain an optimal permutation among all possible allocation plans. The number of permutations (allocation plans) is obtained as:

$$
\begin{aligned}
&{}_nP_m \quad \text{for } n \geq m \\
&{}_mP_n \quad \text{for } n < m
\end{aligned}
\tag{4.1}
$$

where n and m denote the number of the missiles and targets, respectively. In consequence, the cooperative guidance problem is interpreted as a game between missiles and targets: the targets are trying to minimize distances between themselves and defended assets, whereas the missiles to maximize these distances.

Therefore, the allocation problem can be addressed as an optimal problem finding the optimal allocation plan maximizing the minimum safety distance, that is a min max problem. The performance index of the optimal allocation problem for the cooperative mid course guidance problem is given by:

$$\min(d_{ij}^k) \quad \text{for} \left(\begin{array}{l} i = 1, \ldots, p; \\ j = 1, \ldots, \min(n, m); \\ k = 1, \ldots, q \end{array} \right. \tag{4.2}$$

where p and q denote the numbers of defended assets and all possible allocation plans, respectively, and d represents the safety distance between the ith asset and the jth intercept geometry of the kth allocation plan. If each missile uses the EIGGL, d_{ij}^k can be analytically derived as:

$$\begin{aligned} d_{ij}^k &= \sqrt{\left(\boldsymbol{p}_i - \boldsymbol{c}_j^k\right)^T \left(\boldsymbol{p}_i - \boldsymbol{c}_j^k\right)} - r_{Ej}^k \\ r_{Ej}^k &= \frac{\gamma_j^k r_j^k}{1 - \left(\gamma_j^k\right)^2} \end{aligned} \tag{4.3}$$

where $\boldsymbol{p}_i$ denotes the position vector of the ith defended asset, and $\boldsymbol{p}_i$ and r_{Ej}^k are the position vector of centre and radius of the jth EIG of the kth allocation plan, respectively. However, if the IGGL is applied to each missile, we need to calculate the safety distance numerically. In order to reduce the computational load, we evenly select several points of each intercept geometry and calculate the safety distances.

Figure 4.5 illustrates the concept of the proposed optimal allocation algorithm for a simple engagement scenarios: two missiles protect a asset against two incoming treats (targets). The minimum safety distance in the first allocation is d_{11}^1, the distance between the defended asset and the first target. In the second allocation, the minimum distance is the distance with the second target, d_{12}^2. Since d_{11}^1 is greater than d_{12}^2, the optimal allocation plan for this scenario is the first allocation in this scenario.

It is important to consider where the target is likely to head in the area defence. This problem can be resolved using the current heading angle of the target: if an incoming threat is directly heading for a defended asset, then the target is likely to strike the defended asset; on the contrary to this, if an incoming threat is heading

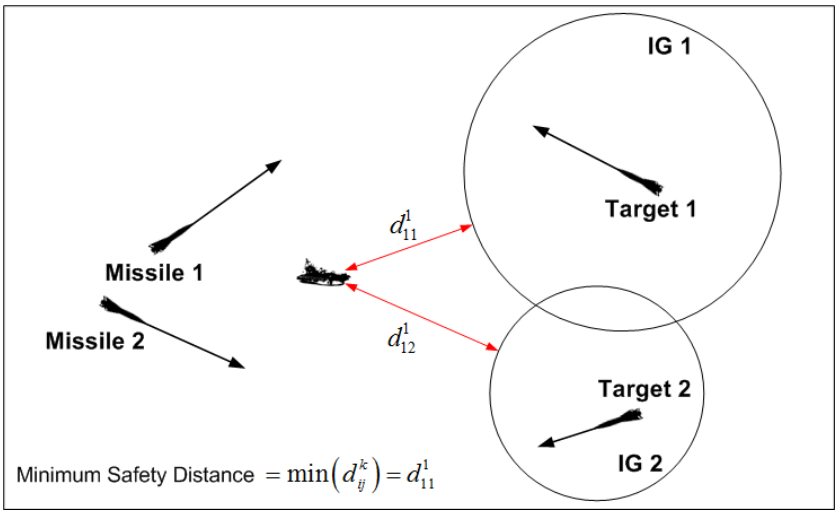

(a) First allocation

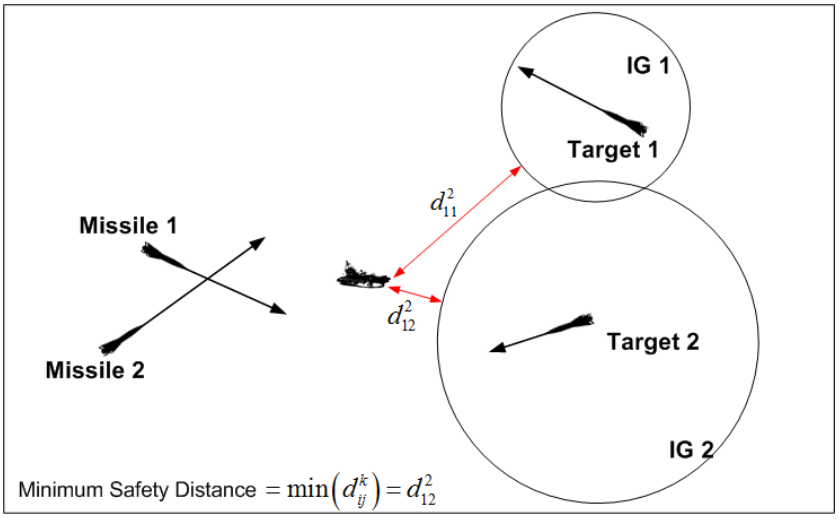

(b) Second allocation

Figure 4.5: Illustration of the concept of the optimal allocation algorithm

for the opposite direction to a defended asset, the incoming threat is not likely to attack the defended asset. In order to consider this striking tendency of the targets in the allocation algorithm, a weighting function is introduced as:

$$W_{ij}^k = \exp\left[-\xi\left(\boldsymbol{p}_i - \boldsymbol{c}_j^k\right) \cdot \boldsymbol{v}_j\right] \tag{4.4}$$

where ξ is a design parameter to adjust the effect of the striking tendency of the incoming threat (target) and $\boldsymbol{v}_j$ is the velocity vector of the jth target. Using this weighting factor, we propose another performance index in the form of:

$$\min(W_{ij}^k \, d_{ij}^k) \tag{4.5}$$

As the optimal allocation problem with the performance index represented in

Equation (4.2). this optimal problem is to find an optimal allocation plan maximizing the cost function derived in equation Equation (4.5).

4.2 Numerical Examples

The proposed cooperative guidance algorithm is verified by numerical simulations. In numerical examples, three different scenarios are considered: the first one is a 2x2 engagement scenario with two defended assets, the second one is another 2x2 engagement scenario, and another is a 3x3 engagement scenario with three assets. Two different 2x2 engagement scenarios are considered to evaluate the effect of the weighting factor on the allocation plan. The target is assumed to use PN guidance after 5 seconds in all scenarios. For the simplicity, we implemented only the EIGGL and the optimal allocation algorithms with two proposed cost functions to the missiles. However, the IGGL can readily replace the EIGGL. In the simulation results, small diamonds represent the initial positions of the missiles, circles the initial positions of the targets, quadrangles the asset positions, and red dashed lined circles are EIGs of the optimal allocation plan at the initial time. Abbreviations 'T' and 'M' stand for the target and missile (named as just missile in the simulation results). For example, 'T1' and 'M2' represent the first target and the second missile.

The simulation results of the first scenario are shown in Figures 4.6 and 4.7. As shown in the figures, the first missile is allocated to the second target and the second missile to the first target in the optimal allocation algorithms with both performance indices. Furthermore, it is shown that the proposed cooperative mid course guidance law effectively achieves the area air defence. Since both targets are heading for their own target in two optimal allocation plans, there exist no differences between them. In order to compare them, another scenario is considered; all initial conditions in the second scenarios remain the same as in the first scenario, but the heading angles of the second target are different. Figures 4.8 and 4.9 depict the simulation results of the second scenario. As shown in figures, the missiles protect the assets and switch the allocation in order to optimize the distances. However, the patterns of two optimal allocation algorithms are different: the frequency of chattering of the second allocation algorithm is higher than the first one. The first target is heading for the opposite direction to the both

assets. Therefore, it is more reasonable that the both missiles are trying to intercept the second target at the beginning of the mid course phase as shown in Figure 4.8(b) and 4.9(b). In order to consider more complicated engagement situation, the third scenario is considered. Figure 4.10 and 4.11 represent the results of the numerical simulation of the third scenario. In the simulation results, it is shown that the cooperative mid course guidance laws with the two performance indices can defend the area even in a complicated engagement condition. Due to the weighting factor in the second performance index, the optimal allocation plan in the second cooperative guidance algorithm (the algorithm considering the second cost function) is different to the allocation plan of the first one (the one implementing the first performance index).

Now, let us check the property of the optimal allocation plan. Figure 4.12 shows the minimum distances between targets and assets: the left one applied the first optimal allocation algorithm (first performance index) and the right one did an arbitrary allocation plan (the first, second, and third targets are respectively allocated to the first, second, and third missiles). As represented in the figure, the first proposed allocation algorithm maximizes its performance index, the minimum safety distance between the targets and assets without considering the weighting factor.

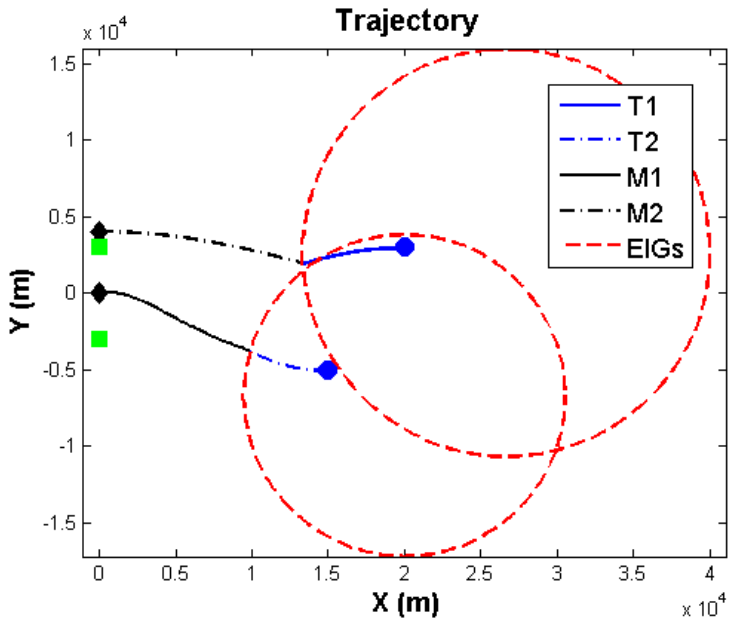

(a) First performance index

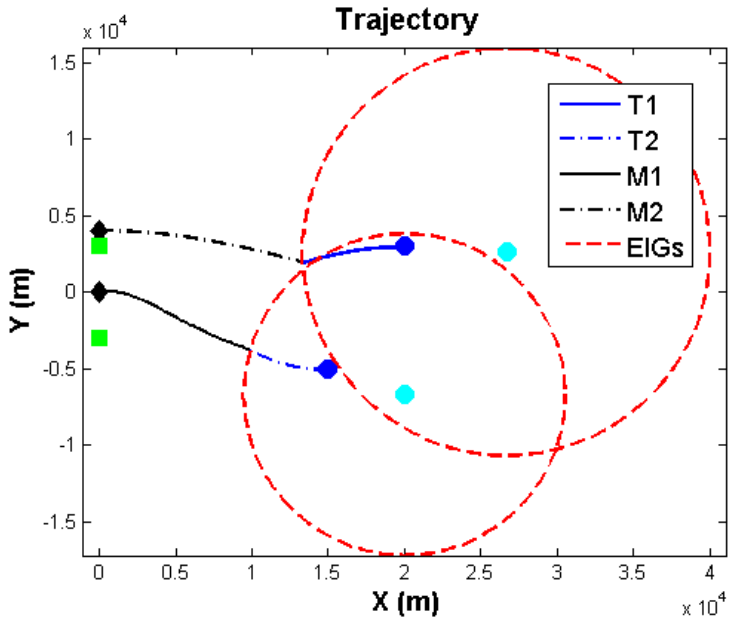

(b) Second performance index

Figure 4.6: Trajectories in the first scenario

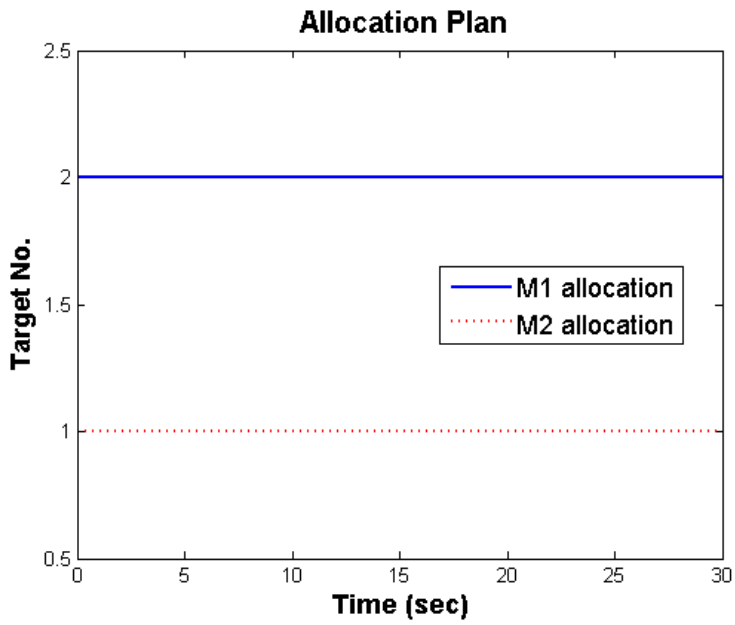

(a) First performance index

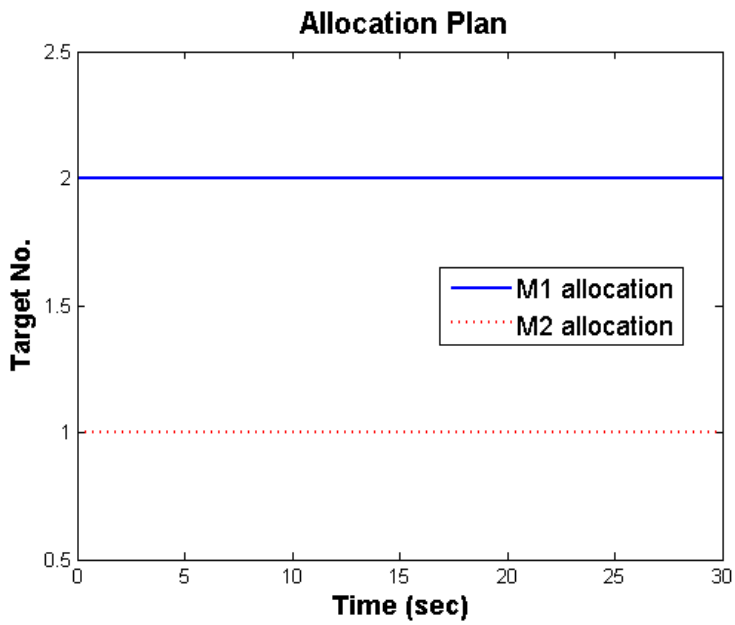

(b) Second performance index

Figure 4.7: Allocation plan in the first scenario

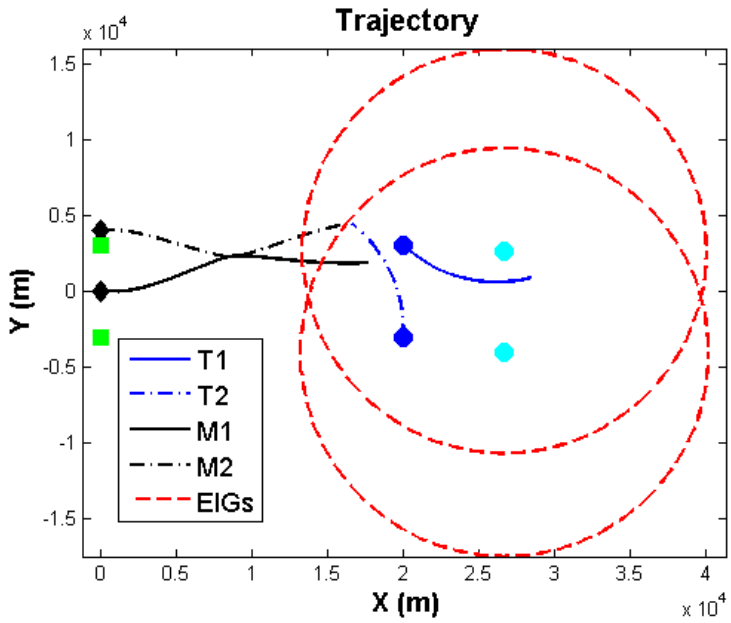

(a) First performance index

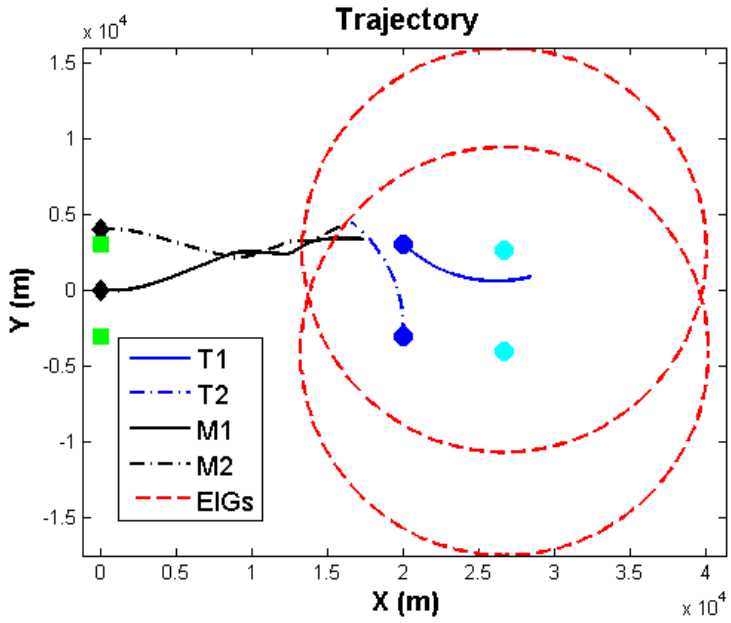

(b) Second performance index

Figure 4.8: Trajectories in the second scenario

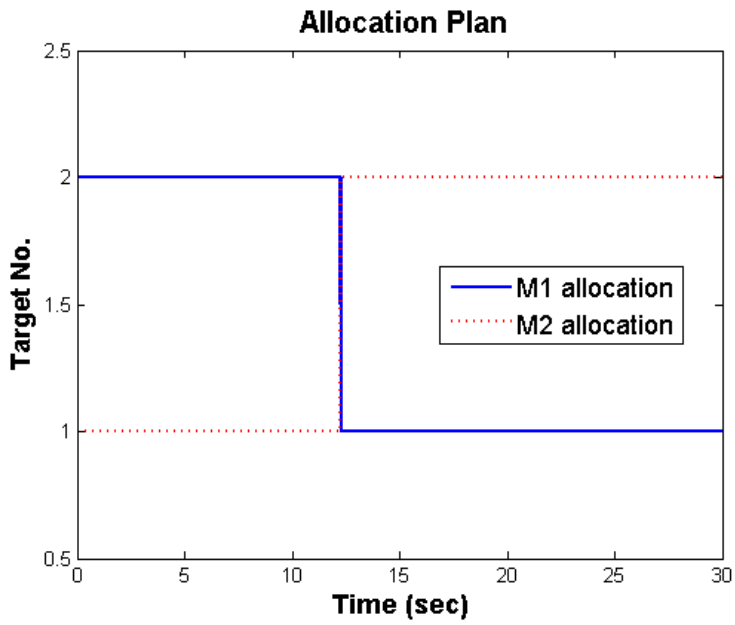

(a) First performance index

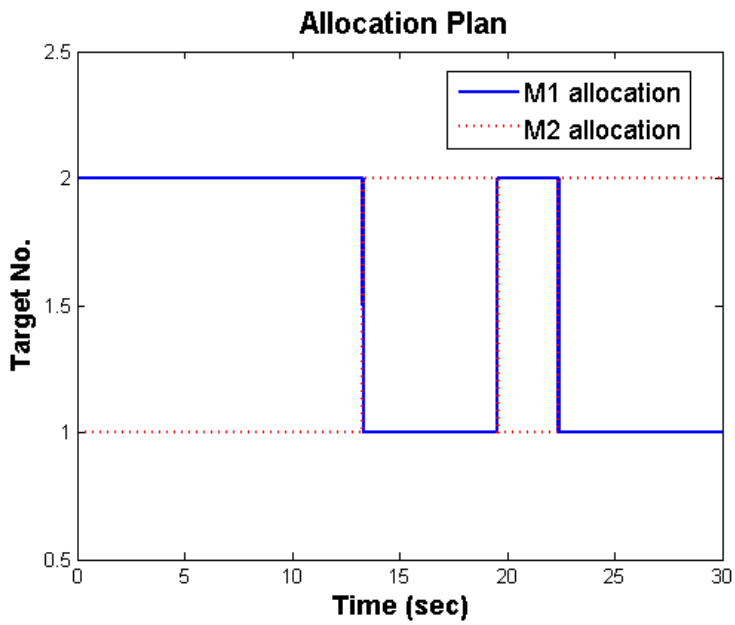

(b) Second performance index

Figure 4.9: Allocation plan in the second scenario

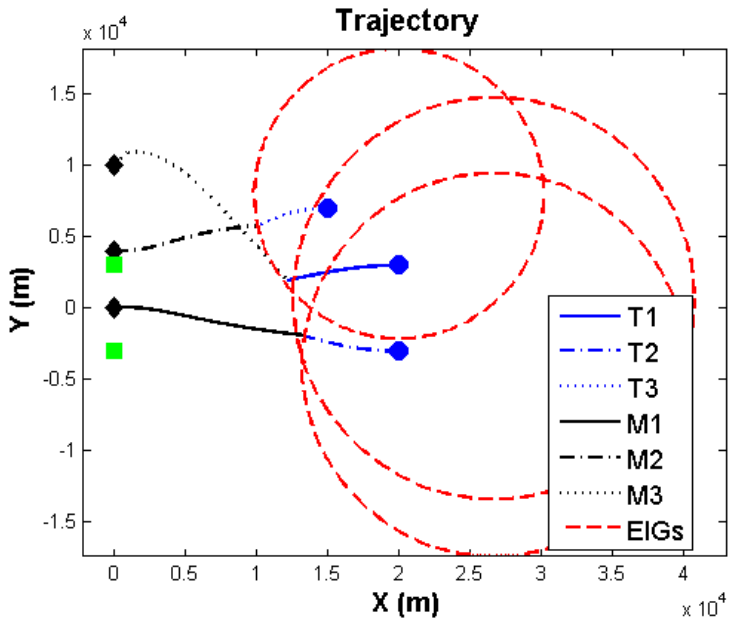

(a) First performance index

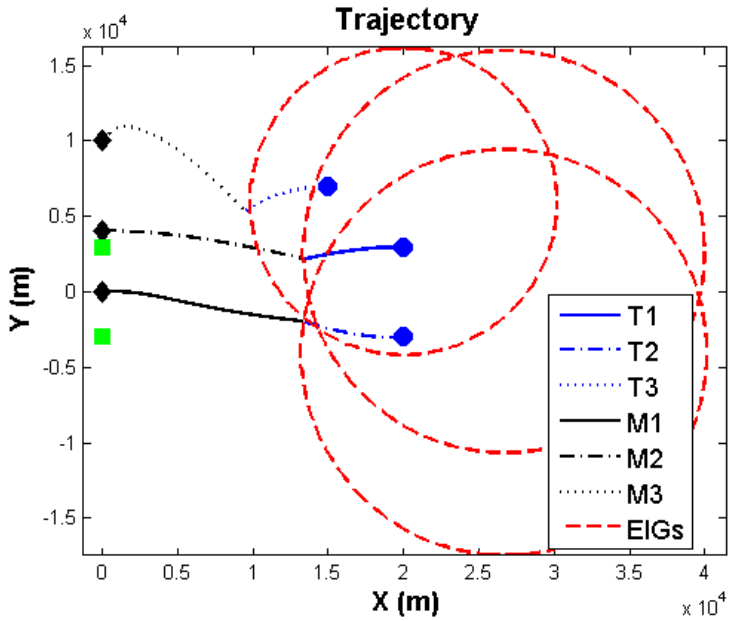

(b) Second performance index

Figure 4.10: Trajectories in the third scenario

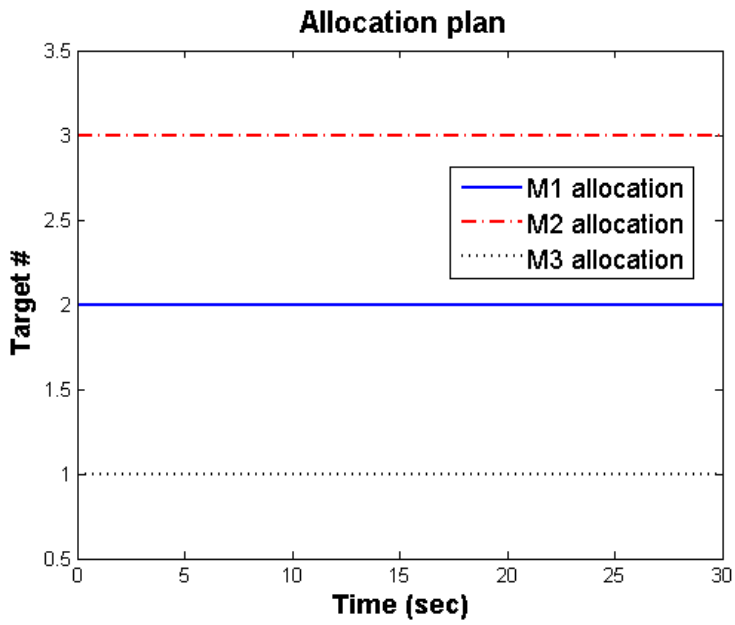

(a) First performance index

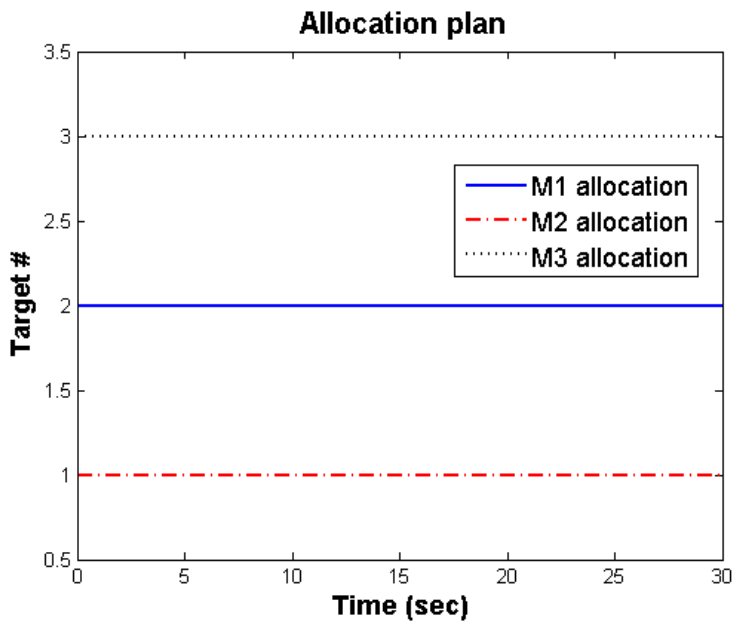

(b) Second performance index

Figure 4.11: Allocation plan in the third scenario

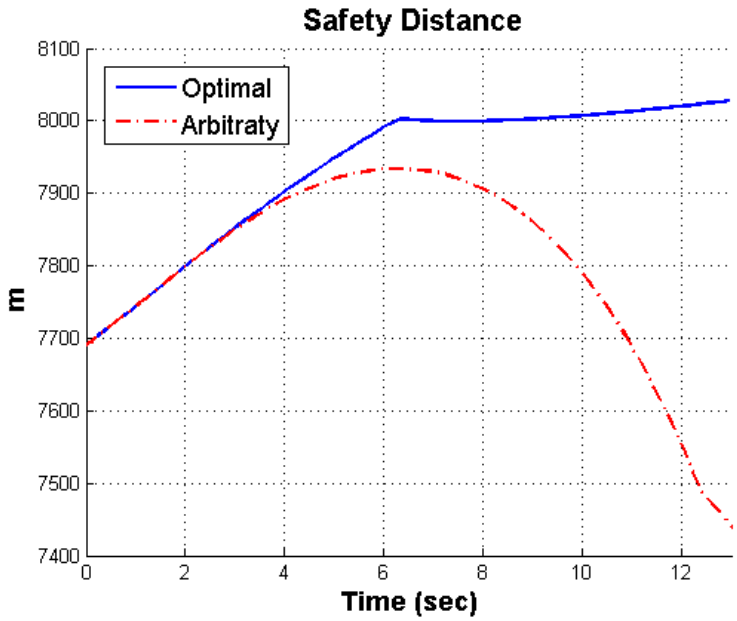

Figure 4.12: Comparison of the safe distances of two allocation plans (First one: applied the optimal allocation algorithm with the first performance index, second one: the first one allocated to the first one, the second one to the second, and the third one to the third)

Chapter 5

Terminal Homing Guidance Law

In the previous chapters, the mid course guidance laws were designed not only to guarantee the intercept of the targets and area air defence, but also to provide better engagement conditions to the terminal homing phase. Now, let us consider the terminal homing guidance.

Any initial angular deviation of the missile from the collision course is known as heading error. It dominantly generates the acceleration command at the initial phase of the terminal homing phase. Therefore, the mid course guidance law is generally designed to reduce the heading error. In practice, however, the homing guidance usually encounters the initial heading error because of different respective hypotheses of future target trajectory in mid course and homing guidance laws. In other words the two guidance laws attempt to drive to zero their own specific versions of heading error. On handover, the mid course guidance version of heading error has approached zero but the homing guidance version will be different, potentially larger.

If terminal homing guidance laws are sensitive to the heading error, the initial angular error results in an abrupt change of the missile acceleration at the beginning of the terminal homing phase. This phenomenon is a undesirable for the terminal homing guidance. A sudden change of the acceleration also causes an abrupt transition manoeuvre. This problem can be alleviated by reducing heading error sensitivity of the homing guidance.

To reduce the heading sensitivity at the beginning of the homing phase, a new performance index is introduced to the optimal control problem. The proposed performance index is formulated with a second order time-to-go weighted polynomial, so that it is possible to distribute the weighting over the flight. This allows the proposed guidance law not only to alleviate the sensitivity of the heading error but also to take into account other important considerations such as small acceleration at the end of the homing phase.

5.1 Motivation

Figure 5.1 shows the two dimensional engagement geometry of a point mass missile and target. In this figure, subscripts $_M$ and $_T$ on the parameters denote

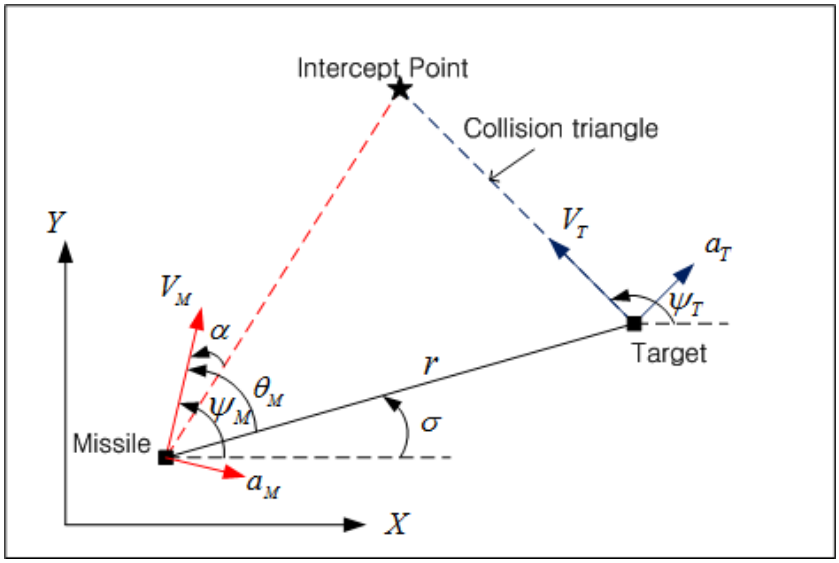

Figure 5.1: Terminal homing guidance geometry

where the motion information belong. For example, $(x_M,\ y_M)$ and V_T denote the position vector of the missile and the target velocity. The flight path angle and line-of-sight angle with respect to the inertial reference frame are denoted as ψ and σ , respectively. a_M and a_T denote the accelerations of the missile and target, which act in perpendicular to the velocity vectors and change the direction of their velocities. It is assumed that the missile system is regarded as a lag-free system and its speed is a constant during the engagement. The flight path angle with respect to the initial LOS is given by

$$\theta_M = \psi_M - \sigma \tag{5.1}$$

If the missile and target continue to fly along a straight line on a collision triangle with constant velocities, the missile will hit the target. In this case, we can calculate the lead angle which is the desired initial flight path angle of the missile with respect to the LOS for the intercept

$$\theta_M^* = \sin^{-1}\left[\frac{V_T \sin\left(\psi_T(t_0) - \sigma\right)}{V_M}\right] \tag{5.2}$$

However, it is difficult to predict an expected intercept point due to different respective hypotheses of future target trajectory in mid course and homing guidance laws. Therefore, the terminal homing guidance generally has heading error at the beginning of the homing phase, so that it is important to reduce the sensitivity to the heading error.

Let us examine the heading sensitivity of the PN guidance law. The PN guidance laws have been widely used for the homing guidance phase and the most common PN law can be represented as

$$a_{PN} = -NV_c\dot{\sigma} \approx -N\left(\frac{y + \dot{y}t_{go}}{t_{go}^2}\right) \tag{5.3}$$

where N is the effective navigation constant, also called the guidance gain, V_c the closing velocity, and $\dot{\sigma}$ the LOS rate. The position error in y-axis and its first time derivative are denoted as y and $\dot{y}$. For the zero initial position error in (5.3) and a small initial angle α, the initial acceleration command is obtained as

$$a_{PN}(t_0) \approx -N\frac{V_c\alpha}{t_f - t_0} \tag{5.4}$$

where α denotes the heading error given by

$$\alpha = \theta_M^* - \theta_M(t_0) \tag{5.5}$$

It indicates that the initial acceleration command the PN guidance law issues abrupt transition of the acceleration command at the handover point, unless the initial heading error α is zero. The acceleration command in Equation (5.4) is proportional to the effective navigation constant N. If we adjust N rather than applying a navigation constant, it should be possible to alleviate an abrupt acceleration transition caused by an initial heading error. Therefore, time varying $N(t)$ will be derived to reduce the sensitivity to the heading error.

5.2 New PN Guidance Law

The relative position between the missile and target on y axis and its time derivative are given by:

$$y(t) = y_T(t) - y_M(t), \tag{5.6}$$

$$\dot{y}(t) = \dot{y}_T(t) - \dot{y}_M(t). \tag{5.7}$$

The state equation is, then, obtained as

$$\dot{\boldsymbol{x}} = A\boldsymbol{x} + Bu \tag{5.8}$$

where

$$\boldsymbol{x} \equiv [x_1,\ x_2]^T = [y,\ \dot{y}]^T, \tag{5.9}$$

and

$$A = \begin{bmatrix} 0 & 1 \\ 0 & 0 \end{bmatrix}, \quad B = \begin{bmatrix} 0 \\ 1 \end{bmatrix}. \tag{5.10}$$

The control input is regarded as the missile acceleration command, $u = -a_M$.

Now, let us consider following optimal control problem: find optimal control command $u(t)$ which minimizes the performance index defined by:

$$J = \frac{1}{2}\int_{t_0}^{t_f} \frac{1}{2}u^T(s)R(t_f - s)u(s)\,\mathrm{d}s, \tag{5.11}$$

subject to Equation (5.8) with terminal constraints in Equation (3.26). For a constant weighting function R equal to 1, if the target is non-manoeuvring and has a constant speed, the optimal solution minimizing the performance index (5.11) is identical to (5.3) with $N = 3$. Substituting a multiplicative inverse for the time-to-go, $\left(t_f - t\right)^{-m}$, into the weighting function yields the optimal solution (5.3) with $N = 3, 4, 5, \cdots$ for $m = 1, 2, 3, \cdots$. In these guidance laws, the effective navigation gain is a constant throughout the flight time.

A new weighting function, which is the form of second order polynomials with time-to-go, is introduced to reshape the control command during the flight

$$R(t_f - s) = \mu_1^2(t_f - s - \mu_2)^2 + 1 \tag{5.12}$$

where μ_1 and μ_2 are the distribution parameters to be designed, and $t_{go}(= t_f - t)$ is time-to-go. Normalizing the weighting function in Equation (5.13) to the time of the flight t_f yields

$$\bar{R}(\tau) = \eta_1^2(\tau - \eta_2)^2 + 1 \tag{5.13}$$

where

$$\tau = \frac{t}{t_f}, \quad \eta_1 = \mu_1 t_f, \quad \eta_2 = 1 - \frac{\mu_2}{t_f} \tag{5.14}$$

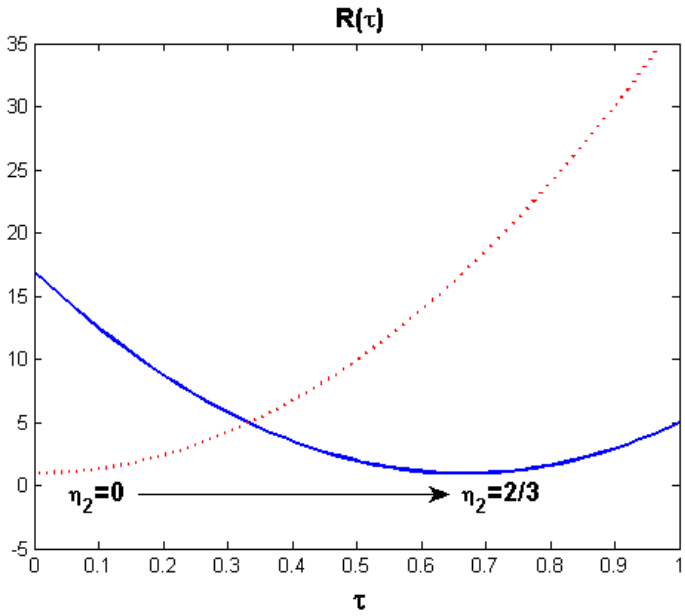

Figure 5.2: Weighting functions $\bar{R}$ for $t_f = 6$: the red dotted line is for $\eta_2 = 0$ and the blue solid line for $\eta_2 = 2/3$

Note that we can simply regulate the weighting on the control input profile with respect to the flight time t_f by tuning two parameters, η_1 and η_2. Figure 5.2 illustrates an example for $t_f = 6$. As shown in the figure, the weighting at the beginning of the homing phase can be released by choosing small η_2. If the initial weighting is greater than the weightings in other interval over the flight, the derived effective navigation gain at the beginning will be smaller than others over the flight. Therefore, introducing the performance index ,Equation (5.13), can allow the homing guidance not only to reduce heading sensitivity at the beginning of the terminal homing phase, but also to take into account the robustness at the end of the homing phase.

In this quadratic problem, we can derive the optimal control law by using the sweep method considering the normality and the convexity condition (Bryson & Ho, 1975) as

$$u^*(t) = K(F\boldsymbol{x} - E) \tag{5.15}$$

where

$$K = \bar{R}^{-1}B^TFG^{-1} \tag{5.16}$$

$$\dot{F} = -A^TF; \quad F(t_f) = D^T, \tag{5.17}$$

$$\dot{G} = F^TB\bar{R}^{-1}B^TF; \quad G(t_f) = 0. \tag{5.18}$$

where the matrix D is given in Equation (3.26). Integrating Equation (5.17) yields,

$$F = \begin{bmatrix} 1 \\ t_f(1-\tau) \end{bmatrix}, \tag{5.19}$$

Substituting this equation, B matrix in Equation (5.10) and Equation (5.13) into Equation (5.18) yields

$$G(t) = -\int_{\tau}^{1} \frac{t_f(1-\tau)^2}{\eta_1^2(\tau-\eta_2)^2+1}\, \mathrm{d}\tau. \tag{5.20}$$

Using simple algebra, Equation (5.20) is obtained as

$$G(\tau) = -\frac{t_f^3}{\eta_1^3}\left\{\eta_1(1-\tau)+\eta_1(\eta_2-1)\ln\frac{\bar{R}(1)}{\bar{R}(\tau)}+(\bar{R}(1)-2)\tan^{-1}\frac{\eta_1(1-\tau)}{1+\eta_1^2(\eta_2-\tau)(\eta_2-1)}\right\}. \tag{5.21}$$

Letting $t \to 0$ and $t_f \to t_{go}$, one can obtain the closed form solution. Thus, from Equation (5.19) and Equation (5.21), the navigation gain K is given by

$$K = \frac{t_{go}}{\bar{R}(0)G(0)}. \tag{5.22}$$

Substituting Equation (5.22) and Equation (5.19) into Equation (5.15), the closed-form guidance command is written by

$$u^*(t_0) = -\bar{N}\left(\frac{y_0}{t_{go}^2}+\frac{\dot{y}_0}{t_{go}}\right), \tag{5.23}$$

where

$$y_0 = y(t_0), \quad \dot{y}_0 = \dot{y}(t_0). \tag{5.24}$$

and

$$\bar{N} = \frac{\bar{\eta}_1^3}{\bar{R}(0)\left\{\bar{\eta}_1+\bar{\eta}_1(\bar{\eta}_2-1)\ln\frac{\bar{R}(1)}{\bar{R}(0)}+(\bar{R}(1)-2)\tan^{-1}\frac{\bar{\eta}_1}{1+\bar{\eta}_1^2\bar{\eta}_2(\bar{\eta}_2-1)}\right\}}. \tag{5.25}$$

In Equation (5.25), $\bar{\eta}_1$ and $\bar{\eta}_2$ are define by

$$\bar{\eta}_1 = \mu_1 t_{go}, \quad \bar{\eta}_2 = 1 - \frac{\mu_2}{t_{go}}. \tag{5.26}$$

From the duality properties, we have

$$\bar{R}(0) = R(t_{go}), \quad \bar{R}(1) = R(0). \tag{5.27}$$

Hence

$$\bar{N} = \frac{\mu_1^3 t_{go}^3}{R(t_{go})\left\{\mu_1 t_{go} + \mu_1\mu_2 \ln \frac{R(t_{go})}{R(0)} + (R(0)-2)\tan^{-1}\varsigma(t_{go})\right\}} \tag{5.28}$$

$$\varsigma(t_{go}) = \frac{\mu_1 t_{go}}{1 - \mu_1^2\mu_2(t_{go} - \mu_2)} \tag{5.29}$$

As shown in Equation (5.28), since the effective navigation gain of the proposed guidance law is varying, the guidance command profile can be controlled. Therefore, the proposed guidance law can simultaneously achieve design requirements on miss distance and heading sensitivity by selecting an appropriate set of the design parameters, $\mu = (\mu_1,\ \mu_2)$.

5.3 Analysis of the guidance law

From Equation (5.28), it is clear that the effective navigation gain of the proposed gain is varying over the flight. When t_{go} converges to 0, we can prove the navigation gain converges to 3 by applying L'Hôspital's rule to Equation (5.28)

$$\lim_{t_{go}\to\infty} \bar{N} = 3. \tag{5.30}$$

For $R(\tau) = 1$, the guidance command in Equation (5.23) is given by

$$u^* = -3\left(\frac{y_0}{t_{go}^2} + \frac{\dot{y}_0}{t_{go}}\right) = a_{PN}. \tag{5.31}$$

This control law is well known as the PN guidance law with the navigation gain of 3. Note that the proposed guidance law becomes identical to conventional PN guidance as the missile homes to the intercept point.

Now, let us examine the effect of μ_1 and μ_2 on the guidance law. If μ_1 is equal to zero in the weighting function $R(t_{go})$, the optimal can be derived as following equation since $R(t_{go})$ is constant

$$\lim_{\mu_1 \to 0} u^* = -3\left(\frac{y_0}{t_{go}^2} + \frac{\dot{y}_0}{t_{go}}\right) = a_{PN}. \tag{5.32}$$

As shown in Equation (5.32), it is identical to the conventional PN guidance law. For $\mu_2 = t_f$, the equivalent gain is obtained as

$$\lim_{\mu_2 \to t_f} \bar{N} = \frac{\kappa^3}{\kappa - \kappa \ln(\kappa^2 + 1) + (\kappa^2 - 1)\tan^{-1}\kappa}, \tag{5.33}$$

where $\kappa = \mu_1 t_{go}$. Since the weighting function is getting larger as the missile approaches the intercept point, the equivalent navigation gain at the beginning of the homing phase is bigger than 3 and converges to 3 at the end of the homing phase. On the other hand, when μ_2 is equal to zero, the weighting becomes smaller as the missile comes closer to the target, and the equivalent navigation gain is derived as

$$\lim_{\mu_2 \to 0} \bar{N} = \frac{\kappa^3}{(\kappa^2 + 1)(\kappa - \tan^{-1}\kappa)}, \tag{5.34}$$

In this case, the equivalent navigation gain is smaller than or equal to 3 over the flight and it converges 3.

5.4 Numerical Examples

In order to analyse the performance of the proposed guidance law, the adjoint method is first applied. Figure 5.3 shows the block diagram of the adjoint simulation model of single-lag guidance system. In the figure, V_c, T and δ denote the closing velocity, time constant and impulse function. The heading error and miss distance and target acceleration are denoted HE, MHE, and MNT respectively. For the adjoint simulation, it is assume that target is non-manoeuvring, the closing velocity is $1000m/s$, initial heading error -5deg, and the flight time $6sec$. The results of the adjoint simulation for $\mu_1 = 0.3$ and $\mu_2 = 0, \ldots, t_f$ are shown in Figure 5.4. From Figure 5.4, it is clear that the performance of the proposed guidance law is similar to that of PN guidance when the flight time is less than

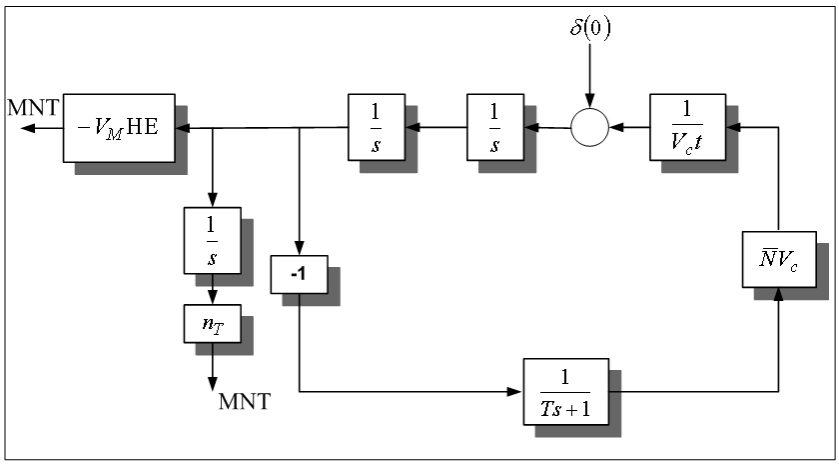

Figure 5.3: Block diagram of the adjoint simulation model (single-lag)

Table 5.1: Initial conditions for the terminal homing guidance simulation

	Position	Heading Angle	Velocity
Missile	$(0\ m, 0\ m)$	$6.7\ deg$	$1000\ m/s$
Target	$(6000\ m, 0\ m)$	$95\ deg$	$600\ m/s$

3 *sec* under the simulation conditions. However, if the flight time is bigger than 3 *sec*, the tendency of the miss distance for the proposed guidance is different and it depends on the value of design parameters $\mu = (\mu_1, \mu_2)$. For $\mu_2 \leq 2$ and $t_f > 3$, the miss distances are bigger than those of PN guidance because the proposed guidance law generates small acceleration. On the other hand, since the proposed guidance law produces large acceleration at a certain region over the flight time, the miss distances are smaller than those of the PN guidance law for $\mu_2 \leq 4$ and $t_f > 3$.

Next, we applied the proposed guidance law to numerical examples to illustrate its performance with various values of μ. Initial conditions for numerical simulations are represented in table 7.2. From the initial conditions, it is clear that the initial heading error is $-30deg$. To examine the effect of the design parameter μ_1, one set of design parameter combinations are considered. In this set, the value of μ_2 is fixed to 3 and $\mu_1 = 0.1, 0, 3, 0.6$. The proposed guidance law is compared with the conventional PN guidance law to fairly evaluate the performance of the proposed guidance law under these simulation conditions. The simulation results are depicted in Figures 5.5, 5.6 and 5.7. The trajectories

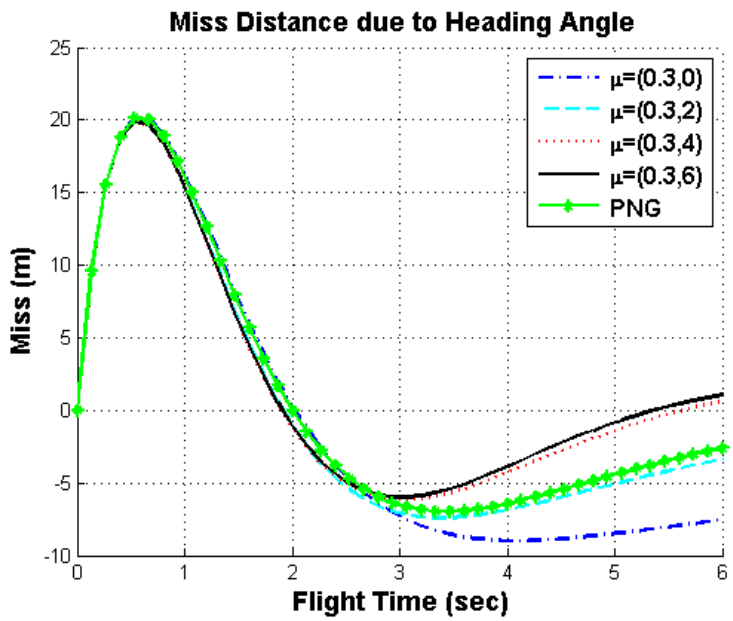

Figure 5.4: Miss distance due to heading error for all flight times

of the missile and targets are illustrated in Figure 5.5. Although the curvatures of the trajectories are slightly different from the one for PN guidance, the proposed guidance law guarantees the interception of the target. Figure 5.6 the profiles of equivalent navigation gains. Increasing the value of μ_1 decreases the gain at the beginning of the homing phase as designed, but it increases the gain at the late homing phase. However, the gain always converges to the effective navigation of the conventional PN guidance law 3 at the end of the homing phased. As shown in Figure 5.7, the acceleration commands generated by various values of μ_1 starts with 94%, 67% and 47% of the initial PN guidance command and converge to the PN guidance command at the end of homing phase. It represents the proposed guidance law can reduce sensitivity to the initial heading error.

To investigate the effect of the design parameter μ_2 to the guidance law, we apply the proposed guidance law with $\mu_1 = 0.3$ and $\mu_2 = 0,\ 3,\ 6$. Figures 5.8, 5.9 and 5.10 shows the results of the numerical simulation. As shown in Fig. 5.8, the proposed guidance law intercepts the target, and modulates the trajectory of the missile in accordance with values of the design parameters. Fig. 5.9 represents the equivalent navigation gains are varying and converges to the gain of the conventional PN guidance law as analysed in section 5.3. However, if μ_1 and μ_2 are respectively equal to 0.3 and 6, the equivalent navigation gain is always

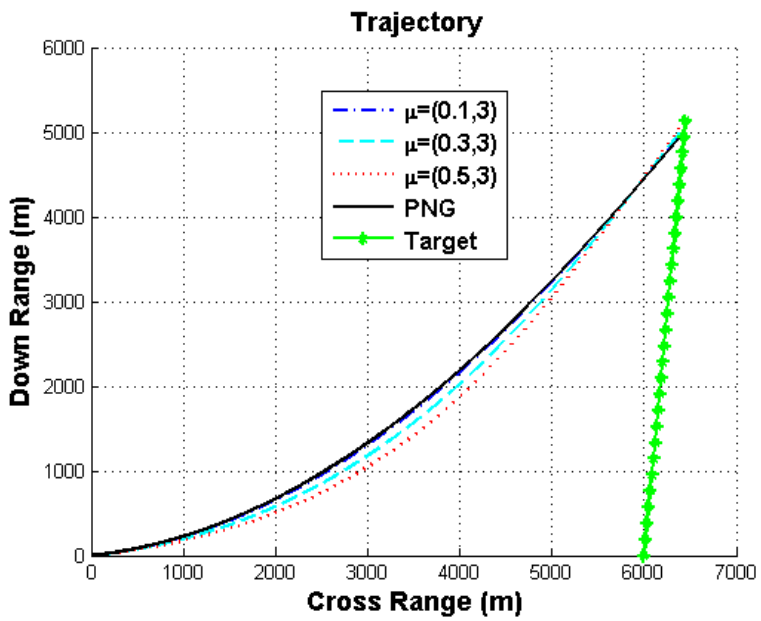

Figure 5.5: Trajectories of the missile and target for the first set of (μ_1, μ_2) combinations

greater than the navigation gain of the PN guidance law, 3, over the flight time. The initial guidance commands are 61%, 67% and 117% of the initial PN guidance command as shown in Fig. 5.10. The proposed guidance with $\mu_1 = 0.3$ and $\mu_2 = 6$ in this numerical example is more sensitive than the conventional PN guidance law. It means that we should select appropriate design parameters, $(\mu_1,\ \mu_2)$ so as not only to reduce alleviate the heading sensitivity, but also to enhance the hit probability.

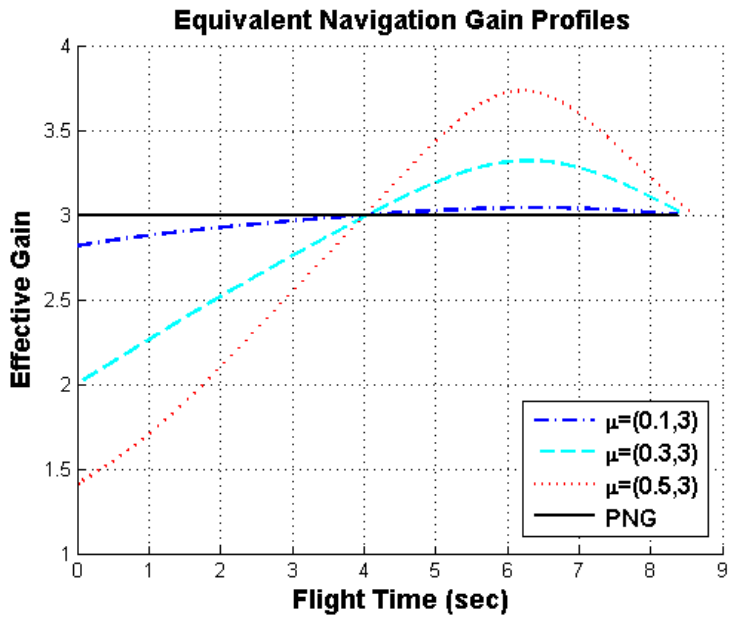

Figure 5.6: Time history of equivalent navigation gains for the first set of (μ_1, μ_2) combinations

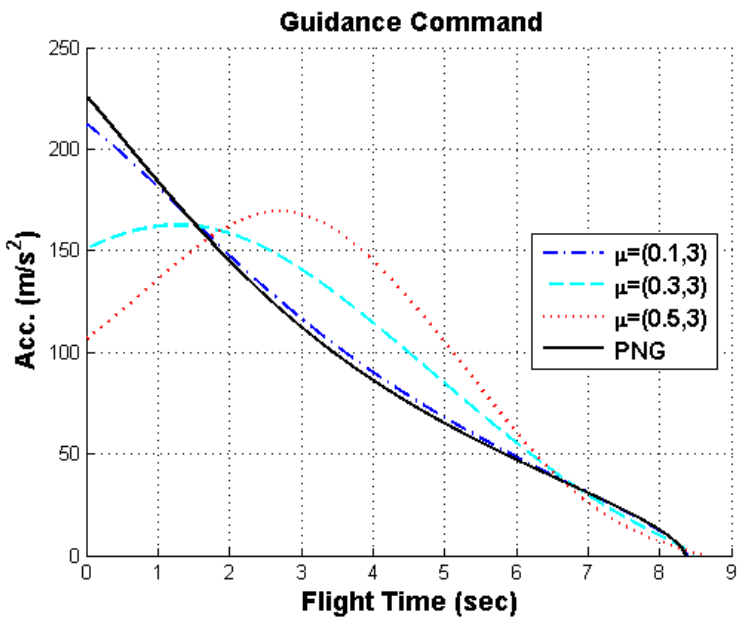

Figure 5.7: Time history of guidance commands for the first set of (μ_1, μ_2) combinations

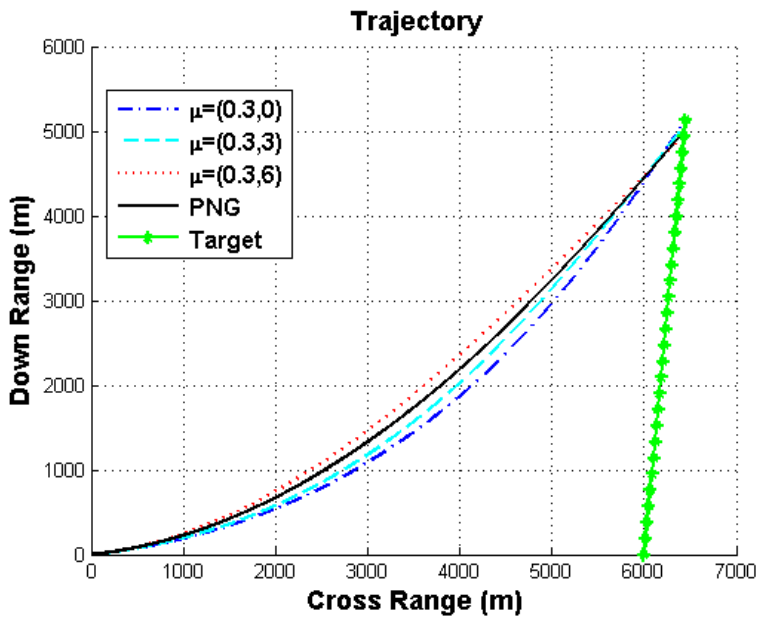

Figure 5.8: Trajectories of the missile and target for the second set of (μ_1, μ_2) combinations

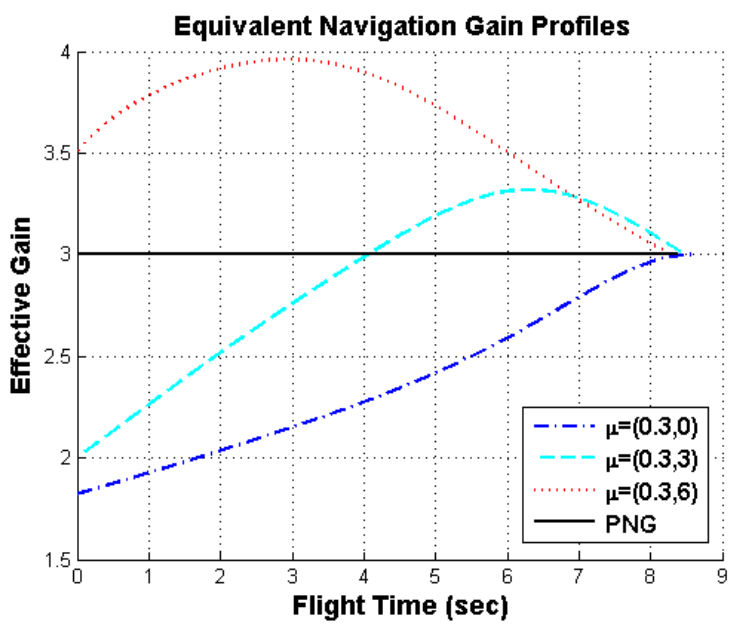

Figure 5.9: Time history of equivalent navigation gains for the second set of (μ_1, μ_2) combinations

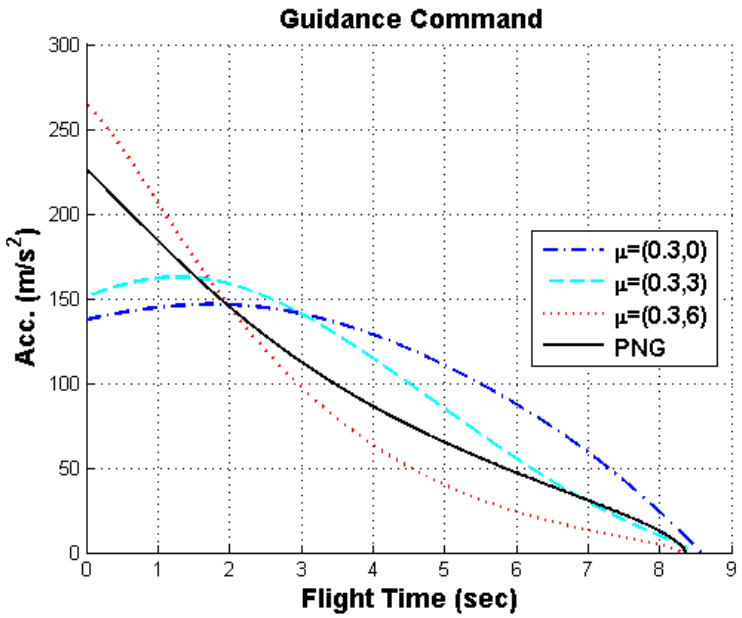

Figure 5.10: Time history of guidance commands for the second set of (μ_1, μ_2) combinations

Chapter 6

Time-to-go Estimation

The linear optimal guidance laws are proposed for the IGGL and terminal homing guidance phase. One of the characteristics of the optimal guidance laws is that they sometimes require accurate time-to-go estimation. In fact, precise time-to-go estimations play important roles in ensuring good performance of the optimal guidance laws. Poor time-to-go estimation not only severely degrades the guidance performance, but also generates the overall trajectory considerably deviated from the optimal one (Hull et al., 1991). The most commonly used time-to-go estimation method is the range over the closing velocity. If the missile uses a PN-type guidance law and is close to the collision path, this estimation is accurate. However, this simple method is erroneous in many engagement situations where the missile trajectory is strongly curved due to big heading error, terminal impact angle constraint, or both. Therefore, in this chapter, an time-to-go estimation algorithm will be introduced to enhance the accuracy of time-to-go estimates.

The time-to-go estimation algorithms can be classified into two categories. In the first category, the time-to-go computation formulae are derived from optimal guidance problems with free terminal time. Although a set of time-to-go equations is a part of the optimal solution, this defies simple solutions. The time-to-go algorithm in the second category tries to provide the best time-to-go estimation possible for a given guidance law.

The second category is more relevant to the optimal guidance laws because the guidance laws have been developed based on the assumption that the flight time is given. In this section, we will address the time-to-go estimation problem of computing better time-to-go estimates especially in the case of strong curvature. Large curvature of the trajectory is major factor contributing to the bad performance. Because the curvature is determined by the guidance command history which can be predicted over the whole flight, we propose a time-to-go estimation algorithm using the guidance command history. As matter of fact, the guidance command has been shown to be represented as a simple function of time-to-go (Zarchan, 1994; Ryoo et al., 2005). Given guidance command profile of the form of time-to-go polynomials, it is possible to obtain time histories of the flight path

angle and position vectors. From the conditions that the missile intercepts the target at the terminal time with some geometrical constraint, we can compute the time-to-go estimate using some optimisation algorithm or zero finding algorithm such as Secant method or Newton method. Since the position vector equations involve the trigonometric functions, the proposed time-to-go estimation algorithm is sensitive to the initial guess of the solutions. For the practical implementation, the sinusoidal functions can be approximated into the polynomial functions of the flight time. If the angle change in the trigonometric functions are big, we approximate these functions around several reference points to reduce approximation error.

6.1 Time-to-go Estimation Using Guidance Command Histories

As shown Equations (3.18) and (3.35) in chapter 3, the linear optimal guidance laws are represented in a form of time-to-go polynomials. Given the constraints of zero miss distance and the terminal impact angle to control the engagement geometry, the general solution of the IAC type guidance problem represented in Equation (3.35) can be rewritten as

$$a_M = t_{go}^N \left(t_{go} C_S + C_R \right), \tag{6.1}$$

for C_S and C_R derived from the definition of u in subsection 3.1.2, and ν_1 and ν_2 in Equation (3.35). For the PN type guidance problem, the optimal guidance command can be also rewritten as

$$a_M = C_S t_{go}^{N+1}, \tag{6.2}$$

A similar result can be found in Zarchan (1994); for $N = 0$ and constant velocities of the missile and target, the optimal control command is obtained as

$$\begin{aligned} a_M =& C_S t_{go}, \\ C_S =& \frac{N' V_C \dot{\sigma}}{t_{go}}, \end{aligned} \tag{6.3}$$

where N' is the effective navigation gain. Note that the guidance law derived in Equation (6.3) is another representation of the conventional PN guidance law.

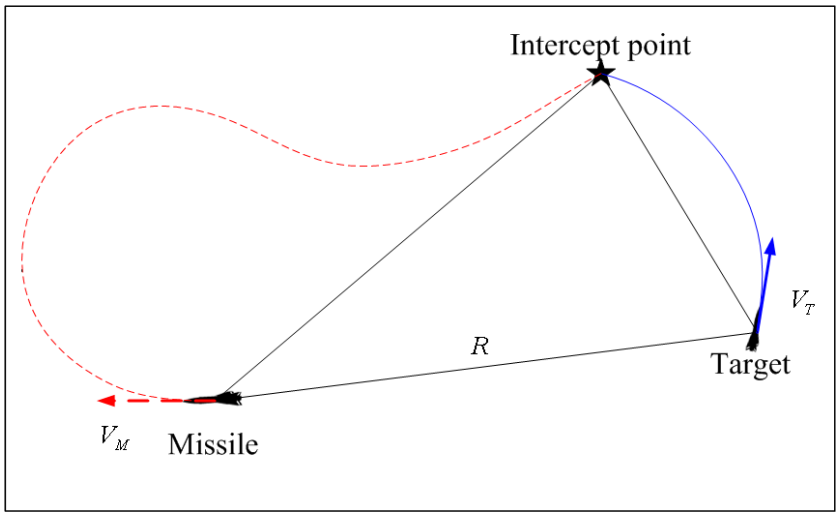

Figure 6.1: Engagement geometry with large initial heading error

The range over the closing velocity, $t_{go} = R/V_C$, provides quite accurate estimation, if the missile applies PN type guidance laws and stays near the collision path. However, this method does not work well when the missile trajectory is considerably curved as shown in Fig. 6.1. Noting that we propose a time-to-go estimation method using time histories of the optimal guidance commands since the curvature of the trajectory is generated by the the guidance command. Indeed, once C_S, C_R and t_f are given, time history of the missile flight path angle can be estimated using the guidance command profile in Equation (6.2):

$$\dot{\psi}_M = \frac{a_M}{V_M}. \tag{6.4}$$

Consequently, Equation (6.4) determines the missile trajectory $(x_M(t)\,, y_M(t))$. The intercept conditions with a terminal impact angle constraint can be represented as

$$\begin{aligned} x_M(t_f) &= x_T(t_f), \\ y_M(t_f) &= y_T(t_f), \\ \psi_M(t_f) &= \psi_T(t_f) + \psi_I. \end{aligned} \tag{6.5}$$

where ψ_I denote the desired terminal impact angle. Assuming the target trajectory is known, three unknown parameters C_S, C_R and t_f can be determined using the three intercept conditions. The solution can be obtained by applying any zero-finding algorithm. Since the guidance command profile is accounted for in the calculation of t_f, the accuracy of the time-go-go estimation is improved.

For the lucid explanation of the details of the proposed time-to-go estimation approach, it is assumed that the velocities of the missile and target are constant. However, this is not a restriction. If a proper functional form of velocity is provided, it can be easily extended to include the effect of the velocity change. The governing equations of the missile in the homing problem are given by

$$\begin{aligned} \dot{x}_M &= V_M \cos\psi_M, \\ \dot{y}_M &= V_M \sin\psi_M, \\ \dot{\psi}_M &= \frac{a_M}{V_M}, \end{aligned} \tag{6.6}$$

with boundary conditions

$$x_M(0) = x_{M0},\ y_M(0) = y_{M0},\ \psi_M(0) = \psi_{M0}, \tag{6.7}$$

$$x_M(t_f) = x_{Mf},\ y_M(t_f) = y_{Mf},\ \psi_M(t_0) = \psi_{Mf}. \tag{6.8}$$

The rate of the flight path angle is given in the form of:

$$\dot{\hat{\psi}}_M(s) = (t_f - s)^N \left\{ C_R + C_S(t_f - s) \right\}, \tag{6.9}$$

for $s \geq t$ and some constant C_R, C_S and t_f. Therefore, we have

$$\hat{\psi}_M(s) = \hat{\psi}_M(t) + \frac{C_R}{N+1}\left\{(t_f - t)^{N+1} - (t_f - s)^{N+1}\right\}, + \frac{C_S}{N+2}\left\{(t_f - t)^{N+2} - (t_f - s)^{N+2}\right\}. \tag{6.10}$$

The position estimates $\hat{x}_M$ and $\hat{y}_M$ are now obtained as

$$\hat{x}_M(s) = x_M(t) + \int_t^s V_M \cos\hat{\psi}_M(s)\ \mathrm{d}s, \tag{6.11}$$

$$\hat{y}_M(s) = y_M(t) + \int_t^s V_M \sin\hat{\psi}_M(s)\ \mathrm{d}s. \tag{6.12}$$

If the target acceleration profile is given as a function of time, we can also compute the target trajectory using the same procedure as in calculating the one of the missile. In our research, for the time-to-go estimation, we use the the target acceleration profile considered to compute the intercept geometries. Now, we define $f = [f_1,\ f_2,\ f_3]$ using

$$\begin{aligned} f_1(t_f, C_R, C_S) &\equiv \hat{\psi}_I(t_f) - \psi_I, \\ f_2(t_f, C_R, C_S) &\equiv x_M(t_f) - x_T(t_f), \\ f_3(t_f, C_R, C_S) &\equiv z_M(t_f) - y_T(t_f), \end{aligned} \tag{6.13}$$

where $\hat{\psi}_I(t_f) = \hat{\psi}_M(t_f) - \hat{\psi}_T(t_f)$ is the terminal impact angle estimated. We can calculate f value by substituting the states of the missile and targets intoEquation (6.13):

$$\begin{aligned} f_1 &= \left\{\hat{\psi}_M(t_f) - \hat{\psi}_T(t_f)\right\} - \psi_I, \\ f_2 &= x_M(t) - x_T(t) + \int_t^{t_f} V_M \cos\hat{\psi}_M(s) - V_T \cos\hat{\psi}_T(s)\ \mathrm{d}s, \\ f_3 &= y_M(t) - y_T(t) + \int_t^{t_f} V_M \sin\hat{\psi}_M(s) - V_T \sin\hat{\psi}_T(s)\ \mathrm{d}s. \end{aligned} \tag{6.14}$$

To meet the intercept conditions, f should be zero. The unknown parameter t_f, C_R and C_S are obtained by applying a optimisation algorithm or some zero finding algorithm such as Secant method or Newton method.

6.2 Computation Issue

The trigonometric integrands in Equation (6.14) can lead to large errors when the initial guess of the solution is far away from the true solution. Furthermore, it might increases computational load of the time-to-go calculation. The Taylor series expansion of the trigonometric integrands can alleviate the problems in implementation issues. However, we should apply Taylor series approximation with care. When the change of current flight path angle is considerably big, it is inadequate to approximate the trigonometric functions about zero as shown in Fig. 6.2. This problem can be alleviated by approximating the integrands about several reference angles as shown in Fig. 6.3.

If we approximate the trigonometric functions into $2nd$ order Maclaurin polynomial around several reference values, the position vector of the missile is represented as:

$$\hat{x}_M(s) = x_M(t) + V_M \sum_{i=1}^{m} \int_{t_{i-1}}^{t_i} MP\left(\cos\hat{\psi}_M(s)\right)\ \mathrm{d}s, \tag{6.15}$$

$$\hat{y}_M(s) = y_M(t) + V_M \sum_{i=1}^{m} \int_{t_{i-1}}^{t_i} MP\left(\sin\hat{\psi}_M(s)\right)\ \mathrm{d}s. \tag{6.16}$$

where $t_0 = t$, MP denotes the $2nd$ order Maclaurin polynomial and m the number of reference points for the Taylor series expansion. The approximated polynomials not only decrease the computational load of the proposed algorithm, but also reduce the sensitivity of the initial guess.

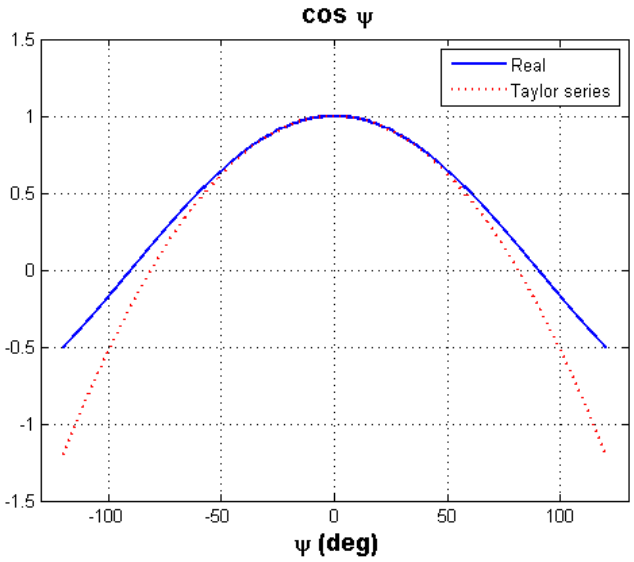

Figure 6.2: Taylor series approximation (2nd order) of $\cos\psi$ *about* $\psi = 0$ *deg*

Table 6.1: Initial conditions for the simulations of the time-to-go estimation algorithm

	Position	Heading Angle	Velocity
Missile	(0 m, 1000 m)	20 or -20 deg	600 m/s
Target	(5000 m, 1000 m)	55 deg	200 m/s

6.3 Numerical Examples

The performance of the proposed algorithm is demonstrated through numerical examples. In the numerical examples, it is assumed that the target velocity is constant and the missile uses the impact angle control guidance command in Equation (3.51) obtained from u in Equation (3.47) with $n = 0$. Initial conditions for nonlinear simulations are represented in table 7.2.

To demonstrate the performance of the proposed time-to-go algorithm, we compare with the most common time-to-go estimation method, R/V_C, and the algorithm proposed by Ryoo et al. (2005), Approximated Length of the Curved Path Over Velocity (ALCPOV). Furthermore, in order to quantify the time-to-go estimate error and analyze its effect on the guidance laws, we introduce two

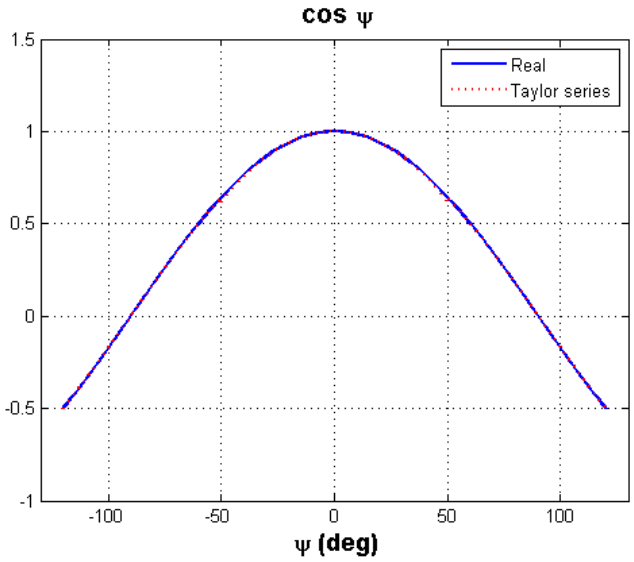

Figure 6.3: Combinations of Taylor series approximations (2nd order) of $\cos\psi$ *about* $\psi = 0$ *deg and* $\psi = \pm 90$ *deg.*

measures

$$J_{t_f} = \frac{\sum \tilde{t}_f(t)\Delta t}{t_f}, \tag{6.17}$$

$$M_{t_f} = \max\left\{|\tilde{t}_f|\right\} / t_f, \tag{6.18}$$

where and Δt is sampling interval and $\tilde{t}_f(t)$ flight time estimation error, which is defined as the error between estimated time of the flight and the the actual total flight time. The meaning of these measures are self evident and we normalize by t_f since the flight time can be different depending on the time-to-go estimation algorithms. Equation (6.17) gives the indication of average performance while Equation (6.18) gives the measure of the worst performance. In tables 6.2 and 6.3, the values of these two measures for the various numerical initial conditions are shown in table 7.2. It is shown that the proposed method generates smaller J_{t_f} and M_{t_f} in the various simulation conditions, i.e., the time-to-go estimation computed by the proposed algorithm is more accurate.

Figures 6.4–6.7 show time histories of the time of flight and the guidance command for the cases of $\psi_I = 10,\ -90(deg)$ and $\psi(t_0) = 20(deg)$. Since the approximated path length is not accurate when the desired impact angle is large, ALCPOV is sometimes less accurate than the range over the closing velocity. The proposed time-to-go estimation method provides better performance than the

Table 6.2: Performance comparison 1: $\left\{\sum \tilde{t}_f(t)\Delta t\right\}/t_f$

ψ_I (deg)	$\psi_M(0)$ (deg)	R/V_C	ALCPOV	Proposed Method
-90	20	0.0213	0.0350	0.0172
	-20	0.5761	1.0606	0.5364
-60	20	0.2205	0.0224	0.0076
	-20	0.3439	0.0970	0.0254
-30	20	0.0954	0.0674	0.0042
	-20	0.3311	0.0296	0.0088
0	20	0.9946	0.1438	0.0301
	-20	1.4226	0.0975	0.0811

range over the closing velocity and ALCPOV as illustrated in Figures 6.4 and 6.6. The trajectories generated by the IAC type guidance law with three time-to-go estimation algorithms are represented in Figures 6.8–6.10 From these figures, it is clear that the time-to-go estimation accuracy also make much effect to the curvature of the trajectory.

Table 6.3: Performance comparison 2: $\max\left\{|\tilde{t}_f|\right\}/t_f, \%$

ψ_I (deg)	$\psi_M(0)$ (deg)	R/V_C	ALCPOV	Proposed Method
-90	20	12.4634	15.0841	6.6930
	-20	12.4634	15.0841	6.6930
-60	20	3.7870	0.3731	0.1058
	-20	7.8665	3.5887	0.7958
-30	20	2.8012	1.5323	0.0496
	-20	8.0019	1.5058	0.0835
0	20	11.6949	3.8956	0.5220
	-20	18.4773	3.7798	3.6328

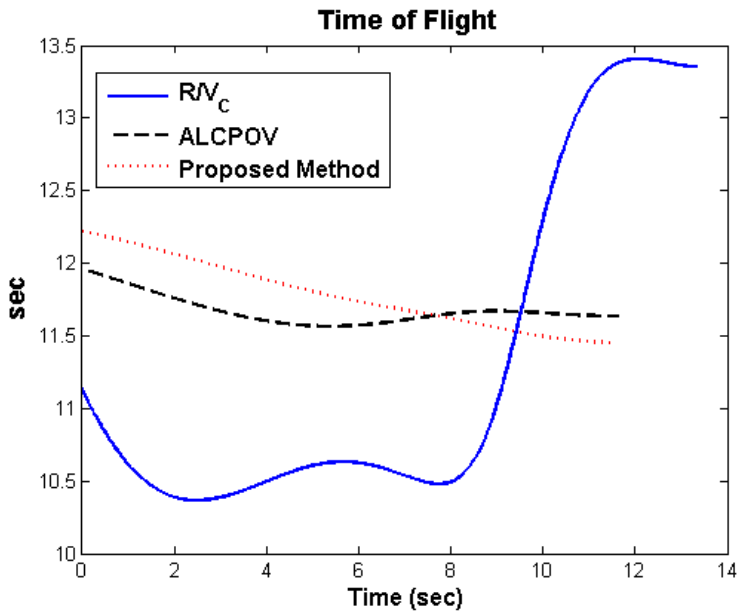

Figure 6.4: Result 1: time-to-go estimation of the optimal IAC guidance law when $\psi_I = 10(deg)$

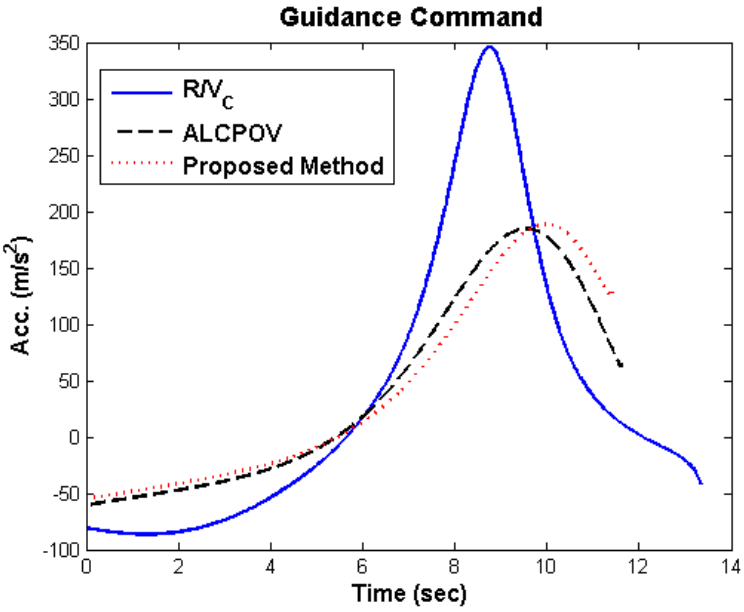

Figure 6.5: Result 1: guidance command history of the optimal IAC guidance law when $\psi_I = 10(deg)$

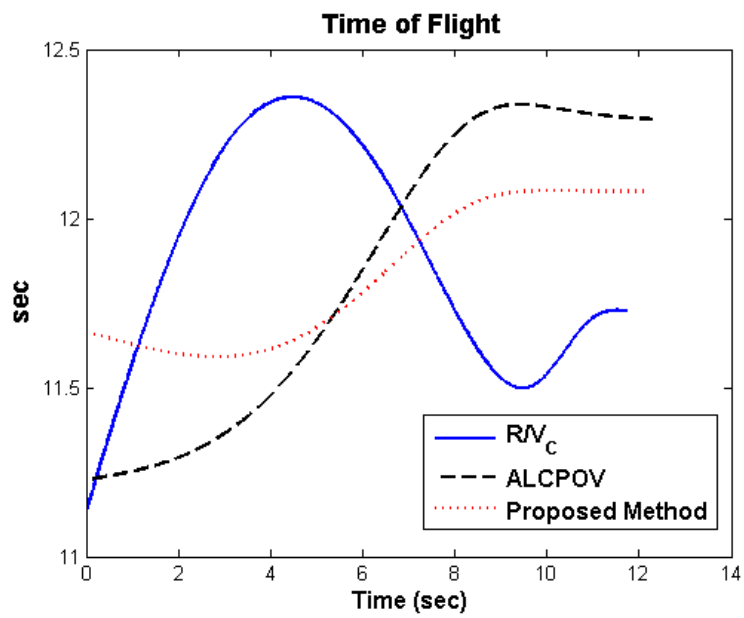

Figure 6.6: Result 2: time-to-go estimation of the optimal IAC guidance law when $\psi_I = 20(deg)$

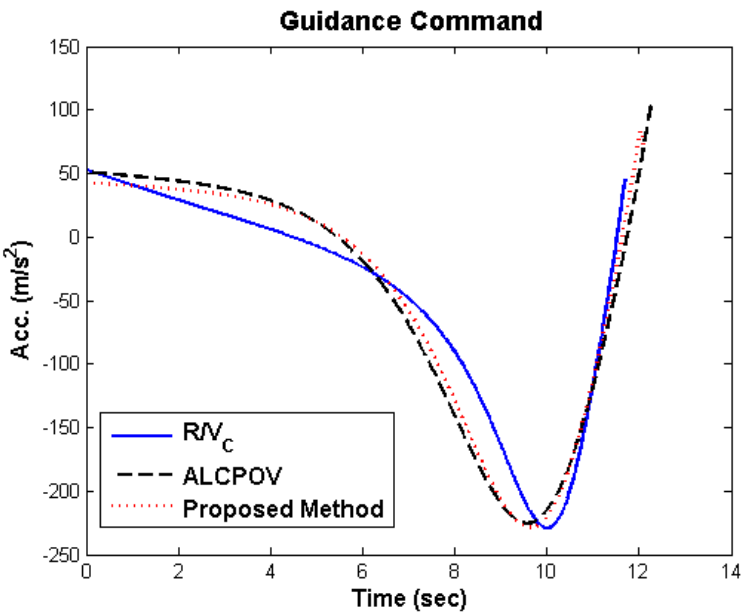

Figure 6.7: guidance command history of the optimal IAC guidance law when $\psi_I = 20(deg)$

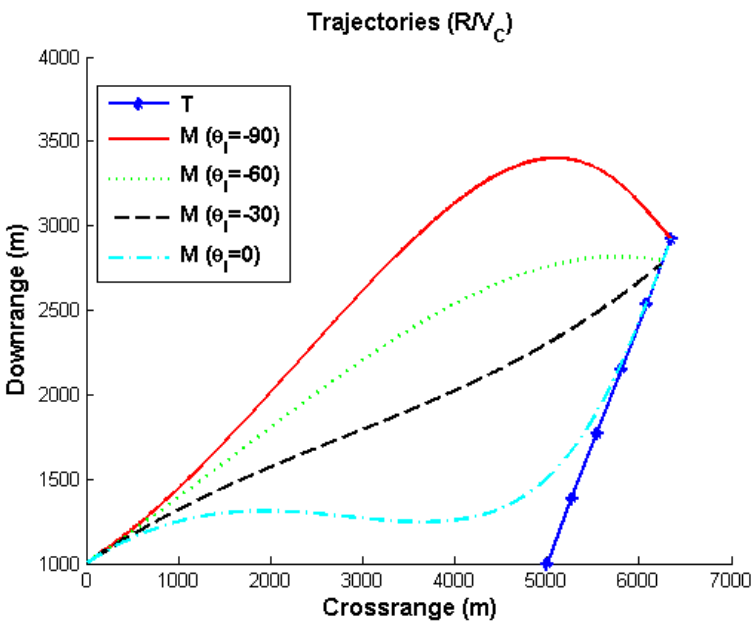

Figure 6.8: Trajectories of the optimal IAC guidance law with the common time-to-go estimation

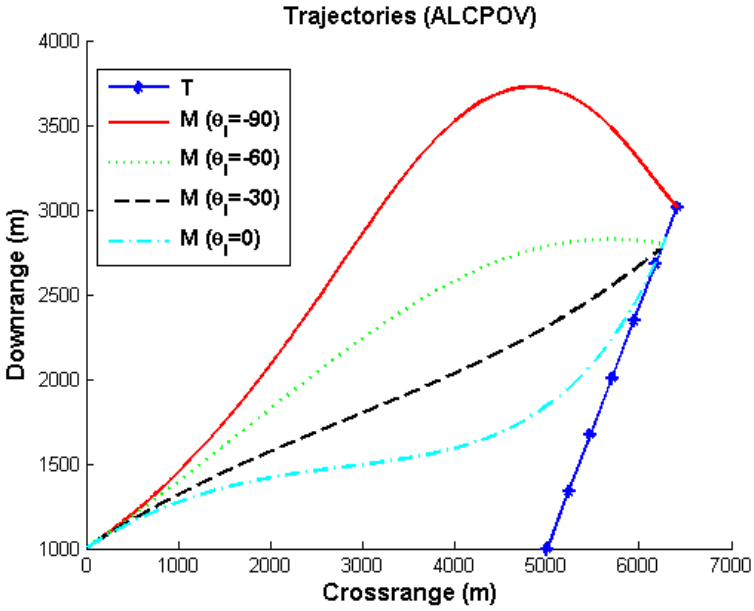

Figure 6.9: Trajectories for the optimal IAC guidance law with AROCV

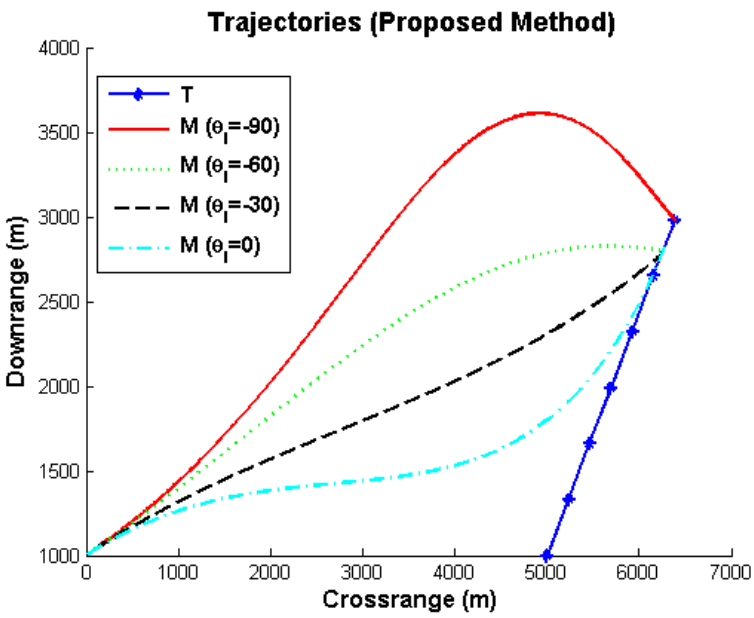

Figure 6.10: Trajectories for the optimal IAC guidance law with the proposed time-to-go estimation

Chapter 7

Applications

In this chapter, for the application of the proposed algorithms, we will first address several practical issues and propose some algorithms to resolve these issues. In order to implement any guidance laws, it is required to estimate the motion information of the target. Since the update from the ground station can be lost and the target acceleration profile is hard to be predicted, the estimation and prediction of the target state is one of main implementation issues. Successful estimation and prediction lie in the quality of extracting useful information about the target's state based on observations and suitable set of hypotheses. This information is greatly enhanced if one uses a suitable model, i.e. one that exploits the knowledge available on the target motion. Classical approach computes the interception control (missile acceleration) using minimum covariance and unbiased estimates of the target state. The determination of the guidance law and its optimality relies on the certainty equivalence principle and a set of assumptions on the final aim of the target (Neslin & Zarchan, 1981; Lin, 1998). However, the performance of the resulting law is tightly linked with the adequacy of these hypotheses and the quality of estimation. In this study, the set estimation is used to resolve this issue. The set estimation algorithm used in this study is designed by Dr Hélène Piet-Lahanier as a part of our joint work for the UK MoD and French DGA MCM-ITP (Materials and Components for Missile - Innovation and Technology Partnership) programme.

In the EIGGL, a desired heading angle of the missile is derived to guide the missile to an intercept point. Since the missile heading angle can be different from the desired angle, we need to design an algorithm to regulate the heading angle at the desired angle. White et al. (2007) considered this problem as a guidance problem to regulate the error between the current and desired heading angles, and then designed the DGGL based on the Lyapunov stability theory. In this chapter, we will also design a regulation algorithm using the DGGL and Lyapunov control theory.

In previous chapters, the performance of each algorithm was analysed and illustrated by working through some numerical examples. However, the satisfac-

tory performance of each algorithm alone cannot guarantee the performance of the whole system. Therefore, we will investigate the overall performance of the proposed cooperative guidance scheme compared to the results of conventional PN guidance with the common existing allocation policy. Since some scenarios are determined to verify the performance of the cooperative guidance laws, the proposed cooperative guidance scheme will be applied to the scenario 3, which is classified as Cat B.

7.1 Target estimation and prediction

Tracking manoeuvring targets is mostly performed using a state-space discrete model with additive noise of the following form

$$X_{k+1} = f_k(X_k, u_k) + w_k \tag{7.1}$$

$$Z_k = h_k(X_k) + v_k \tag{7.2}$$

where X_k, Z_k and u_k are the target state, observation and control input vectors, respectively, at the discrete time t_k; w_k and v_k are process and measurement noise sequences, respectively; and f_k and h_k are some vector-valued (possibly time-varying) functions. Measurement and process noises are usually assumed to be gaussians whereas the control input is defined so that the target aims at a given (valuable) objective. The measurements are provided either by ground-based device with a slow uplink frequency or by missile-borne seeker with higher frequency. According to model dynamics and measurement structure, the Kalman or extended Kalman filter are used to estimate the target state vector consisting mostly often of its position, velocity and acceleration in an inertial frame.

However, this approach suffers several drawbacks. Firstly, the prediction of the state vector is based on the combination of a gaussian evolution and a deterministic trajectory aimed at a given objective. The adequacy of the prediction is then tightly linked to the credibility of this assumption. Secondly, it might be difficult to provide a suitable gaussian description of the measurement noise as they are obtained usually via a nonlinear transform. In order to overcome these difficulties, the approach used here is based on the following assumptions. The state perturbations and noise measurements are only assumed to remain within

known bounds. The values of the target control inputs are determined to ensure that the target is enabled to reach a priori defended area.

7.1.1 Set estimation

Estimation of the target state vector under these hypotheses consists in seeking for the set of all values of state vector that is consistent in the sense that all errors fall within specified known bounds. This approach corresponds to guaranteed estimation that was initially introduced by Schweppe (1968) and followed by Bertsekas & Rhodes (1971). Several methods have been developed to define the boundary of this set or to compute a set properly containing this boundary. The main approach computes a set approximation under the form of an ellipsoid, but other approaches determine a characterized polyhedral boundary or the union of intervals to which all state vectors belong. In this study, the set estimation procedure is based on the ellipsoidal approximation algorithm in Maksarov & Norton (2002).

In the implementation, if the measurement data of the target states are available, the estimates of the target states are obtained from the measurement update. When the measurement update is not available, the guidance algorithm uses the states computed by the prediction.

7.1.1.1 Ellipsoidal description

The initial step of the estimation algorithm consists in defining an ellipsoid that is assumed to contain all values of the initial state vector. It is characterized by its center $\hat{X}_0$ and associated matrix P_0 that defines its main axes and amplitude (P_0 is Semi-Positive Definite (SPD) matrix):

$$\begin{aligned}\Xi_0 &= \{X_0 \in \xi(\hat{X}_0, P_0)\} \\ &= \{X_0 \in \mathfrak{R}^n / (X_0 - \hat{X}_0)^T P_0^{-1} (X_0 - \hat{X}_0) \leq 1\}\end{aligned} \tag{7.3}$$

where n is the space dimension. As the target state vector consists in position, velocity and acceleration components, this ellipsoid is of dimension 9, x_0 is a 9-dimensional vector and P_0 a 9 by 9 positive matrix. The system is modeled as a

discretized first-order linearised system

$$\begin{cases} X_{k+1} = A_k X_k + B_k u_k + w_k \\ Z_k = C_k X_k + v_k \end{cases} \quad \text{for } k = 1, 2, \ldots \tag{7.4}$$

where state variables with subscription $_k$ or $_{k+1}$ denote those at time t_k or t_{k+1}, and w_k and v_k are input and measurement noises at t_k which belong to the following ellipsoids

$$\begin{aligned} \xi_1 &= \{w_k \in \xi(0, W_k)\} = \{w_k \in \mathfrak{R}^n / w_k^T W_k^{-1} w_k \leq 1\} \\ \xi_2 &= \{v_k \in \xi(0, V_k)\} = \{v_k \in \mathfrak{R}^p / v_k^T V_k^{-1} v_k \leq 1\} \end{aligned} \tag{7.5}$$

where W_k and V_k are covariances of noise w_k and v_k.

7.1.1.2 Measurement updating

Let $\Xi_{k/k-1}$ be the ellipsoid predicted at time t_{k-1} for time t_k with center $\hat{X}_{k/k-1}$ and characteristic matrix $P_{k/k-1}$. Let Z_k be the new measurement, the ellipsoid Ξ_k consistent with $\Xi_{k/k-1}$ and the new measurement is characterized by its center $\hat{X}_k$ and characteristic matrix P_k defined by

$$\hat{X}_k = \hat{X}_{k/k-1} + \tau_k \frac{P_{k/k-1} h_k}{\sqrt{h_k^T P_{k/k-1} h_k}} \tag{7.6}$$

and

$$P_k = \beta_k (P_{k/k-1} - \sigma_k \frac{P_{k/k-1} h_k h_k^T P_{k/k-1}}{h_k^T P_{k/k-1} h_k}) \tag{7.7}$$

where

$$\begin{aligned} \tau_k &= \frac{1 + n\rho}{1 + n}, \qquad \sigma_k = \frac{2\tau_k}{(1 + \rho)} \\ \beta_k &= \frac{n^2(1 - \rho^2)}{n^2 - 1}, \quad h_k = C_k^T V_k^{-1} e_k, \end{aligned} \tag{7.8}$$

and ρ is given by equation (7.9)

$$\rho = \frac{e_k^T V_k^{-1} e_k - \sqrt{e_k^T V_k^{-1} e_k}}{\sqrt{h_k^T P_{k/k-1} h_k}} \tag{7.9}$$

where e_k is the innovation ($e_k = Z_k - C_k\hat{X}_{k/k+1}$).
Updating is performed when ρ belongs to the interval $]1, \frac{-1}{n}[$. If ρ is lower than $\frac{-1}{n}$, the resulting intersection is empty which means that either the measurement is erroneous or the hypothesis on the bounds is wrong. In order to avoid loss of target tracking, when such a situation occurs, we operate a translation of the resulting ellipsoid towards the measurement image, halfway to the exact measurement image. This corresponds to weight the confidence in the new measurement by 1/2.

7.1.1.3 Prediction

Any X belonging to Ξ_k should be considered as a candidate to be the state initial value for the characterization of the attainability domain. As X describes Ξ_k, it is possible to determine the extreme vector values reached. They consist in $2n$ points obtained by determining the eigen values and eigen vectors of the matrix P_k. They are obtained as the vector starting from $\hat{X}_k$ along one of the eigen vector of P_k multiply by plus or minus the associated eigen value. These points will be used as starting points for the trajectories that will define the limit of the attainability domain. These trajectories are assumed to aim at reaching a priori defended area characterized as a convex envelope of a set of n_{sk} points, S_{ki}. A bundle of trajectories is determined linking each of the extreme points to one of the S_{ki}. The predicted set at time t_{k+1} is obtained as the smallest convex domain containing the points of these trajectories for the given time (refer to e.g. Abdel-Malek & Hassan (1991)).

7.1.1.4 Chebyshev centre

After characterizing the trajectory bundle at time t_k as a set of points or a bounded ellipsoid, it is of interest to define a specific point that would present suitable properties to be chosen as the objective for the defending missile guidance. Such a point is the Chebyshev centre of the convex hull of this set of points, i.e. the point which minimizes the maximal distance between itself and any point of the set. Determination of this centre is performed using the method described in Botkin & Turova-Botkina (1994). As a minmax estimate of the potential state of

Table 7.1: Positions of the defended assets

Ground Base 1	Ground Base 2	Ground Base 3
(4 Km, 1 Km)	(-4 Km, -1 Km)	(-2 Km, 1 Km)

Table 7.2: Initial conditions for the simulation of the target estimation and prediction algorithm

	Position	Velocity
Missile	(0 Km, 0 Km)	(400 m/s, 100 m/s)
Target	(20 Km, 0 m)	(498 m/s, 32 m/s)

the target, this point limits the amount of lateral acceleration necessary to reach the real target position whenever additional measurement becomes available.

7.1.2 Numerical Examples

In order to verify the target estimation and prediction algorithm with the proposed guidance laws, we considered two engagement scenarios in which a target endeavour to destroy one of the assets in a defended area and the missile defends the assets. Figures in Figure 7.1 show these two engagement scenarios without missile intervention. As shown in these figures, the target homes to the first ground base in the first scenario, and to the second ground base in the second scenario.

For the numerical simulations, it is assumed that the speeds of the missile and target are constant and PN guidance law is applied to the target. The number of the assets is three and their positions are represented in table 7.1. Table 7.2 represents initial conditions of the missile and target for the numerical simulations.

Since there are three ships and the target flies to one of those, three possible PN guidance commands are considered in the target estimation and prediction. Figures 7.2(a) and 7.2(b) show the performance of the proposed algorithm when the measurement data are always available. Figures 7.3(a) and 7.3(b) illustrate the performance if there is no measurement update from 7 *sec* to 18 *sec* of the flight

time. In the figures, the Chebyshev centre represents the estimated trajectory of the target. As shown in Figure 7.2, the performance of the proposed algorithm is satisfactory when the system can always obtain the measurement data. If the measurement data are partially unavailable, the performance could be degraded as illustrated in Figure 7.4. However, it is shown that the set estimation can effectively reduce the estimation error when the measurement data are obtained again.

We also demonstrate the performance of the IGGL, which uses the estimated target states computed by the set estimation algorithm. For the numerical simulations, it is again assumed that the measurement update is not available from 7 *sec* to 18 *sec*. Figures 7.4(a) and 7.4(b) show the performance of the IGGL with the set estimation algorithm. From the results, it is shown the proposed algorithm effectively intercept the target before it reaches the defended area. As expected, the target intercept of the proposed algorithm is earlier than that of PN guidance law as illustrated in the figures.

7.2 Regulation Algorithm for the EIGGL

The matching condition for the direct intercept is given by Equation (2.6). In Equation (2.6), the reference frame for the EIGGL is the LOS frame, whose x axis is tangent to the LOS line and y axis is normal to this line, and thus the angles θ_M and θ_T are measured from the LOS line. In this section, the angle satisfying the matching condition will be denoted as θ_M^* to be distinguished from the current heading angle θ_M. The missile heading angle can be controlled to the desired one, if we regulate the heading error, θ_ϵ, of the form

$$\theta_\epsilon = \theta_M^* - \theta_M. \tag{7.10}$$

Therefore, the regulating algorithm of the heading angle can be determined by use of a simple Lyapunov function V of the form:

$$V = \frac{1}{2}\theta_\epsilon^2. \tag{7.11}$$

The time derivative of the Lyapunov candidate function V is given by

$$\frac{dV}{dt} = \dot{\theta}_\epsilon \theta_\epsilon. \tag{7.12}$$

Hence, for stability, we require

$$\dot{\theta}_\epsilon \theta_\epsilon < 0. \tag{7.13}$$

From a definition of θ_ϵ, we have

$$\dot{\theta}_\epsilon = \dot{\theta}_M^* - \dot{\theta}_M, \tag{7.14}$$

First time derivative of the matching condition for the direct intercept is obtained as

$$\begin{aligned} \dot{\theta}_M^* &= \gamma \frac{\cos(\theta_T)}{\cos(\theta_M)} \dot{\theta}_T, \\ &= \frac{\cos(\theta_T)}{\sqrt{\gamma^2 - \sin^2(\theta_T)}} \dot{\theta}_T. \end{aligned} \tag{7.15}$$

This means

$$-\frac{1}{\gamma}\dot{\theta}_T \leq \dot{\theta}_M^* \leq \frac{1}{\gamma}\dot{\theta}_T. \tag{7.16}$$

From the definition of θ_T, we have

$$\dot{\theta}_T = \dot{\psi}_T - \dot{\theta}_S, \tag{7.17}$$

where ψ_T denotes the heading angle of the target in the inertial reference frame and θ_S represents the LOS angle. Since the EIGGL guides the missile to the intercept point against the missile which flies in a straight line with the heading angle θ_T, Equation (7.17) becomes

$$\dot{\theta}_T = -\dot{\theta}_S, \tag{7.18}$$

Hence:

$$-\frac{1}{\gamma}\dot{\theta}_S \leq \dot{\theta}_M^* \leq \frac{1}{\gamma}\dot{\theta}_S. \tag{7.19}$$

From the Liapunov equation, we have:

$$\begin{aligned} \frac{dV}{dt} &= \dot{\theta}_\epsilon \theta_\epsilon, \\ &= (\dot{\theta}_M^* - \dot{\theta}_M)\theta_\epsilon, \end{aligned} \tag{7.20}$$

Table 7.3: Initial conditions for the simulations of the regulation algorithm

	Target	Missile
Position(Km,Km)	(30, 10)	(0, 0)
Velocity(m/s)	300	600
Heading angle(deg)	130	-100

thus a missile tangent vector control algorithm is proposed as

$$\dot{\theta}_M = \frac{K}{\gamma}|\dot{\theta}_S|\text{sign}(\theta_\epsilon), \tag{7.21}$$

$$K > 1, \tag{7.22}$$

$$\text{sign}(\theta_\epsilon) = \frac{|\theta_\epsilon|}{\theta_\epsilon}, \tag{7.23}$$

to give:

$$\frac{dV}{dt} = \dot{\theta}_M^* \theta_\epsilon - \frac{K}{\gamma}|\dot{\theta}_S||\theta_\epsilon| \leq 0. \tag{7.24}$$

which is negative semi define. Since $\dot{\theta}_M$ is given by

$$\dot{\theta}_M = a_M / V_M, \tag{7.25}$$

the lateral acceleration command of the missile a_M is obtained as

$$a_M = V_M \frac{K}{\gamma}|\dot{\theta}_S|\text{sign}(\theta_\epsilon). \tag{7.26}$$

The performance of the EIGGL with the regulating algorithm is demonstrated through numerical simulations. The initial simulation conditions of the missile and target are represented in Table 7.3. Note that the initial heading error in these conditions is about 146(*deg.*). The target is assumed to fly in a straight line in the first scenario, and to manoeuvre with a constant lateral acceleration $15m/s^2$ in the second scenarios. In both scenarios, it is assumed that two assets are defended by the missile. Figures 7.5 depicts the simulation results of the first scenario. If the heading error was zero, the intercept points of the first and second EIG (denoted as EIG1 and EIG2) should be the same as stated. From the figures, it is shown that the heading error results in the intercept delay, although the EIGGL with the regulating algorithm successfully protects the assets. The

safety margin introduced in Chapter 2 can resolve the problem resulting from this delay. The simulation results of the second scenario are illustrated in Figure 7.6. Even thought the heading error delays the intercept of the target, the EIGGL still can intercept the manoeuvring target inside the capture zone (EIG) as shown in the figure.

7.3 Numerical Simulation of the Overall System

Figures 7.7 and 7.8 illustrate the ground to air and surface to air scenario 3, when there is no missile intervention. The second target is the incoming missile launched from an aircraft, which is the first target. The aircraft is manoeuvring away from the defended area after firing the missile. The maximum acceleration of the missile is assumed to be $600m/s^2$. In order to compare the proposed guidance scheme to the common approach, the PN guidance law with the navigation gain 4 is first implemented for the mid and terminal phases. Moreover, the targets are allocated to the missiles using a sequential allocation policy; the first missile is allocated to the first and the second missile to the second target. Many existing naval firing policies generally fire a single missile to the target at long range and fire another missile until later when, if there were sufficient time, a kill assessment would be undertaken before firing a second round. Thus, the existing systems tend to follow a more sequential approach. Simulation results are shown in Figure 7.9. In the both scenarios, the PN guidance law with a general allocation policy cannot intercept the first target. Since the first target (aircraft) can fire other missiles, this might result in other threats to the defending system.

Now, we apply a simple combination of the proposed algorithms: the EIGGL, the target allocation using the EIG, the target estimation and prediction algorithm, and the proposed terminal homing guidance and time-to-go estimation algorithm. The allocation plan is activated when the many-on-many engagement is encountered, that is the second missile is launched in this scenario. The simulation results of the ground to air scenario are shown in Figures 7.10 and 7.11. Figures 7.10(a) and 7.10(b) illustrate the performance of the proposed guidance strategy, whose target allocation plan is obtained from the first performance index

in Equation (4.2), and Figures 7.11(a) and 7.11(b) depict the simulation results of the guidance with the weighted performance index in Figures 7.10(a) and 7.10(b). As shown in the figures, the initial EIGs are not overlapping with the defended area and missiles intercept the targets inside the EIGs, that is the capture zone; the proposed guidance scheme effectively protect the defended area. Compare to the PN guidance law with the general allocation policy, the proposed guidance scheme moves up the interception of the second missile and can reach to the target on the run.

The simulation results for the surface to air scenario are illustrated in Figures 7.12 and 7.13. In the surface to air scenario, the proposed guidance scheme guarantees the intercept of the targets before they reach to any defended asset. Moreover, similar to the results in the ground to air scenario, it is shown that the proposed guidance scheme advances the interception and catch the escaping target.

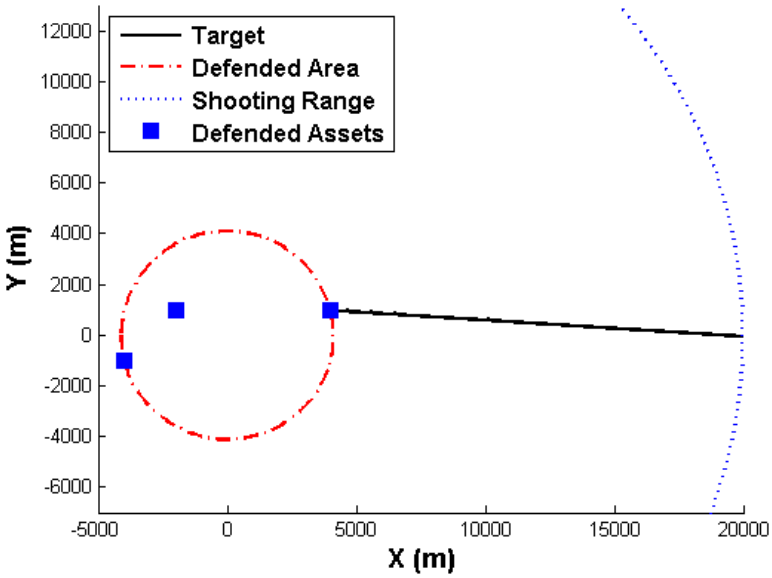

(a) First scenario

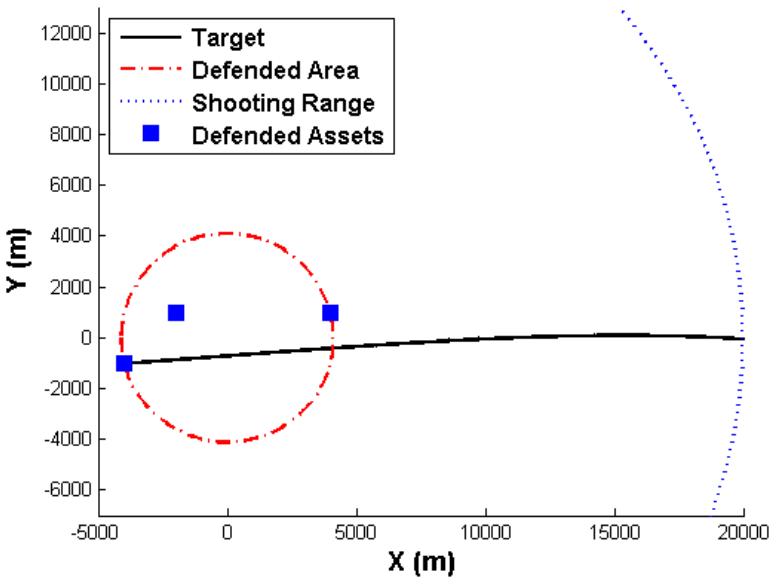

(b) Second scenario

Figure 7.1: Engagement scenarios

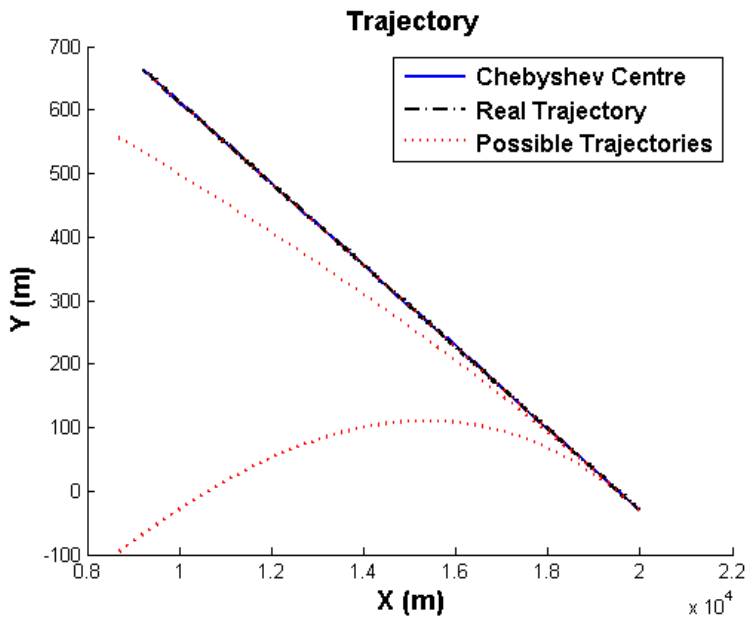

(a) First scenario

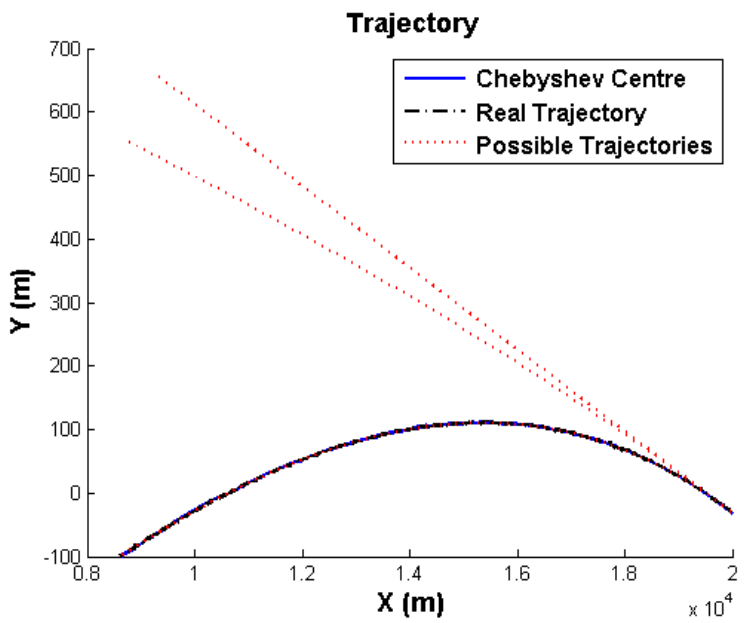

(b) Second scenario

Figure 7.2: The performance of the set estimation algorithm when the measurement data are always available

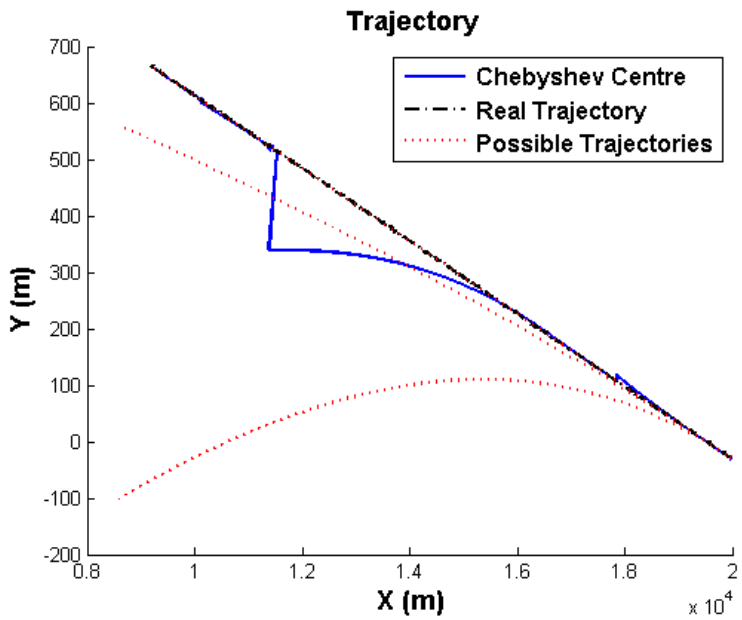

(a) First scenario

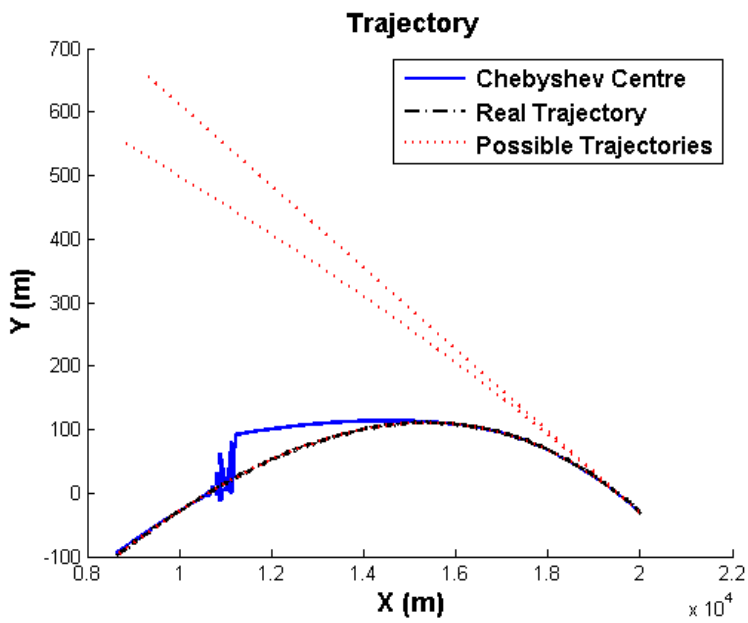

(b) Second scenario

Figure 7.3: The performance of the set estimation algorithm when the measurement data are partially available

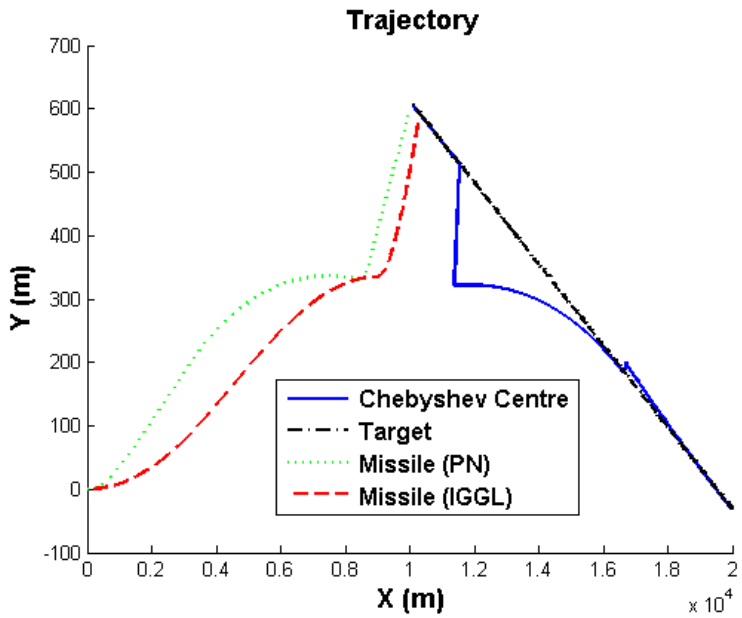

(a) *First scenario*

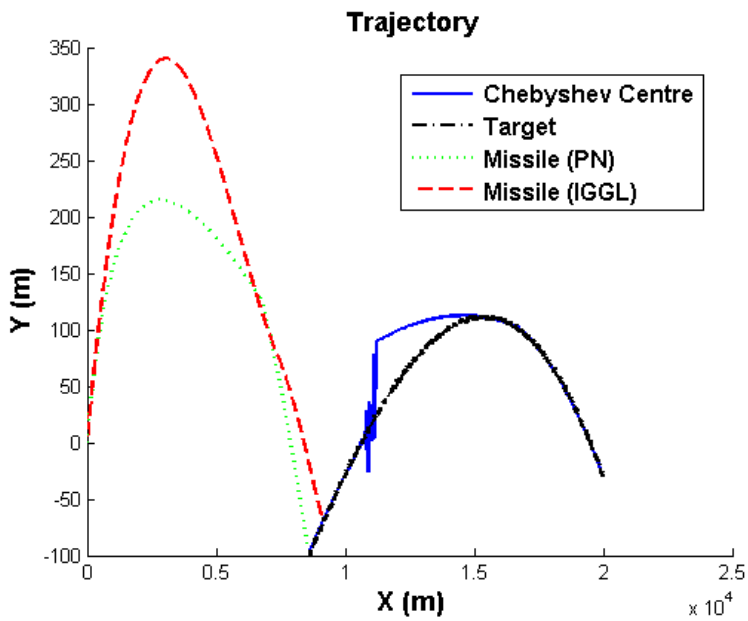

(b) *Second scenario*

Figure 7.4: Trajectory result of the IGGL with the set estimation algorithm

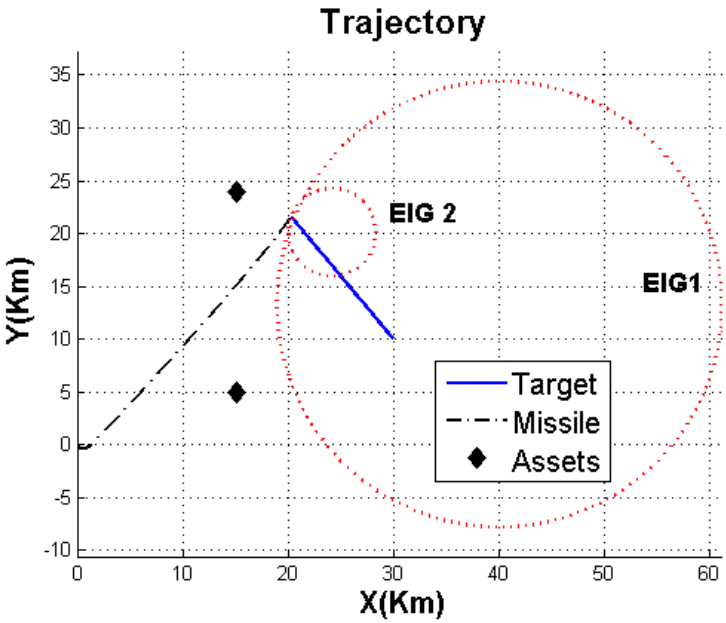

Figure 7.5: EIG and trajectories: when the lateral acceleration of the target is zero (first scenario)

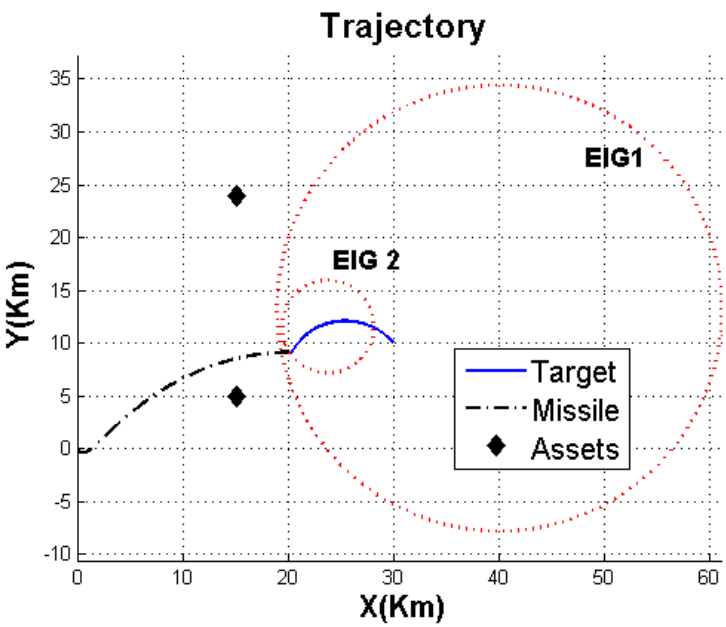

Figure 7.6: EIG and trajectories: when target is manoeuvring (second scenario)

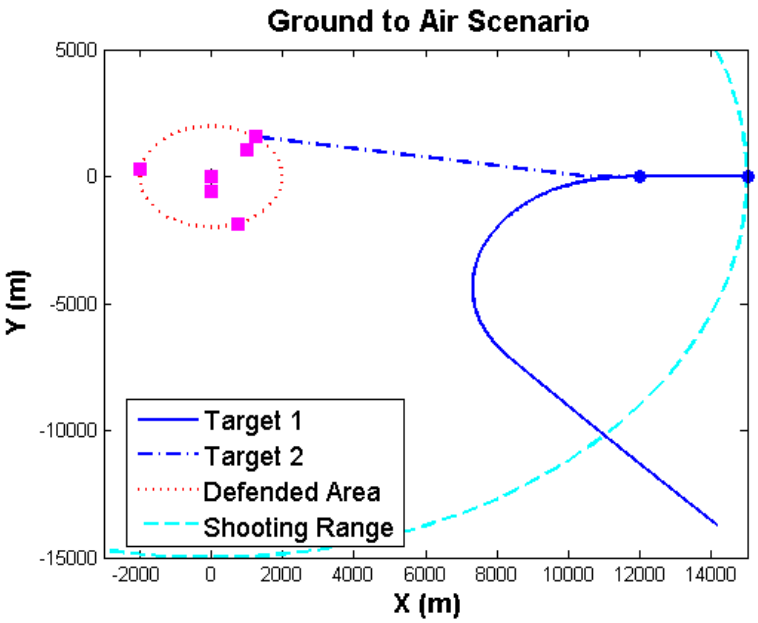

Figure 7.7: Ground to air scenario 3

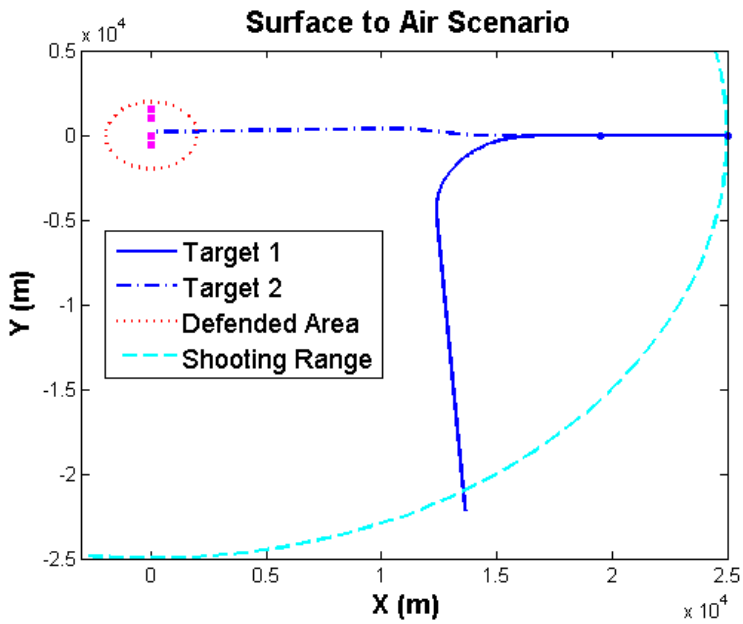

Figure 7.8: Surface to air scenario 3

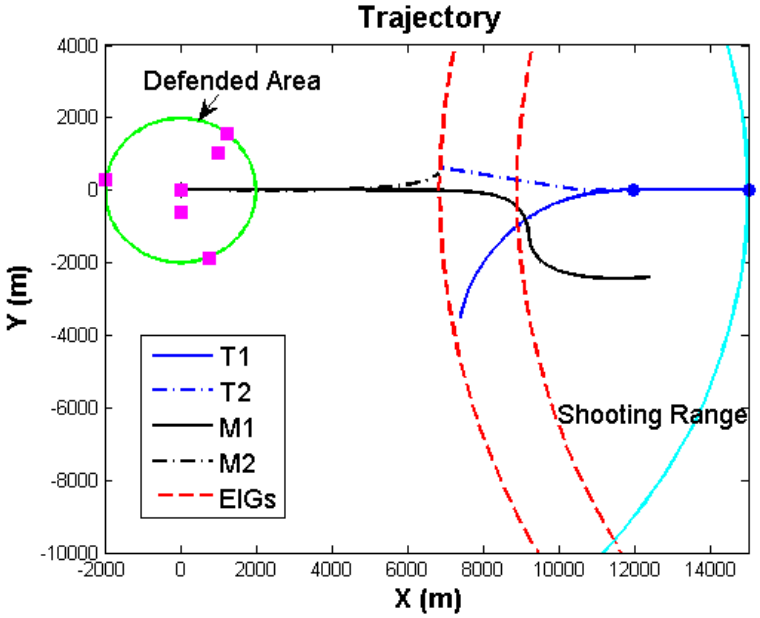

(a) Ground to air scenario 3

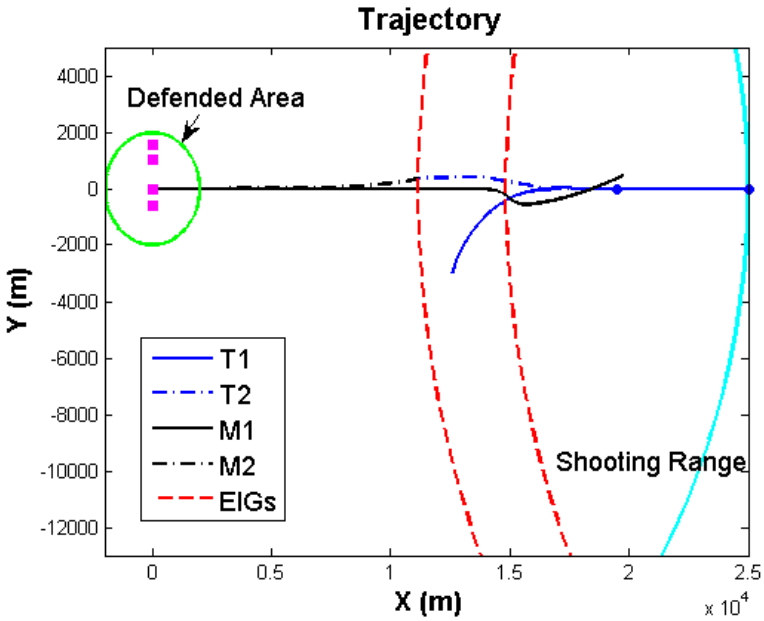

(b) Surface to air scenario 3

Figure 7.9: Trajectory result of the PN guidance law

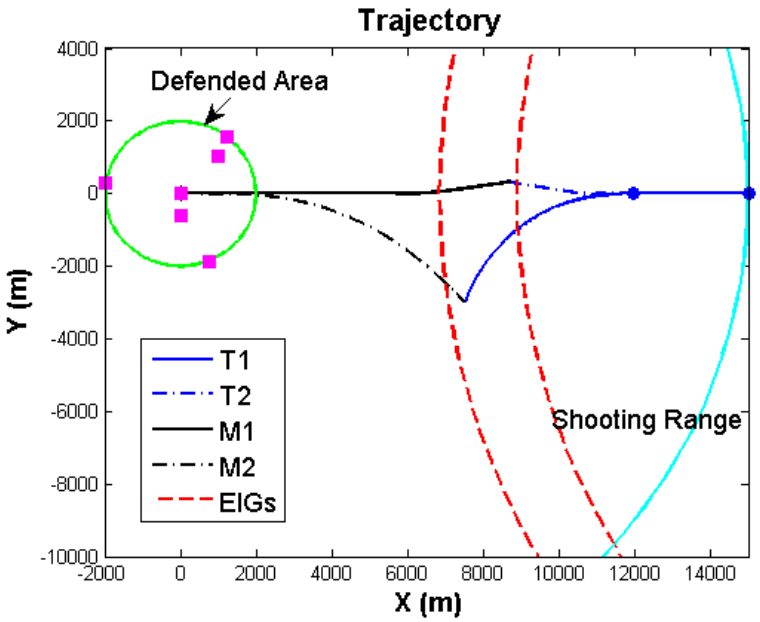

(a) Trajectories

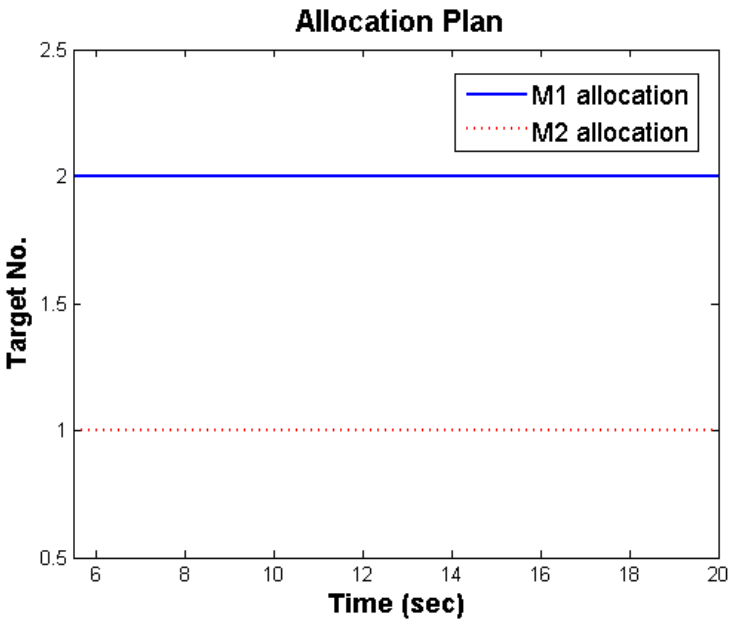

(b) Allocation plan

Figure 7.10: Simulation results of the cooperative guidance strategy for the ground to air scenario 3

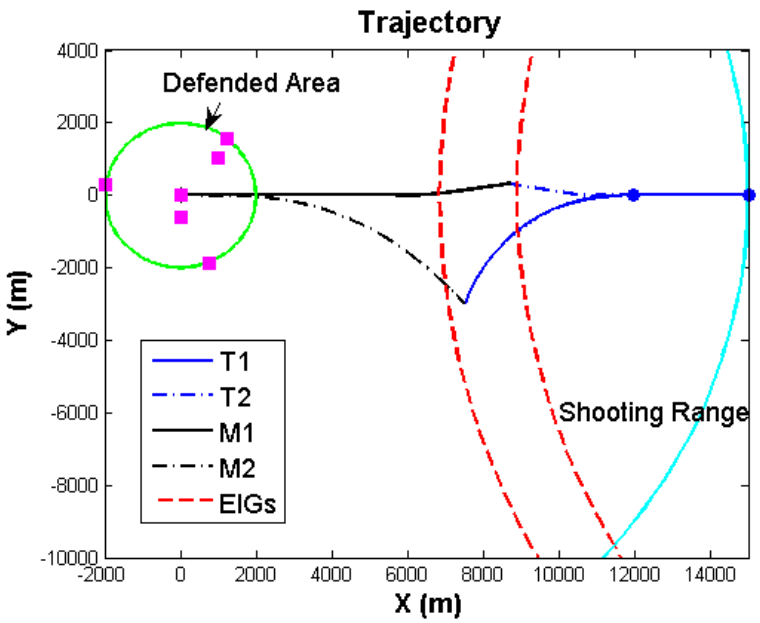

(a) Trajectories

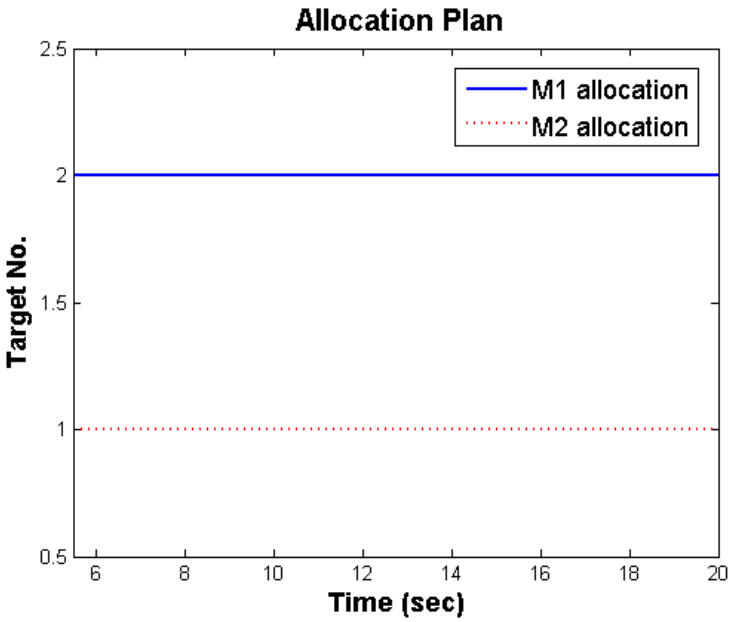

(b) Allocation plan

Figure 7.11: Simulation results of the cooperative guidance strategy (with the weighted performance index) for the ground to air scenario 3

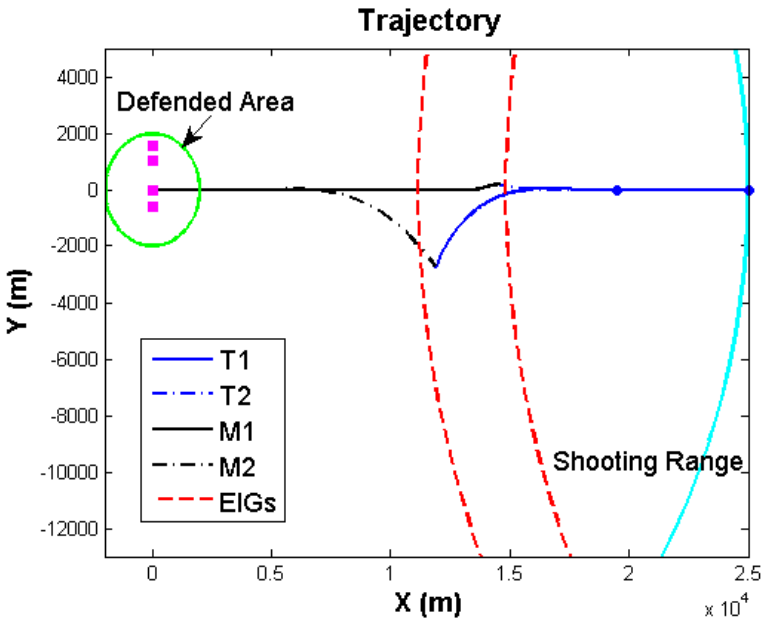

(a) Trajectories

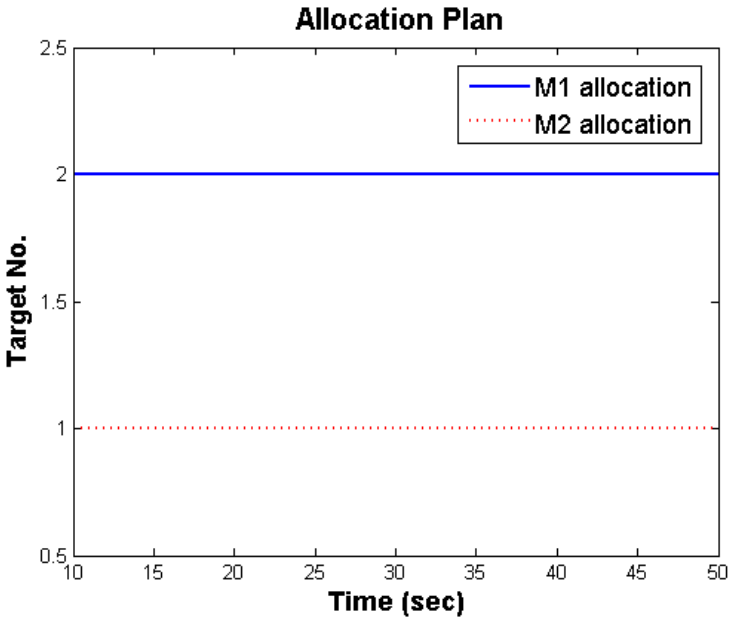

(b) Allocation plan

Figure 7.12: Simulation results of the cooperative guidance strategy for the surface to air scenario 3

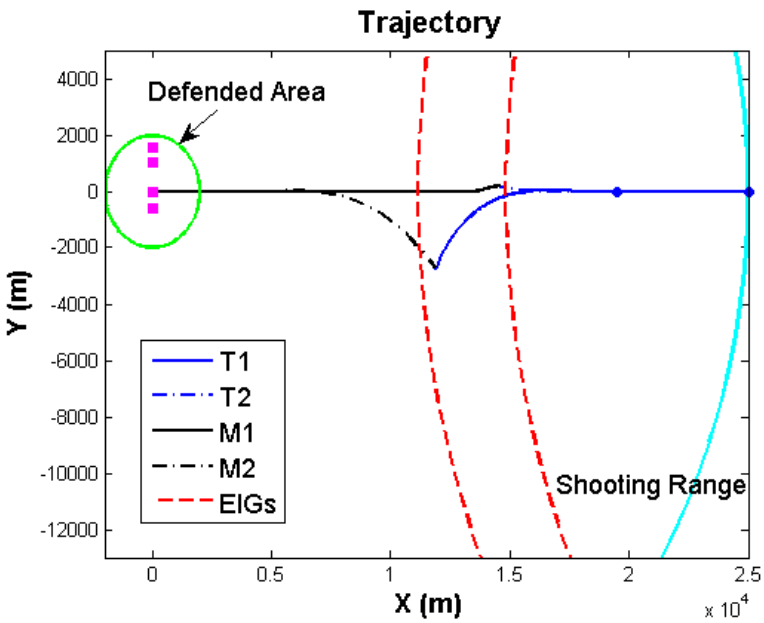

(a) Trajectories

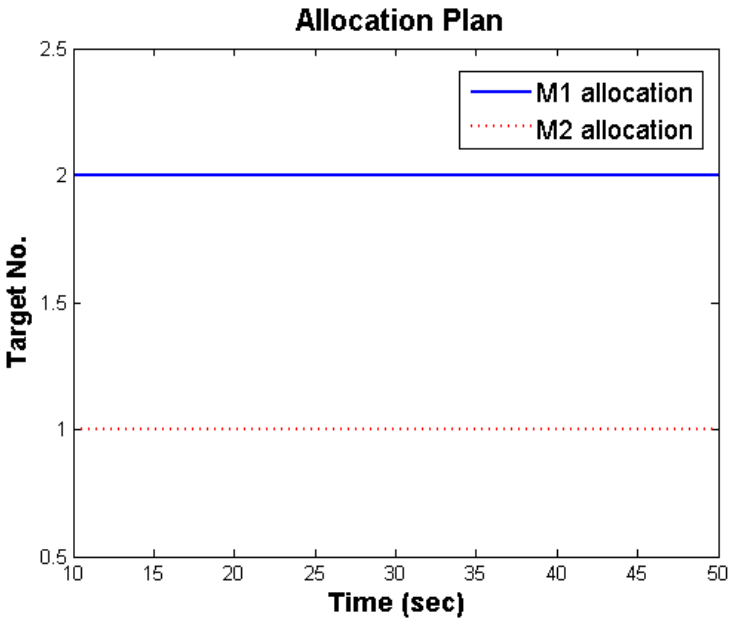

(b) Allocation plan

Figure 7.13: Simulation results of the cooperative guidance strategy (with the weighted performance index) for the surface to air scenario 3

Chapter 8

Conclusions and Future Work

8.1 Conclusions

Cooperative guidance is a challenging technique which is likely to emerge as a technology in future weapon systems (Rabbath, 2007; Ge et al., 2006; Jang & Tomlin, 2005; Shaferman & Oshman, 2009). Future weapon system scenarios will include the need to engage multiple threats which places greater demands on the guidance chain compared with single-to-single. As a part of UK MoD and French DGA MCM-ITP (Materials and Components for Missile - Innovation and Technology Partnership) programme, a project was launched in year 2008 to examine this cooperative guidance problem for area air defence. MBDA-UK, MBDA-France, ONERA, and Cranfield Univeristy have jointly developed various component technologies supporting the concept of cooperative guidance for the area defence. This thesis summarizes various algorithms and integration frameworks proposed by the author for the cooperative guidance.

For long or medium range engagements, since the missile cannot lock on to the target, mid course guidance is generally applied to the missile. Mid course guidance phase refers to the stage in which the missile is guided to a handover point in order to acquire the target motion from its on-board sensor. The real-life problem in this phase is that the guidance uses the target motion information which are updated by the external source with a relatively slow update rate. Due to this problem, one of the most challenging issues is the probability of future target manoeuvres. It is difficult to predict where the target would head for, because it usually flies to some point and change its heading at the late stage of the engagement to increase its survivability. If the missile reacts against the current target acceleration as in the typical guidance laws, the guidance law with a slow update rate would considerably waste the energy, consequently the missile could miss the target.

For the mid course design, the most important idea was that we can determine the capture zone with certainty although we cannot predict the target acceleration

profile with certainty. In this research, the capture zone is obtained using either the Earliest Intercept Geometry (EIG) or Intercept Geometry (IG). The intercept geometries are the involutes of the all possible extremal Earliest Intercept Points (EIPs) or Intercept Points (IPs) against the target acceleration hypotheses. As long as the guidance algorithm provides better engagement conditions to the terminal homing phase whilst guaranteeing that the capture zone is not overlapping with defended area (keep out zone), the missile can protect all assets in the defended area. The key challenge was how to keep this capture zone outside the defended area, when the target manoeuvre is unpredictable. In order to resolve this issue, the change of the intercept geometries was first derived in accordance with the missile and target manoeuvre. Then, the guidance command is derived using this geometry change. The proposed mid course guidance heads to one of the derived possible intercept points, not to the target. When the IG is away from the defended area, the missile is guided to the IP against the target which is assumed to fly in a straight line. When any defended asset is in danger, the missile guided to the intercept point which can push the IG away from the asset.

The Earliest Intercept Geometry Guidance Law (EIGGL) was analytically derived using the concept of controlling the EIG away from the defended area. Since the EIG was derived under assumption that the target and missile can change their heading angles instantaneously, the EIG changes when the missile heading angle is deviated from the desired one. In order to take this change into consideration, we introduced a safety margin. If the distances between the EIG and the assets, called the safety distances, are bigger than this margin, the missile flies to the intercept point against the target trajectory of the straight line. Otherwise, it is guided to the intercept point which pushes the EIG away from the asset in danger. The Intercept Geometry Guidance Law (IGGL) was proposed using the IG to alleviate this undesirable EIG change and consider physical and operational constraints. The optimal guidance laws are also proposed and the missile is assumed to apply the optimal guidance law to calculate the IG and leave more energy and manoeuvrability to the terming homing phase. Because the IG is numerically calculated, the computational load might be high. Therefore, the IPs are calculated in interval to compute the IG and the number of the IPs can be determined depending on the computational power.

Since the performance of the cooperative guidance algorithms depends on

the target allocation policy, we should design the allocation plan. The concepts of the intercept geometry were applied to develop an optimal target allocation plan. The intercept geometries in the cooperative guidance problem are determined by which missile is allocated to which target. Therefore, it is possible to push away the IGs from the defended area by changing the allocation plan, i.e. enhance the guidance performance. In the same engagement scenario, if we can increase the safety distance, which is minimum distance between the IGs and the defended assets, we can advance the interception and provide the more time and manoeuvrability to the terminal homing phase. Therefore, we considered the target allocation problem as the problem of maximising this safety distance. Since it is hard to find an analytical solution for this optimal problem, a numerical approach is proposed. In order to reduce the computational load to solve the problem, the proposed approach divides the optimal problem into several steps and made each step simple.

Common terminal homing guidance algorithms such as Proportional Navigation (PN) control the missile onto the collision course. Due to the different hypotheses of the target acceleration at the mid course and terminal homing phase, the collision triangle at the handover point can be different for that predicted in the mid course phase. Any initial angular deviation from the collision course, called the heading error, generates a sudden change of the missile acceleration. Since an abrupt acceleration change also generates a sudden transition manoeuvre, it is undesirable. Therefore, we proposed a new PN guidance law for reducing sensitivity to heading error based on the optimal control theory. The main idea was that it should be possible to alleviate the heading sensitivity, if we change the navigation gain over the flight time: relatively small navigation gain at the beginning of the terminal homing phase. To distribute the navigation gain over the time of flight, we introduced a new time-varying weighting function which is the second order polynomial of time-to-go. The characteristic of the terminal guidance law is mathematically analysed and its performance is illustrated via adjoint simulations and engagement simulations. The proposed guidance law not only guarantees the interception of the target, but also reduce sensitivity of the initial heading error.

The performance of the proposed optimal guidance laws depends on the accuracy of the time-to-go estimation, because the derived guidance commands are

polynomial functions of the time-to-go. Hence, we considered the problem of computing accurate time-to-go estimates for various forms of the optimal guidance laws. Predicted guidance command histories are used in computing the time-to-go. The proposed algorithm naturally takes the curvature of the trajectory into account so as to improve the accuracy of the time-to-go estimation. For the implementation issue, trigonometric integrands in computing the time-to-go is approximated to polynomial functions of the flight time. If the change of the angular values in the trigonometric integrands is big, they are approximated about several reference points. Various numerical simulations show that the performance of the proposed time-to-go estimation algorithm is satisfactory for the optimal guidance laws.

The performance of each algorithm analysed and demonstrated using some numerical examples. However, the good performance of the proposed algorithms cannot guarantee the satisfactory performance of the overall system. In our joint project to develop the cooperative guidance algorithms, several scenarios for air defence in ground and naval context have been defined. Therefore, some unclassified scenarios among them were considered to investigate the performance of the whole system, which consists of the proposed mid course guidance, target allocation, terminal homing guidance, and time-to-go estimation algorithms. The numerical results of the proposed guidance were compared to those of the conventional PN guidance law with a sequential allocation policy. Moreover, in Chapter 7, we addressed some issues for the application of the proposed cooperative guidance strategy and proposed algorithms to resolve those issues.

8.2 Future Work

Whilst the proposed guidance concept using the intercept geometries is promising, there are several issues to be addressed before this guidance concept can be implemented. Some numerical examples were simulated using scenarios and a Simulink Common Model (CM) shared between the partners and the numerical results show the satisfactory performance. However, in order to explore its possible use to other than naval air defence, we need to verify the proposed algorithms using various scenarios and quantitatively analyse the effect of the dynamics and

characteristics of the control system on the proposed guidance system. Some other issues to consider are:

- Effect of finite missile energy on the IG and EIG (limited reachability),
- Maximising reachability by appropriate guidance in the vertical plane ,
- Constraints on handover geometry (eg. seeker nmax look angle, sightline depression angle to avoid clutter).

A clear limitation of this research is that the proposed guidance law considered only a 2D world. Except the sea-skimming missiles, this is unacceptable for the medium and long range missiles which apply mid course guidance. We just started considering the problem to extend the proposed algorithms into the 3D plane and expect it would be relatively simple to obtain the intercept geometries. However, it might be challenging to derive the change of the intercept geometries in 3D to establish the guidance strategy for the area air defence.

Before the proposed guidance concept is brought to the real world, the practical implementations of the proposed concept to the other fields will remain narrow. However, the possible applications of the proposed concept are wide. The IG concept can be implemented into most of moving vehicles such as Unmanned Ground Vehicles (UGVs) or Unmanned Aerial Vehicles (UAVs). Especially, the proposed guidance scheme can be used for Unmanned Combat Aerial Vehicles (UCAVs). The IG concept can be also applied to the aircraft avoidance. We already explored the possibility of this application and a paper on the initial work, *'UAV Conflict Detection and Resolution for Static and Dynamic Obstacles'* , has been accepted for presentation at AIAA 2009.

Even though the proposed guidance scheme was developed to defend assets in an area, this can be directly used to design the cooperative guidance policy for the attacking missiles such as the fire shadow[1]. On the contrary to the cooperative defending guidance, the intercept geometries can be used to find the guidance strategy which minimizes the distances between the defended assets and the intercept geometries.

[1]http://www.mbdasystems.com/mbda/site/ref/scripts/EN_FireShadow_353.html

References

References

Abdel-Malek, H. L. & Hassan, A. K. S. O. (1991). The ellipsoidal technique for design centering and region approximation. *IEEE Transactions on Computer-Aided Design*, *10*, 1006–1014.

Becker, K. (1990). Closed-form solution of pure proportional navigation. *IEEE Transactions on Aerospace and Electronic Systems*, *26*(3), 526–533.

Ben-Asher, J. Z. & Yaesh, I. (1998). Advances in missile guidance theory. In *Progress in Astronautics and Aeronautics AIAA*, Reston, USA.

Bertsekas, D. & Rhodes, I. (1971). Recursive state estimation for a set-membership description of uncertainty. *IEEE Transactions on Automatic Control*, *16*, 117–128.

Botkin, N. & Turova-Botkina, V. (1994). An algorithm for finding the chebyshev center of a convex polyhedron. *Applied Mathematics and Optimization*, *29(2)*, 211–222.

Bryson, A. E. & Ho, J. Y. C. (1975). *Applied Optimal Control*. Hemisphere Publishing Corporation.

Chakravarthy, A. & Ghose, D. (1996). Capturability of realistic generalized TPN. *IEEE Transactions on Aerospace and Electronic Systems*, *32*(1), 407–418.

Cheng, V. H. L. & Gupta, N. K. (1986). Advanced midcourse guidance for air-to-air missiles. *Journal of Guidance, Control, and Dynamics*, *9(2)*, 135–142.

Cho, H. J., Ryoo, C. K., & Tahk, M. J. (1999). Implementation of optimal guidance laws using predicted velocity profiles. *Journal of Guidance, Control, and Dynamics*, *22(4)*, 579–588.

Dougherty, J. & Speyer, J. L. (1997). Near-optimal guidance law for ballistic missile interception. *Journal of Guidance, Control, and Dynamics*, *20(2)*, 355–362.

Dubins, L. E. (1957). On curves of minimal length with a constraint on average curvature and with prescribed initial and terminal positions and tangent. *American Journal of Mathematics*, *79*, 497–516.

Ge, J., Tang, L., Reimann, J., & Vachtsevanos, G. (2006). Suboptimal approaches to multiplayer pursuit-evasion differential games. In *Proceedings of AIAA Gudance, Navigation, and Control Conference and Exhibit*, Keystone, Colorado.

Ghose, D. (1992). True proportional navigation with manoeuvring target. *IEEE Transactions on Aerospace and Electronic Systems*, *30*(1), 229–237.

Glizer, V. Y. (1996). Optimal planar interception with fixed end conditions: Closed-from solution. *Journal of Optimization Theory and Applications*, *88(3)*, 503–539.

Guelman, M. (1972). Proportional navigation with a manoeuvring target. *IEEE Transactions on Aerospace and Electronic Systems*, *8*(3), 364–371.

Hull, D. G., Radke, J. J., & Mack, R. E. (1991). Time-to-go prediction for homing missiles based on minimum-time intercepts. *Journal of Guidance, Control, and Dynamics*, *14(5)*, 865–871.

Imado, F. & Kuroda, T. (2009). Optimal midcourse guidance system against hypersonic targets. In *Proceedings of AIAA Gudance, Navigation, and Control Conference and Exhibit*, Hilton Head, SC, USA.

Imado, F., Kuroda, T., & Miwa, S. (1990). Optimal midcourse guidance for medium-range air-to-air missiles. *Journal of Guidance, Control, and Dynamics*, *13(4)*, 603–608.

Imado, F., Kuroda, T., & Tahk, M. J. (1998). A new missile guidance algorithm against a manoeuvring target. In *AIAA Conference on Guidance, Control and Navigation*, (pp. 145–153).

Isaacs, R. (1665). *Differential Games*. Dover Publications.

Jane's (Aug 2002). Multinational aaw programmes. *Jane's Navy International*.

Jang, J. S. & Tomlin, C. J. (2005). Control strategies in multi-player pursuit and evasion game. In *Proceedings of AIAA Gudance, Navigation, and Control Conference and Exhibit*.

Jeon, I. S., Lee, J. I., & Tahk, M. J. (2006). Impact-time-control guidance law for anti-ship missiles. *IEEE Transactions on Control Systems Technology*, *14(2)*, 260–266.

Kim, B., Lee, J., & Han, H. (1998). Biased PNG law for impact with angular constraint. *IEEE Transactions on Aerospace and Electronic Systems*, *34*(1), 277–288.

Kreindler, E. (1973). Optimality of proportional navigation. *AIAA Journal*, *11*, 878–880.

Lee, J. I., Jeon, I. S., & Tahk, M. J. (2007). Guidance law to control impact time and angle. *IEEE Transactions on Aerospace and Electronic Systems*, *43(1)*, 301–310.

Le Ménec, S., Shin, H. S., Tsourdos, A., White, B. A., Zbikowski, R., & Markham, K. (2009). Cooperative missile guidance strategies for maritime area air defence. In *Proceedings of 1st IFAC Workshop on Distributed Estimation and Control in Networked Systems (NecSys09)*, Venice, Italy.

Lin, C. (1998). *Modern Navigation, Guidance, and Control Processing*. England: Prentice-Hall.

Mahapatra, P. & Shukla, U. (1989). Accurate solution of proportional navigation for manoeuvring targets. *IEEE Transactions on Aerospace and Electronic Systems*, *25*(1), 81–89.

Maksarov, D. G. & Norton, J. P. (2002). Computationally efficient algorithms for state estimation with ellipsoidal approximations. *International Journal of Adaptive Control and Signal Processing*, 411–434.

Menon, P. K. A. & Briggs, M. M. (1990). Near-optimal midcourse guidance for air-to-air missiles. *Journal of Guidance, Control, and Dynamics*, *13(4)*, 596–602.

Neslin, F. W. & Zarchan, P. (1981). New look at classical vs modern homing missile guidance. *Journal of Guidance, Control, and Dynamics*, *4*, 78–85.

Rabbath, D. D. C. A. (2007). Real-time decentralized pursuer-evader assignment for cooperating ucavs using the dtc algorithm. In *Proceedings of AIAA Gudance, Navigation, and Control Conference and Exhibit*, South Carolina, USA.

Robb, M., Tsourdos, A., & White, B. (August 2006). Earliest intercept line guidance using a game theory approach. In *Proceedings of AIAA Guidance, Navigation, and Control Conference and Exhibit*.

Robb, M., White, B. A., & Tsourdos, A. (August 2005). Earliest intercept line guidance: a novel concept for improving mid-course guidance in area air defence. In *Proceedings of AIAA Gudance, Navigation, and Control Conference and Exhibit*, San Francisco, California.

Robb, M., White, B. A., Tsourdos, A., & Rulloda, D. (June 2005). Reachability guidance: a novel concept to improve mid-course guidance. In *Preceedings of American Control Conference*, Portland, OR, USA.

Rusnak, I. & Meir, L. (1990). Optimal guidance for acceleration constrained missile and manoeuvring target. *IEEE Transactions on Aerospace and Electronic Systems*, *26*(4), 618–623.

Ryoo, C. K., Cho, H. J., & Tahk, M. J. (2005). Optimal guidance laws with terminal impact angle constraint. *Journal of Guidance, Control, and Dynamics*, *28(4)*, 724–732.

Ryoo, C. K., Cho, H. J., & Tahk, M. J. (2006). Time-to-go weighted optimal guidance with impact angle constraints. *IEEE Transactions on Control Systems Technology*, *14(3)*, 483–492.

Schweppe, F. (1968). Recursive state estimation: Unknown but bounded errors and system inputs. *IEEE Transactions on Automatic Control*, *13(1)*, 22–28.

Shaferman, V. & Oshman, Y. (2009). Cooperative interception in a multi-missile engagement. In *Proceedings of AIAA Gudance, Navigation, and Control Conference and Exhibit*, Chicago, Illinois, USA.

Shin, H. S., A. Tsourdos, B. A. W., & Tahk, M. J. (2009). Earliest intercept geometry guidance to improve mid-course guidance in area air-defence. In *Proceedings of Mediterranean Conference on Control and Automation*, Thessaloniki, Greece.

Shin, H. S., Le Ménec, S., Tsourdos, A., White, K. M. B. A., & Zbikowski, R. (2010a). Cooperative guidance for naval area defence. In *IFAC ACA*, Nara, Japan.

Shin, H. S., Le Ménec, S., Tsourdos, A., White, K. M. B. A., & Zbikowski, R. (2010b). Cooperative mid course guidance for area air defence. In *Proceedings of AIAA Gudance, Navigation, and Control Conference and Exhibit*, Toronto, Canada.

Shin, H. S., Tahk, M. J., A. Tsourdos, A., & White, B. A. (2010). Earliest intercept geometry guidance to improve mid-course guidance in area air-defence. *International Journal of Aeronautical and Space Science*, *11(2)*, 118–125.

Shinar, J. (2001). On the feasibility of 'hit to kill' in the interception of a manoeuvring target. In *American Control Conference*, (pp. 3358–3363).

Shinar, J., Guelman, M., Silberman, G., & Green, A. (1989). Ieee international conference on control and applications. In *On optimal missile avoidance - a comparison between optimal control and differential game solutions*, (pp. 453–459).

Shinar, J. & Shima, T. (1996). A game theoretical interceptor guidance law for ballistic missile defence. In *IEEE Conference on Decision and Control*, (pp. 2780–2785).

Shinar, J., Siegel, A., & Gold, Y. (1988). On the analysis of a complex differential game using artificial intelligence. In *IEEE Conference on Decision and Control*, (pp. 1436–1441).

Shinar, J. & Turetsky, V. (2002). On improved estimation for interceptor guidance. In *American Control Conference*, (pp. 203–208).

Shneydor, N. A. (1998). *Missile guidance and Pursuit*. Horwood Publishing.

Shukla, U. S. & Mahapatra, P. R. (1990). The proportinal navigation dilemma-pure or true. *IEEE Transactions on Aerospace Electronic Systems*, *16(2)*, 382–392.

Siouris, G. M. & Leros, A. P. (1998). Minimum-time intercept guidance for tactical missiles. *Control Theory and Advanced Technology*, *4*, 251–263.

Song, E. J. & Tahk, M. J. (1998). Real-time midcourse guidance with intercept point prediction. *Control Engineering Pratice*, *6(8)*, 957–967.

Song, E. J. & Tahk, M. J. (1999). Real-time midcourse missile guidance robust against launch conditions. *Control Engineering Practice*, *7(4)*, 507–515.

Song, E. J. & Tahk, M. J. (2001). Real-time neural-network midcourse guidance. *Control Engineering Practice*, *9(10)*, 1145–1154.

Tahk, M. J., Ryoo, C. K., & Cho, H. J. (2002). Recursive time-to-go estimation for homing guidance of varying velocity missiles. *IEEE Transactions on Aerospace and Electronic Systems*, *38(1)*, 13–24.

White, B. A. & Tsourdos, A. (2011). Modern missile guidance design: An overview. In *IFAC Automatic Control in Aerospace*.

White, B. A., Zibkowski, R., & Tsourdos, A. (2007). Direct intercept guidance using differential geometry concepts. *IEEE Transactions on Aerospace and Electronic Systems*, *43(3)*, 899–919.

Yang, C. D. & Yang, C. C. (1997). Optimal pure proportional navigation for maneuvering targets. *IEEE Transactions on Aerospace Electronic Systems*, *33(3)*, 949–957.

Yang, S. M. (1996). Analysis of optimal mid-course guidance law. *IEEE Transactions on Aerospace and Electronic Systems*, *32*(1), 419–425.

Yuan, P. J. & Chern, J. S. (1992). Analytic study of biased proportional navigation. *Journal of Guidance, Control, and Dynamcis*, *15(1)*, 185–190.

Zarchan, P. (1994). *Tactical and Strategic Missile Guidance*. AIAA tactical missile series.

Appendices

Appendix A

Optimal Solution for the Linear System with Additional Forcing Term

Let us consider state equations of the linear system with additional forcing terms defined as:

$$\dot{x} = Ax + Bu + \Delta, \quad x(t_0) = x_0, \tag{A.1}$$

where Δ is continuous differential function of time t. Moreover, consider a linear optimal control problem with the additional forcing term Δ: find $u(t)$, which minimizes J, given by

$$J = \int_{t_0}^{t_f} L(x, u, t)\ \mathrm{d}t + F(x(t_f)), \tag{A.2}$$

where

$$L = \frac{1}{2}x^T Q x + u^T C x + \frac{1}{2}u^T R u, \quad (Q \geq 0,\ \ R > 0) \tag{A.3}$$

$$F = \frac{1}{2}x(t_f)^T S_f x(t_f) \tag{A.4}$$

subject to Eqn. (A.1) with terminal constraint

$$Dx(t_f) = E \tag{A.5}$$

From the Prontryagin necessary condition, we have

$$\begin{aligned} \dot{\lambda} &= H_x^T \\ &= -A^T\lambda - Qx - C^T u \end{aligned} \tag{A.6}$$

$$\lambda(t_f) = S_f x(t_f) + D^T \nu \tag{A.7}$$

and

$$0 = H_u^T = Cx + Ru + B^T\lambda \tag{A.8}$$

$$u = -R^{-1}(Cx + B^T\lambda) \tag{A.9}$$

Substituting Eqn. (A.9) into Eqn. (A.1) and repeating Eqn.(A.6) yields following two-point boundary-value problem (TPBVP):

$$\begin{bmatrix} \dot{x} \\ \dot{\lambda} \end{bmatrix} = \begin{bmatrix} A - BR^{-1}C & -BR^{-1}B^T \\ -Q + C^T R^{-1} C & -(A - BR^{-1}C)^T \end{bmatrix} \begin{bmatrix} x \\ \lambda \end{bmatrix} + \begin{bmatrix} \Delta \\ 0 \end{bmatrix} \tag{A.10}$$

$$x(t_0) = x_0, \quad \lambda(t_f) = S_f x(t_f) + D^T \nu \tag{A.11}$$

Now, let the Hamiltonian matrix H be

$$H(t) = \begin{bmatrix} A - BR^{-1}C & -BR^{-1}B^T \\ -Q + C^T R^{-1} C & -(A - BR^{-1}C)^T \end{bmatrix} \tag{A.12}$$

The transition matrix for H is represented as:

$$\Phi_H = \begin{bmatrix} \phi_{11} & \phi_{12} \\ \phi_{21} & \phi_{22} \end{bmatrix} \tag{A.13}$$

The solution of Equation (A.10) is given by:

$$\begin{aligned} \begin{bmatrix} x(t) \\ \lambda(t) \end{bmatrix} &= \Phi_H(t, t_0) \begin{bmatrix} x(t_0) \\ \lambda(t_0) \end{bmatrix} + \int_{t_0}^{t} \Phi_H(t, \tau) \begin{bmatrix} \Delta(\tau) \\ 0 \end{bmatrix} \mathrm{d}\tau \\ &= \begin{bmatrix} \phi_{11}(t, t_0) x(t_0) + \phi_{12}(t, t_0)\lambda(t_0) + \phi_{\Delta 1}(t, t_0) \\ \phi_{21}(t, t_0) x(t_0) + \phi_{22}(t, t_0)\lambda(t_0) + \phi_{\Delta 2}(t, t_0) \end{bmatrix} \end{aligned} \tag{A.14}$$

where

$$\begin{cases} \phi_{\Delta 1}(t, s) = \int_s^t \phi_{11}(t, \tau)\Delta(\tau) \ \mathrm{d}\tau \\ \phi_{\Delta 2}(t, s) = \int_s^t \phi_{21}(t, \tau)\Delta(\tau) \ \mathrm{d}\tau \end{cases} \tag{A.15}$$

For $t = t_f$, it is clear:

$$x(t_f) = \phi_{11}(t_f, t_0) x_0 + \phi_{12}(t_f, t_0)\lambda(t_0) + \phi_{\Delta 1}(t_f, t_0) \tag{A.16}$$

$$\lambda(t_f) = \phi_{21}(t_f, t_0) x_0 + \phi_{22}(t_f, t_0)\lambda(t_0) + \phi_{\Delta 2}(t_f, t_0) \tag{A.17}$$

Substituting Equation (A.16) into Equation (A.7) yields

$$\begin{aligned} \lambda(t_f) &= S_f x(t_f) + D^T \nu \\ &= S_f \phi_{11} x_0 + S_f \phi_{12} \lambda(t_0) + S_f \phi_{\Delta 1}(t_f, t_0) + D^T \nu \end{aligned} \tag{A.18}$$

From Equation (A.17) and (A.18), we have:

$$(\phi_{22} - S_f \phi_{12})\lambda(t_0) = -(\phi_{21} - S_f \phi_{11}) x_0 + S_f \phi_{\Delta 1}(t_f, t_0) - \phi_{\Delta 2}(t_f, t_0) + D^T \nu \tag{A.19}$$

Defining $\bar{\Phi}_H$ as

$$\bar{\Phi}_H \equiv \begin{bmatrix} I & 0 \\ -S_f & I \end{bmatrix} \Phi_H \tag{A.20}$$

yields:

$$\bar{\Phi}_H = \begin{bmatrix} \bar{\phi}_{11} & \bar{\phi}_{12} \\ \bar{\phi}_{21} & \bar{\phi}_{22} \end{bmatrix} \equiv \begin{bmatrix} \phi_{11} & \phi_{12} \\ \phi_{21} - S_f\phi_{11} & \phi_{21} - S_f\phi_{12} \end{bmatrix} \tag{A.21}$$

Now, we define $\bar{\phi}_\Delta$ as:

$$\bar{\phi}_\Delta(t,s) = S_f\phi_{\Delta 1}(t_f,s) - \phi_{\Delta 2}(t_f,s) \tag{A.22}$$

Then, Equation (A.19) can be rewritten as:

$$\bar{\phi}_{22}(t_f,t_0)\lambda(t_0) = -\bar{\phi}_{21}(t_f,t_0)x_0 - \bar{\phi}_\Delta(t_f,t_0) + D^T\nu \tag{A.23}$$

If $\bar{\phi}_{22}$ is nonsingular, this equation is given by:

$$\lambda(t_0) = -\bar{\phi}_{22}^{-1}\bar{\phi}_{21}x_0 + \bar{\phi}_{22}^{-1}(D^T\nu - \bar{\phi}_\Delta) \tag{A.24}$$

where:

$$\begin{cases} \phi_{ij} \equiv \phi_{ij}(t_f,t_0), & \bar{\phi}_{ij} \equiv \bar{\phi}_{ij}(t_f,t_0), \\ \phi_\Delta \equiv \phi_\Delta(t_f,t_0), & \phi_{\Delta i} \equiv \phi_{\Delta i}(t_f,t_0); \end{cases} \quad i,j = 1,2. \tag{A.25}$$

Substituting Equation (A.24) into Equation (A.16) and using the definition Φ_H yield:

$$\begin{aligned} x(t_f) &= \phi_{11}x_0 + \phi_{12}\left[-\bar{\phi}_{22}^{-1}\bar{\phi}_{21}x_0 + \bar{\phi}_{22}^{-1}(D^T\nu - \bar{\phi}_\Delta)\right] + \phi_{\Delta 1} \\ &= (\bar{\phi}_{11} - \bar{\phi}_{12}\bar{\phi}_{22}^{-1}\bar{\phi}_{21})x_0 + \bar{\phi}_{12}\bar{\phi}_{22}^{-1}D^T\nu - \bar{\phi}_{12}\bar{\phi}_{22}^{-1}\bar{\phi}_\Delta + \phi_{\Delta 1} \end{aligned} \tag{A.26}$$

Terminal constraint then becomes:

$$D(\bar{\phi}_{11} - \bar{\phi}_{12}\bar{\phi}_{22}^{-1}\bar{\phi}_{21})x_0 + D\bar{\phi}_{12}\bar{\phi}_{22}^{-1}D^T\nu = E + D\bar{\phi}_{12}\bar{\phi}_{22}^{-1}\bar{\phi}_\Delta - D\phi_{\Delta 1} \tag{A.27}$$

Since it is well known that Φ_H is a symplectic matrix, i.e.,

$$\Phi_H(t,t_0)\begin{bmatrix} 0 & I \\ -I & 0 \end{bmatrix}\Phi_H(t,t_0)^T = \begin{bmatrix} 0 & I \\ -I & 0 \end{bmatrix} \tag{A.28}$$

following relations can be derived:

$$\begin{aligned} \phi_{11}\phi_{12}^T &= \phi_{12}\phi_{11}^T \\ \phi_{21}\phi_{22}^T &= \phi_{22}\phi_{21}^T \\ \phi_{11}\phi_{22}^T - \phi_{12}\phi_{21}^T &= I \end{aligned} \tag{A.29}$$

From this equation, we have:

$$\begin{aligned} \phi_{22}^{-1}\phi_{21} &= \phi_{21}^T\phi_{22}^{-T} \\ \phi_{11} - \phi_{12}\phi_{21}^T\phi_{22}^{-T} &= \phi_{22}^{-T} \end{aligned} \tag{A.30}$$

where $\phi_{ij}^{-T} = (\phi_{ij}^T)^{-1} = (\phi_{ij}^{-1})^T$. Note that $\bar{\Phi}_H$ defined in Equation (A.20) is also a symplectic matrix, so that $\bar{\phi}_{ij}^{'}$s satisfy Equation (A.29) and (A.30). Therefore, Equation (A.24) and (A.27) can be rewritten as:

$$\begin{bmatrix} \lambda(t_0) \\ E \end{bmatrix} = \begin{bmatrix} \bar{\phi}_{22}^{-1}\bar{\phi}_{21} & \bar{\phi}_{22}^{-1}D^T \\ D\bar{\phi}_{22}^{-T} & D\bar{\phi}_{12}\bar{\phi}_{22}^{-1}D^T \end{bmatrix} \begin{bmatrix} x_0 \\ \nu \end{bmatrix} - \begin{bmatrix} \bar{\phi}_{22}^{-1}\bar{\phi}_{\Delta} \\ D\bar{\phi}_{12}\bar{\phi}_{22}^{-1}\bar{\phi}_{\Delta} - D\phi_{\Delta 1} \end{bmatrix} \tag{A.31}$$

Let us define:

$$S(t_f,t) = -\bar{\phi}_{22}^{-1}(t_f,t)\bar{\phi}_{21}(t_f,t) \tag{A.32}$$

$$F(t_f,t) = \bar{\phi}_{22}^{-1}(t_f,t)D^T \tag{A.33}$$

$$G(t_f,t) = D\bar{\phi}_{12}(t_f,t)\bar{\phi}_{22}^{-1}(t_f,t)D^T \tag{A.34}$$

$$F_{\Delta}(t_f,t) = -\bar{\phi}_{22}^{-1}(t_f,t)\bar{\phi}_{\Delta}(t_f,t) \tag{A.35}$$

$$G_{\Delta}(t_f,t) = D\bar{\phi}_{12}(t_f,t)\bar{\phi}_{22}^{-1}(t_f,t)\bar{\phi}_{\Delta}(t_f,t) - D\phi_{\Delta 1}(t_f,t) \tag{A.36}$$

Since any time $t < t_f$ is a possible initial time, Equation (A.31) can be rewritten as:

$$\lambda(t) = S(t_f,t)x(t) + F(t_f,t)\nu + F_{\Delta}(t_f,t) \tag{A.37}$$

$$E = F^T(t_f,t)x(t) + G(t_f,t)\nu + G_{\Delta}(t_f,t) \tag{A.38}$$

These relations must be valid for $t = t_f$:

$$\begin{aligned} &S(t_f,t_f) = S_f, \quad F(t_f,t_f) = D^T, \quad G(t_f,t_f) = 0 \\ &F_{\Delta}(t_f,t_f) = 0, \quad G_{\Delta}(t_f,t_f) = 0 \end{aligned} \tag{A.39}$$

If Equation (A.31) can be solved for $S(t_f,t)$, $F(t_f,t)$, $G(t_f,t)$, $F_{\Delta}(t_f,t)$, and $G_{\Delta}(t_f,t)$, it is possible to derive $\lambda(t_0)$ and ν. Time derivative of S is given by:

$$\dot{S} = -\left(\frac{\mathrm{d}}{\mathrm{d}t}\bar{\phi}_{22}^{-1}\right)\bar{\phi}_{21} - \bar{\phi}_{22}^{-1}\left(\frac{\mathrm{d}}{\mathrm{d}t}\bar{\phi}_{21}\right) \tag{A.40}$$

Using the property of the state transition matrix $\bar{\Phi}_H(t_f, t)$ given by:

$$\frac{\mathrm{d}}{\mathrm{d}t}\bar{\Phi}_H(t_f, t) = -\bar{\Phi}_H(t_f, t)H(t) \tag{A.41}$$

we have:

$$\frac{\mathrm{d}}{\mathrm{d}t}\bar{\phi}_{21} = -\bar{\phi}_{21}(A - BR^{-1}C) - \bar{\phi}_{22}(-Q + C^T R^{-1}C) \tag{A.42}$$

Differentiating following equation:

$$\bar{\phi}_{22}^{-1}(t_f, t)\bar{\phi}_{22}(t_f, t) = I \tag{A.43}$$

and again using Equation (A.30) and (A.41), we have:

$$\frac{\mathrm{d}}{\mathrm{d}t}\bar{\phi}_{22}^{-1} = \left[SBR^{-1}B^T - (A - BR^{-1}C)^T\right]\bar{\phi}_{22}^{-1} \tag{A.44}$$

Therefore, $\dot{S}(t_f, t)$ is obtained as:

$$\begin{aligned}\dot{S} &= -\left[SBR^{-1}B^T - (A - BR^{-1}C)^T\right]\bar{\phi}_{22}^{-1}\bar{\phi}_{21} \\ &\quad +\bar{\phi}_{22}^{-1}\left[\bar{\phi}_{21}(A - BR^{-1}C) + \bar{\phi}_{22}(-Q + C^T R^{-1}C)\right]\end{aligned} \tag{A.45}$$

The definition $S(t_f, t)$ in Equation (A.32) yields:

$$\begin{aligned}\dot{S} &= -(A - BR^{-1}C)^T S - S(A - BR^{-1}C) \\ &\quad +(-Q + C^T RC) + SBR^{-1}B^T S; \quad S(t_f, t_f) = S_f\end{aligned} \tag{A.46}$$

Now, let us differentiate Equation (A.33):

$$\dot{F} = \left(\frac{\mathrm{d}}{\mathrm{d}t}\bar{\phi}_{22}^{-1}\right)D^T \tag{A.47}$$

From Equation (A.44) and Equation (A.33), this equation can be derived as:

$$\dot{F} = -(A - BR^{-1}C)^T F + SBR^{-1}B^T F; \quad F(t_f, t_f) = D^T \tag{A.48}$$

The first time derivative of $G(t_f, t)$ is obtained as:

$$\dot{G} = D\left(\frac{\mathrm{d}}{\mathrm{d}t}\bar{\phi}_{12}\bar{\phi}_{22}^{-1}\right) \tag{A.49}$$

From Equation (A.41), $\mathrm{d}/\mathrm{d}t\bar{\phi}_{12}$ can be derived of the form:

$$\frac{\mathrm{d}}{\mathrm{d}t}\bar{\phi}_{12} = -\left[-\bar{\phi}_{11}BR^{-1}B^T - \bar{\phi}_{12}(A - BR^{-1}c)^T\right]\bar{\phi}_{22}^{-1} \tag{A.50}$$

Hence:

$$\frac{\mathrm{d}}{\mathrm{d}t}(\bar{\phi}_{12}\bar{\phi}_{22}^{-1}) = (\bar{\phi}_{11} + \bar{\phi}_{12}S)BR^{-1}B^T\bar{\phi}_{22}^{-1} \tag{A.51}$$

Since $\bar{\phi}'_{ij}s$ also satisfy Equation (A.30), we have:

$$\bar{\phi}_{11} + \bar{\phi}_{12}S = \bar{\phi}_{22}^{-T} \tag{A.52}$$

$$\frac{\mathrm{d}}{\mathrm{d}t}\left(\bar{\phi}_{12}\bar{\phi}_{22}^{-1}\right) = \bar{\phi}_{22}^{-T}BR^{-1}B^T\bar{\phi}_{22}^{-1} \tag{A.53}$$

Therefore, $\dot{G}$ is given by:

$$\begin{aligned}\dot{G} &= D\bar{\phi}_{22}^{-T}BR^{-1}B^T\bar{\phi}_{22}^{-1}D^T \\ &= F^TBR^{-1}B^TF; \quad G(t_f, t_f) = 0\end{aligned} \tag{A.54}$$

Note that, for $t \leq t_f$, $G(t_f, t) \leq 0$ because $\dot{G}(t_f, t) \geq 0$ and $G(t_f, t_f) = 0$. Next, let us differentiate $F_\Delta(t_f, t)$ from Equation (A.35):

$$\frac{\mathrm{d}}{\mathrm{d}t}F_\Delta = -\left(\frac{\mathrm{d}}{\mathrm{d}t}\bar{\phi}_{22}\right)\bar{\phi}_\Delta - \bar{\phi}_{22}\frac{\mathrm{d}}{\mathrm{d}t}\bar{\phi}_\Delta \tag{A.55}$$

Here, $\mathrm{d}/\mathrm{d}t\bar{\phi}_\Delta(t_f, t)$ can be shortened using the definition of $\bar{\phi}_{21}$:

$$\frac{\mathrm{d}}{\mathrm{d}t}\bar{\phi}_\Delta = \left(-\phi_{21} + S_f\phi_{11}\right)\Delta = -\bar{\phi}_{21}\Delta \tag{A.56}$$

Substituting Equation (A.15), (A.22), and (A.56) into Equation (A.55) yields:

$$\frac{\mathrm{d}}{\mathrm{d}t}F_\Delta = \left[SBR^{-1}B^T - (A - BR^{-1}C)^T\right]\bar{\phi}_{22}^{-1}\bar{\phi}_\Delta + \bar{\phi}_{22}^{-1}\bar{\phi}_{21}\Delta \tag{A.57}$$

Using definitions of F_Δ and S, $\dot{F}_\Delta$ can be rewritten as:

$$\frac{\mathrm{d}}{\mathrm{d}t}F_\Delta = -\left[(A - BR^{-1}C)^T - SBR^{-1}B^T\right]F_\Delta - S\Delta; \quad F_\Delta(t_f, t_f) = 0 \tag{A.58}$$

The first time derivative of $G_\Delta(t_f, t)$ is obtained as:

$$\frac{\mathrm{d}}{\mathrm{d}t}G_\Delta = D\frac{\mathrm{d}}{\mathrm{d}t}(\bar{\phi}_{12}\bar{\phi}_{22}^{-1})\bar{\phi}_\Delta + D\bar{\phi}_{12}\bar{\phi}_{22}^{-1}\frac{\mathrm{d}}{\mathrm{d}t}\bar{\phi}_\Delta - D\frac{\mathrm{d}}{\mathrm{d}t}\phi_{\Delta 1} \tag{A.59}$$

and

$$\frac{\mathrm{d}}{\mathrm{d}t}\phi_{\Delta 1} = -\phi_{11}\Delta \tag{A.60}$$

Now, we substitute Equation (A.53), (A.56), and (A.60) into Equation (A.59):

$$\begin{aligned}\frac{\mathrm{d}}{\mathrm{d}t}G_\Delta &= D\bar{\phi}_{22}^{-T}BR^{-1}B^T\bar{\phi}_{22}^{-1}\bar{\phi}_\Delta - D\bar{\phi}_{12}\bar{\phi}_{22}^{-1}\bar{\phi}_{21}\Delta + D\phi_{11}\Delta \\ &= -F^TBR^{-1}B^TF_\Delta + D(\phi_{11} - \bar{\phi}_{12}\bar{\phi}_{22}^{-1}\bar{\phi}_{21})\Delta \\ &= -F^TBR^{-1}B^TF_\Delta + F^T\Delta; \quad G_\Delta(t_f, t_f) = 0 \end{aligned} \tag{A.61}$$

At a particular initial time $t = t_0$, if G is invertible, Equation (A.38) can be solved for v:

$$v = G^{-1}(t_f, t_0)E - G^{-1}(t_f, t_0)F^T(t_f, t_0)x_0 + G^{-1}(t_f, t_0)G_\Delta(t_f, t_0) \tag{A.62}$$

In a shortened form:

$$v = G^{-1}E - G^{-1}F^Tx_0 + G^{-1}G_\Delta \tag{A.63}$$

Hence:

$$\begin{aligned}\lambda(t_0) &= Sx_0 + FG^{-1}E - FG^{-1}F^Tx_0 + FG^{-1}G_\Delta + F_\Delta \\ &= (S - FG^{-1}F^t)x_0 + FG^{-1}(E + G_\Delta) + F_\Delta \end{aligned} \tag{A.64}$$

Let $\bar{S}$ be $(S - FG^{-1}F^T)$, then:

$$\lambda(t_0) = \bar{S}x_0 + FG^{-1}(E + G_\Delta) + F_\Delta \tag{A.65}$$

Since Equation (A.65) is valid for any possible initial time $t_0 = t$ for which $G(t_f, t)$ is invertible, we have

$$\lambda(t) = \bar{S}(t_f, t)x(t) + F(t_f, t)G^{-1}(t_f, t)(E + G_\Delta(t_f, t)) + F_\Delta(t_f, t) \tag{A.66}$$

Substituting Equation (A.66) into Equation (A.9) gives optimal control of the form:

$$\begin{aligned}u^*(t) &= -R^{-1}\left[C + B^T\bar{S}(t_f, t)\right]x(t) \\ &\quad -R^{-1}B^TF(t_f, t)G^{-1}(t_f, t)(E + G_\Delta(t_f, t)) - R^{-1}B^TF_\Delta(t_f, t) \end{aligned} \tag{A.67}$$

Summary

We are interested in solve the optimal control problem. Since it is possible to derive following matrices

$$\begin{cases} \bar{S} = S - FG^{-1}F^T \\ \dot{S} = -(A - BR^{-1}C)^T S - S(A - BR^{-1}C) + (-Q + C^T RC) + SBR^{-1}B^T S \\ \dot{F} = -(A - BR^{-1}C)^T F + SBR^{-1}B^T F \\ \dot{G} = F^T BR^{-1}B^T F \\ \dot{F}_\Delta = -\left[(A - BR^{-1}C)^T - SBR^{-1}B^T\right] F_\Delta - S\Delta \\ \dot{G}_\Delta = -F^T BR^{-1}B^T F_\Delta + F^T \Delta \end{cases} \tag{A.68}$$

with terminal conditions

$$\begin{aligned} &S(t_f, t_f) = S_f, \quad F(t_f, t_f) = D^T, \quad G(t_f, t_f) = 0 \\ &F_\Delta(t_f, t_f) = 0, \quad G_\Delta(t_f, t_f) = 0 \end{aligned} \tag{A.69}$$

we can evaluate following optimal feedback control law:

$$u^*(t) = -R^{-1}(C + B^T \bar{S})x(t) - R^{-1}B^T \left[FG^{-1}(E + G_\Delta) + F_\Delta\right] \tag{A.70}$$